User Guide for

# ABC – Analysis of Bearing Capacity

Version 1.0

C.M. Martin

Department of Engineering Science
University of Oxford

OUEL Report No. 2261/03

| | |
|---|---|
| Initial draft | September 2003 |
| Revised for v1.0 | October 2004 |
| | |
| | |
| | |
| | |
| | |

## DISCLAIMER



## TECHNICAL SUPPORT

Address: Dr C.M. Martin
Department of Engineering Science
University of Oxford
Parks Road
Oxford OX1 3PJ
U.K.

Email: chris.martin@eng.ox.ac.uk

Web: http://www-civil.eng.ox.ac.uk/people/cmm/software/abc

## ACKNOWLEDGEMENTS

For their help with the beta testing:

- Dave White (University of Cambridge) and his students in 4D5 Foundation Engineering
- Mark Randolph (University of Western Australia)

For thinking up the program's name:

- Geraldine Johnson (University of Oxford)

# CONTENTS

# 1. INTRODUCTION

## 1.1 Program description

ABC is a computer program that uses the method of stress characteristics (also known as the slip line method) to solve the classical geotechnical bearing capacity problem of a rigid foundation, resting on a cohesive-frictional soil mass, loaded to failure by a central vertical force. Figure 1.1 shows the terminology used.

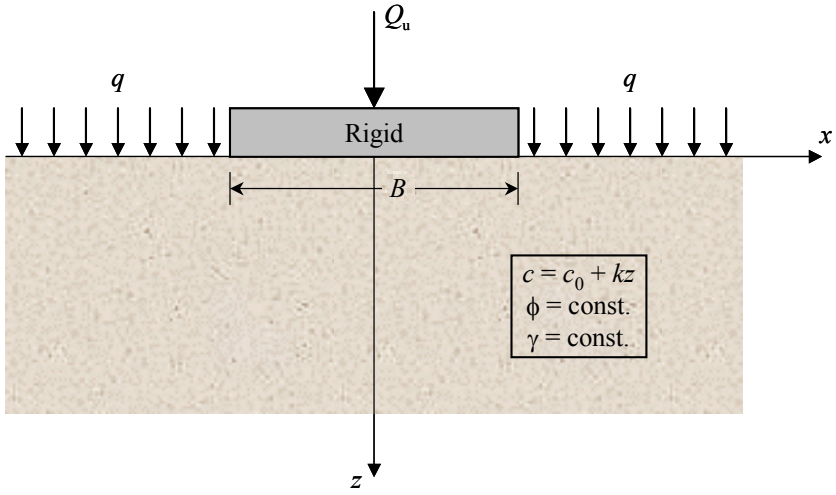


**Figure 1.1** Problem definition

*Soil*

- The soil is modelled as a rigid–perfectly plastic Mohr-Coulomb material, assumed to be isotropic and of semi-infinite extent.
- The cohesion $c$ can vary linearly with depth ( $c = c_0 + kz$ ).
- The friction angle $\phi$ and unit weight $\gamma$ are taken to be constant.

*Footing*

- Plane strain (strip footing) and axially symmetric (circular footing) analyses can be performed.
- The soil–footing interface can be modelled as smooth or rough.
- A uniform surcharge pressure $q$ can be applied to the soil adjacent to the footing.

*Solution*

- The mesh or 'net' of characteristics is constructed in an interactive environment.
- A sequence of increasingly accurate calculations, each one involving a finer mesh, can be used to obtain a converged solution.
- A variety of automated strategies, including mesh adaptivity, maintain the accuracy and efficiency of the method when solving difficult problems.

*Results*

- The bearing capacity is reported as a force $Q_u$ and an average pressure $q_u$.
- The mesh of characteristics can be annotated to show the footing tractions (as used to obtain the bearing capacity), and/or the principal stresses in the soil.

### 1.2 Status of solutions

In the terminology of limit analysis, a converged solution obtained using ABC is classified as a 'partial' or 'incomplete' lower-bound collapse load (see e.g. Bishop, 1953). This is because only part of the stress field at collapse, namely the part needed to compute the bearing capacity, is constructed. For many problems in both plane strain and axial symmetry it has been shown that the bearing capacity obtained in this manner is identical to the exact collapse load, but various additional calculations (not currently performed by ABC) are needed to establish this formally for a particular combination of parameters[1]. Specifically, these calculations involve proving that the partial lower-bound stress field can

- be extended throughout the rest of the soil mass without violating equilibrium or yield;
- be associated with a velocity field that gives a coincident upper-bound collapse load.

It is important to realise that the bound and uniqueness theorems of limit analysis are only valid for ideal materials that exhibit perfect plasticity, i.e. no post-yield hardening or softening, and an associated flow rule. The latter requirement means that, in the case of a Mohr-Coulomb soil, the theorems are only applicable if the dilation angle $\psi$ is equal to the friction angle $\phi$. Even though real soils only exhibit such behaviour in the special case of undrained shearing ( $\phi_u = \psi_u = 0$ ), calculations based on associativity remain an important point of reference, e.g. the bearing capacity design methods in codes and standards are invariably based on factors $N_c$, $N_q$ and $N_\gamma$ that pertain to soil with an associated flow rule. Investigations into the effect of non-associativity on the bearing capacity of shallow foundations are ongoing – see the references cited in Martin (2003).

### 1.3 Possible applications

*Rigorous checks of traditional $N_c$ - $N_q$ - $N_\gamma$ calculations, such as those prescribed in design codes.*

These methods rely on the superposition of three separate bearing capacities – a technique that is inherently conservative – but they also rely on tabulated or curve-fitted values of the bearing capacity factor $N_\gamma$, which may be unconservative. Further approximations are introduced if the footing is circular (multiplicative shape factors are used to modify the plane strain values of $N_c$, $N_q$ and $N_\gamma$) or if the soil is non-homogeneous (calculations must then be based on some representative strength). By contrast, ABC constructs a numerical solution from first principles, without resorting to superposition, shape factors or any other form of approximation.

*Establishing benchmarks for the validation of other calculation methods.*

To validate the performance of, say, a commercial finite element package that is to be used for bearing capacity calculations, a series of test problems could be specified and solved using ABC. These problems could then be analysed using the FE package, ensuring that the settings adopted were consistent with ABC (Mohr-Coulomb yield criterion, associated flow rule, etc.). Assuming that the comparisons were satisfactory, the FE package could then be applied with confidence to more complex bearing capacity problems, perhaps involving a different yield criterion or flow rule, non-vertical loading, 3D footing geometry, etc.

*Education.*

Students learning about the theory of bearing capacity will find ABC a useful tool for understanding the method of characteristics, and for visualising the stress fields obtained with various combinations of parameters.

[1] In the small number of axially symmetric problems where crossing characteristics arise (see Section 3.6.2), the calculated bearing capacity has no formal status – not even as an 'incomplete' lower-bound collapse load.

## 2. HOW ABC WORKS

### 2.1 Introduction

If it is assumed *a priori* that the soil is at yield, the two-dimensional stress state at a point $(x, z)$ can be fully specified in terms of two auxiliary variables, namely the mean stress $\sigma$ and the orientation $\theta$ of the major principal stress, together with a function $R(x, z, \sigma, \theta)$ that defines the radius of Mohr's circle of stress (and thus the strength of the soil). The sign conventions adopted for $x$, $z$, $\sigma$ and $\theta$ are indicated in Figure 2.1, which also shows the yield criterion used in ABC:

$$R = c\cos\phi + \sigma\sin\phi \tag{2.1}$$

This is the two-dimensional form of the Mohr-Coulomb criterion. By definition, a Mohr-Coulomb soil is *isotropic*, because at a given point $(x, z)$ the strength does not depend on the orientation of the principal stresses – equation (2.1) is independent of $\theta$. If the strength parameters $c$ and $\phi$ are constant, the soil is described as *homogeneous*; if $c$ and/or $\phi$ vary with position, the soil is *non-homogeneous* (though still isotropic, as defined above). For simplicity, ABC only allows vertical non-homogeneity in $c$, via the linear equation

$$c = c_0 + kz \tag{2.2}$$

The friction angle $\phi$ is taken to be constant throughout the soil.

When the stresses-at-yield of Figure 2.1 are combined with the equations of equilibrium, a pair of coupled partial differential equations is obtained (spatial variables $x$ and $z$, field variables $\sigma$ and $\theta$). Standard techniques can be used to show that this equation system is hyperbolic, and hence there are two distinct characteristic directions – here denoted $\alpha$ and $\beta$ – along which the partial differential equations reduce to (coupled) ordinary differential equations. The relevant equations for plane strain and axial symmetry are summarised in the next section. For a concise summary of the derivation using the same terminology as that adopted here, see Martin (2003).

### 2.2 Governing equations

In the tables below, $\varepsilon$ $(= \pi/4 - \phi/2)$ denotes the angle between the direction of the major principal stress $\sigma_1$ and the directions of the $\alpha$ and $\beta$ characteristics (Figure 2.1a). Note that the characteristics coincide with the planes on which the Mohr-Coulomb criterion is satisfied (Figure 2.1b).

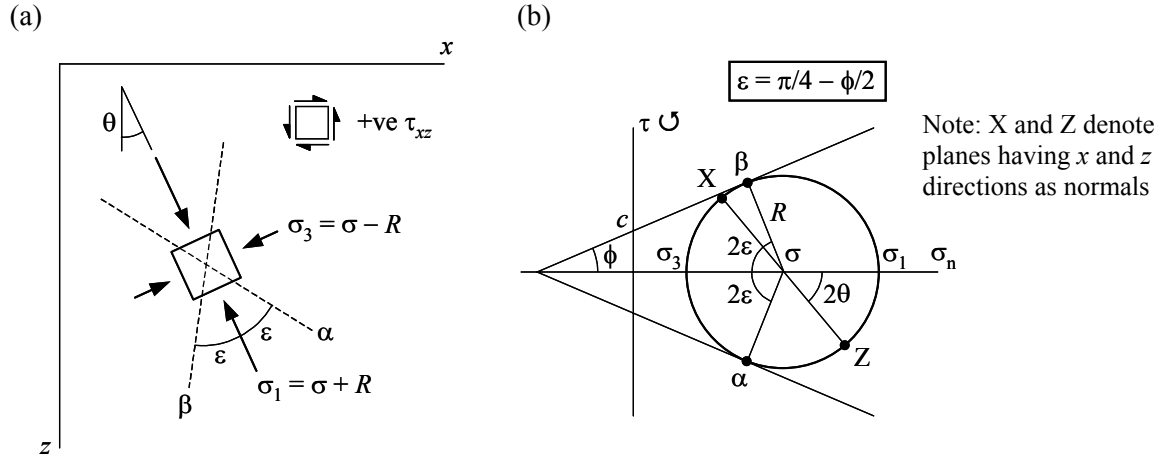


**Figure 2.1** Notation and sign conventions

*2.2.1 Plane strain*

Stresses in terms of auxiliary variables:

$$\begin{aligned} \sigma_{xx} &= \sigma - R\cos 2\theta \\ \sigma_{zz} &= \sigma + R\cos 2\theta \\ \tau_{xz} &= R\sin 2\theta \end{aligned} \tag{2.3}$$

Characteristics:

| | Directions (2.4) | Ordinary differential equations (2.5) |
|---|---|---|
| $\alpha$ | $\dfrac{\mathrm{d}x}{\mathrm{d}z} = \tan(\theta + \varepsilon)$ | $\mathrm{d}\sigma + \dfrac{2R}{\cos\phi}\mathrm{d}\theta = (\gamma_x - \gamma_z \tan\phi - k)\,\mathrm{d}x + (\gamma_z + \gamma_x \tan\phi)\,\mathrm{d}z$ |
| $\beta$ | $\dfrac{\mathrm{d}x}{\mathrm{d}z} = \tan(\theta - \varepsilon)$ | $\mathrm{d}\sigma - \dfrac{2R}{\cos\phi}\mathrm{d}\theta = (\gamma_x + \gamma_z \tan\phi + k)\,\mathrm{d}x + (\gamma_z - \gamma_x \tan\phi)\,\mathrm{d}z$ |

In equations (2.5), $\gamma_x$ and $\gamma_z$ denote body forces per unit volume in the *x* and *z* directions. In the current version of ABC it is always assumed that $\gamma_x = 0$ and $\gamma_z = \gamma$, so the governing equations can be simplified slightly.

*2.2.2 Axial symmetry*

Stresses in terms of auxiliary variables (note $\sigma_{yy}$ = hoop stress from Haar-von Karman hypothesis):

$$\begin{aligned} \sigma_{xx} &= \sigma - R\cos 2\theta \\ \sigma_{zz} &= \sigma + R\cos 2\theta \\ \sigma_{yy} &= \sigma - R \\ \tau_{xz} &= R\sin 2\theta \end{aligned} \tag{2.6}$$

Characteristics:

| | Directions (2.7) | Ordinary differential equations (2.8) |
|---|---|---|
| $\alpha$ | $\dfrac{\mathrm{d}x}{\mathrm{d}z} = \tan(\theta + \varepsilon)$ | $\mathrm{d}\sigma + \dfrac{2R}{\cos\phi}\mathrm{d}\theta = (\gamma_x^* - \gamma_z^* \tan\phi - k)\,\mathrm{d}x + (\gamma_z^* + \gamma_x^* \tan\phi)\,\mathrm{d}z$ |
| $\beta$ | $\dfrac{\mathrm{d}x}{\mathrm{d}z} = \tan(\theta - \varepsilon)$ | $\mathrm{d}\sigma - \dfrac{2R}{\cos\phi}\mathrm{d}\theta = (\gamma_x^* + \gamma_z^* \tan\phi + k)\,\mathrm{d}x + (\gamma_z^* - \gamma_x^* \tan\phi)\,\mathrm{d}z$ |

where

$$\begin{aligned} \gamma_x^* &= \gamma_x + \frac{R(\cos 2\theta - 1)}{x} \\ \gamma_z^* &= \gamma_z - \frac{R\sin 2\theta}{x} \end{aligned} \tag{2.9}$$

In equations (2.9), $\gamma_x$ and $\gamma_z$ denote actual body forces per unit volume in the *x* (now radial) and *z* directions, which as above are taken to be 0 and $\gamma$ respectively. The variables $\gamma_x^*$ and $\gamma_z^*$ can be viewed as fictitious plane strain body forces that have been modified to incorporate the effect of axial symmetry; this is simply a convenience that allows concise expression and coding of the equations. Note that $\gamma_x^*$ and $\gamma_z^*$ are not constants – they depend on the local values of *x* and $\theta$, as well as (through *R*) on the local values of *c* and $\sigma$.

An important feature of equations (2.9) is that they become singular on – and highly nonlinear in the vicinity of – the axis of symmetry, $x = 0$. Furthermore, they would give meaningless results if the radius $x$ were to become negative during the construction of a trial mesh of characteristics (see Section 2.9). For these reasons, the solution of a bearing capacity problem using the method of characteristics is considerably more difficult in axial symmetry than in plane strain.

## 2.3 Boundary conditions

### *2.3.1 Soil surface*

As shown in Figure 1.1, the soil adjacent to the footing is subjected to a uniform surcharge $q$, and is (by assumption) in a state of passive failure. The values of $\sigma$ and $\theta$ at the soil surface are therefore:

$$\sigma_{\text{passive}} = \frac{q + c_0 \cos\phi}{1 - \sin\phi}$$
$$\theta_{\text{passive}} = \pi/2 \tag{2.10}$$

The first of these equations can be obtained from the relevant Mohr's circle construction (Figure 2.2), noting that $c = c_0$ since $z = 0$, and that the minor principal stress $\sigma_3$ is vertical and equal to $q$. The $\alpha$ and $\beta$ characteristics are inclined at $\pm\varepsilon$ to the horizontal. The second of equations (2.10) simply states that the major principal stress $\sigma_1$ is horizontal (see Figure 2.1a).

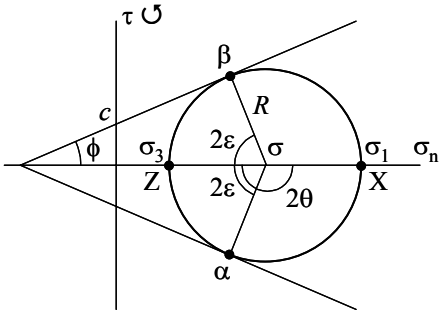


$$R = c\cos\phi + \sigma\sin\phi$$
$$c = c_0 \qquad 2\theta = \pi$$
$$\sigma_3 = q = \sigma - R \qquad \theta = \pi/2$$
$$\therefore \quad \sigma = \frac{q + c_0\cos\phi}{1 - \sin\phi}$$

**Figure 2.2** Mohr's circle for soil surface

### *2.3.2 Underside of footing*

The soil directly beneath the footing is (by assumption) in a state of active failure. The orientation $\theta$ of the major principal stress depends on the roughness of the underside of the footing. If it is smooth, the major principal stress is vertical:

$$\theta_{\text{footing}} = 0 \tag{2.11s}$$

If it is rough (and full roughness is mobilised, see Section 2.5.2) then the Mohr-Coulomb criterion is satisfied on the plane of the interface, hence:

$$\theta_{\text{footing}} = -\pi/4 - \phi/2 \tag{2.11r}$$

Mohr's circles for the two cases are shown in Figure 2.3. In the smooth case the interface shear stress is zero, and the $\alpha$ and $\beta$ characteristics are inclined at $\pm\varepsilon$ to the vertical. In the rough case the footing exerts an inward shear stress on the soil, with the $\beta$ characteristic tangential to the interface.

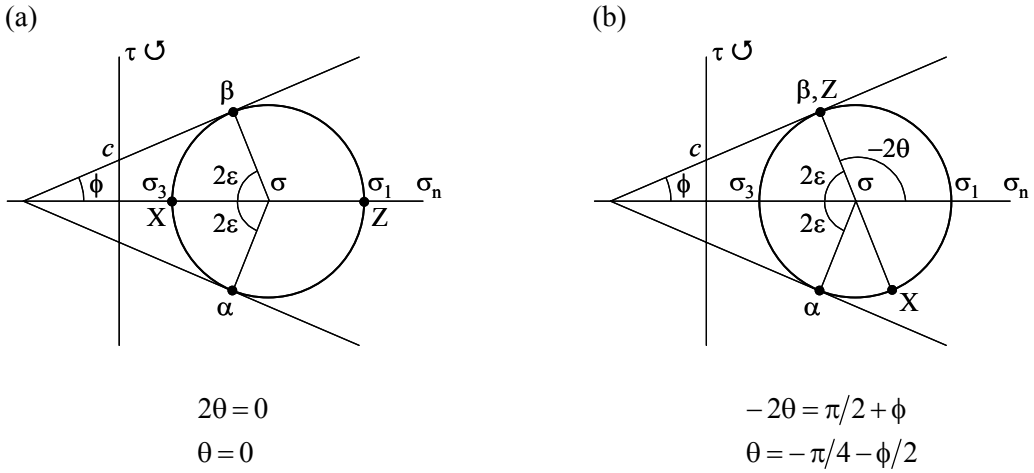


$2\theta = 0$ $\qquad$ $-2\theta = \pi/2 + \phi$

$\theta = 0$ $\qquad$ $\theta = -\pi/4 - \phi/2$

**Figure 2.3** Mohr's circle for underside of footing: (a) smooth (b) rough

## 2.4 Finite difference formulation

*2.4.1 Plane strain*

The basis of the method of characteristics is as follows. Referring to Figure 2.4, if the solution[1] is known at two points A (on an α characteristic) and B (on a β characteristic), it can be propagated to a new point C by integrating the governing equations simultaneously along the α segment AC and the β segment BC. It is sometimes possible to devise special patterns of characteristics that allow these integrations to be performed analytically, notably in plane strain when the soil is either

- homogenous and purely cohesive ( $c_0 > 0$ , $k = 0$ , $\phi = 0$ , $\gamma \geq 0$ );
- homogeneous and weightless ( $c_0 \geq 0$ , $k = 0$ , $\phi > 0$ , $\gamma = 0$ ).

In general, however, an approximate numerical integration must be carried out.

To solve the four nonlinear equations (2.4α,β) and (2.5α,β) for the solution[1] at the new point, it is convenient and customary to adopt a midpoint finite difference scheme, in conjunction with a fixed-point iteration strategy. In detail, the algorithm used in ABC is as follows:

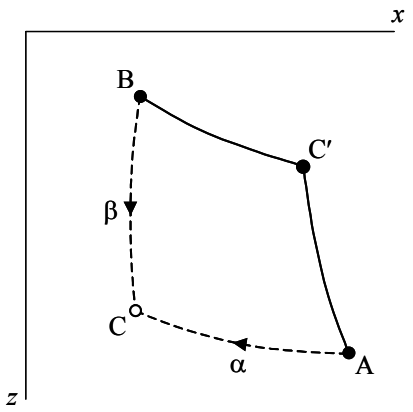


**Figure 2.4** Calculation of new solution point in body of soil (CalcAB)

[1] i.e. the coordinates and the auxiliary variables, conveniently stored as a vector [$x$, $z$, σ, θ]

**CalcAB**

In: $[x_A, z_A, \sigma_A, \theta_A]$, $[x_B, z_B, \sigma_B, \theta_B]$, $\sigma_C^i$, $\theta_C^i$, *Tol*, *MaxIt1, MaxIt2*

Out: $[x_C, z_C, \sigma_C, \theta_C]$

0. Preliminaries.

Calculate $R_A = c_A \cos\phi + \sigma_A \sin\phi$ (where $c_A = c_0 + kz_A$) and $R_B = c_B \cos\phi + \sigma_B \sin\phi$ (where $c_B = c_0 + kz_B$). Initialise $\sigma_C = \sigma_C^i$ and $\theta_C = \theta_C^i$.

1. Intersect chord AC with chord BC.

Solve, cf. equation (2.4) but avoiding the singularity-prone $\tan(\bullet)$ functions,

$$\begin{aligned}(x_C - x_A)\cos\left(\frac{\theta_A + \theta_C}{2} + \varepsilon\right) &= (z_C - z_A)\sin\left(\frac{\theta_A + \theta_C}{2} + \varepsilon\right)\\ (x_C - x_B)\cos\left(\frac{\theta_B + \theta_C}{2} - \varepsilon\right) &= (z_C - z_B)\sin\left(\frac{\theta_B + \theta_C}{2} - \varepsilon\right)\end{aligned} \tag{2.12}$$

for $x_C$ and $z_C$.

2. Update field variables.

Calculate $R_C = c_C \cos\phi + \sigma_C \sin\phi$ (where $c_C = c_0 + kz_C$) and solve, cf. equation (2.5),

$$\begin{aligned}\sigma_C - \sigma_A + \frac{R_A + R_C}{\cos\phi}(\theta_C - \theta_A) &= (-\gamma\tan\phi - k)(x_C - x_A) + \gamma(z_C - z_A)\\ \sigma_C - \sigma_B - \frac{R_B + R_C}{\cos\phi}(\theta_C - \theta_B) &= (\gamma\tan\phi + k)(x_C - x_B) + \gamma(z_C - z_B)\end{aligned} \tag{2.13}$$

for $\sigma_C$ and $\theta_C$.

3. Check convergence.

If on the first iteration, set $x_C^{old} = x_C$, $z_C^{old} = z_C$, $\sigma_C^{old} = \sigma_C$, $\theta_C^{old} = \theta_C$ and repeat from Step 1. Otherwise, test each of the four components for convergence:

$$\begin{aligned}\left|x_C - x_C^{old}\right| &\le Tol\\ \left|z_C - z_C^{old}\right| &\le Tol\\ \left|\sigma_C - \sigma_C^{old}\right| &\le Tol \cdot \left|\sigma_C\right|\\ \left|\theta_C - \theta_C^{old}\right| &\le Tol\end{aligned} \tag{2.14}$$

If any component fails, set $x_C^{old} = x_C$, $z_C^{old} = z_C$, $\sigma_C^{old} = \sigma_C$, $\theta_C^{old} = \theta_C$ and repeat from Step 1. Otherwise, return the converged solution.

4. Back-up strategy.

If convergence has not been achieved within *MaxIt1* iterations, solve the four nonlinear equations (2.4α,β) and (2.5α,β) using the MINPACK subroutine HYBRD (Moré et al., 1980), specifying a convergence tolerance *Tol* and an iteration limit *MaxIt2*, and taking the latest fixed-point iterate $[x_C, z_C, \sigma_C, \theta_C]$ as the initial approximation to the solution. If HYBRD fails to converge, report a fatal error. Otherwise, return the converged solution.

Although straightforward, subroutine CalcAB is critical because it is called many millions of times during the construction of a highly refined mesh of characteristics. This piece of code has therefore been optimised quite carefully.

As indicated in Step 3, simple convergence checks based on absolute error are used for the quantities where this is appropriate ($x$, $z$, $\theta$). The convergence check for $\sigma$ – which can vary by many orders of magnitude within certain stress fields – is based on relative error. The method used to obtain the initial approximations $\sigma_C^i$ and $\theta_C^i$ depends on the availability of a known solution point C′ diagonally opposite C in the current cell of the mesh (Figure 2.4). If there is such a point, then good initial approximations can be found by linear extrapolation:

$$\begin{aligned} \sigma_C^i &= \sigma_A + \sigma_B - \sigma_{C'} \\ \theta_C^i &= \theta_A + \theta_B - \theta_{C'} \end{aligned} \tag{2.15}$$

If no C′ point is available, as is the case when a new $\alpha$ characteristic has just been initiated at the soil surface, an alternative procedure must be used. This is explained in Section 2.5.1.

As well as calculating new solution points in the body of the soil, it is also necessary to perform 'one-legged' calculations in which $\alpha$ characteristics are stepped onto the underside of the footing. This is illustrated in Figure 2.5. As before, there are four unknowns to be found: $x$, $z$, $\sigma$ and $\theta$ at C. Two of the necessary equations come from the integration (in finite difference form) of equations (2.4$\alpha$) and (2.5$\alpha$) along the $\alpha$ segment AC. These are supplemented by the geometrical condition $z_C = 0$ and the fact that $\theta_C = \theta_{\text{footing}}$, where $\theta_{\text{footing}}$ is evaluated from one of equations (2.11). Details of the calculation procedure are given below.

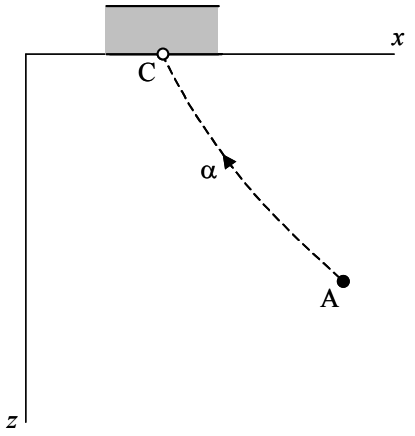


**Figure 2.5** Calculation of new solution point on underside of footing (CalcA)

**CalcA**

In: $[x_A, z_A, \sigma_A, \theta_A]$

Out: $[x_C, z_C, \sigma_C, \theta_C]$

0. Preliminaries.

   Calculate $R_A = c_A \cos\phi + \sigma_A \sin\phi$ (where $c_A = c_0 + kz_A$). Set $\theta_c = \theta_{\text{footing}}$, using equation (2.11s) or (2.11r) as appropriate.

1. Intersect chord AC with footing.

   Solve, cf. equation (2.4α),

$$\left(x_C - x_A\right)\cos\left(\frac{\theta_A + \theta_C}{2} + \varepsilon\right) = \left(z_C - z_A\right)\sin\left(\frac{\theta_A + \theta_C}{2} + \varepsilon\right) \tag{2.16}$$

$$z_C = 0 \tag{2.17}$$

   for $x_C$ and $z_C$.

2. Evaluate $\sigma_C$.

   Noting that $R_C = c_C\cos\phi + \sigma_C\sin\phi$ (where $c_C = c_0$) is a function of $\sigma_C$, solve, cf. equation (2.5α),

$$\sigma_C - \sigma_A + \frac{R_A + R_C}{\cos\phi}\left(\theta_C - \theta_A\right) = \left(-\gamma\tan\phi - k\right)\left(x_C - x_A\right) + \gamma\left(z_C - z_A\right) \tag{2.18}$$

   for $\sigma_C$. Return the solution.

CalcA requires no iteration, so its code is simpler and faster than that of CalcAB. It is, however, called far less frequently.

*2.4.2 Axial symmetry*

For circular footing problems, only (2.13) and (2.18) of the plane strain finite difference equations need to be modified. For example equation (2.13β) becomes, cf. equation (2.8β),

$$\sigma_C - \sigma_B - \frac{R_B + R_C}{\cos\phi}\left(\theta_C - \theta_B\right) = \left(\gamma^*_{x,BC} + \gamma^*_{z,BC}\tan\phi + k\right)\left(x_C - x_B\right) + \left(\gamma^*_{z,BC} - \gamma^*_{x,BC}\tan\phi\right)\left(z_C - z_B\right) \tag{2.19}$$

where, cf. equation (2.9),

$$\begin{aligned}\gamma^*_{x,BC} &= \frac{\left(R_B + R_C\right)\left[\cos\left(\theta_B + \theta_C\right) - 1\right]}{x_B + x_C}\\ \gamma^*_{z,BC} &= \gamma - \frac{\left(R_B + R_C\right)\sin\left(\theta_B + \theta_C\right)}{x_B + x_C}\end{aligned} \tag{2.20}$$

Clearly the computational burden in terms of floating-point operations is significantly higher in axial symmetry than it is in plane strain. This is another reason why it invariably takes ABC somewhat longer to solve a circular footing problem than a comparable strip footing problem.

**2.5 Stress field construction**

*2.5.1 Smooth footings (solution type 1)*

Figure 2.6a shows a completed mesh of characteristics for a smooth strip footing problem. For clarity, very coarse subdivision counts are used for both $d_1$ and the fan zone (5 and 10 respectively). This type of mesh, in which all of the α characteristics proceed to the footing, is referred to in ABC as solution type 1. Note that it is only necessary to calculate half of the stress field, which is symmetric about the *z* axis. Suppose that the mesh has been partially constructed to the stage shown in Figure 2.6b, and that a new α characteristic is to be added. The calculation of solution points proceeds in a clockwise direction, using the finite difference procedures CalcAB and CalcA described in the

(a) Solution type 1 – all α characteristics progress to footing

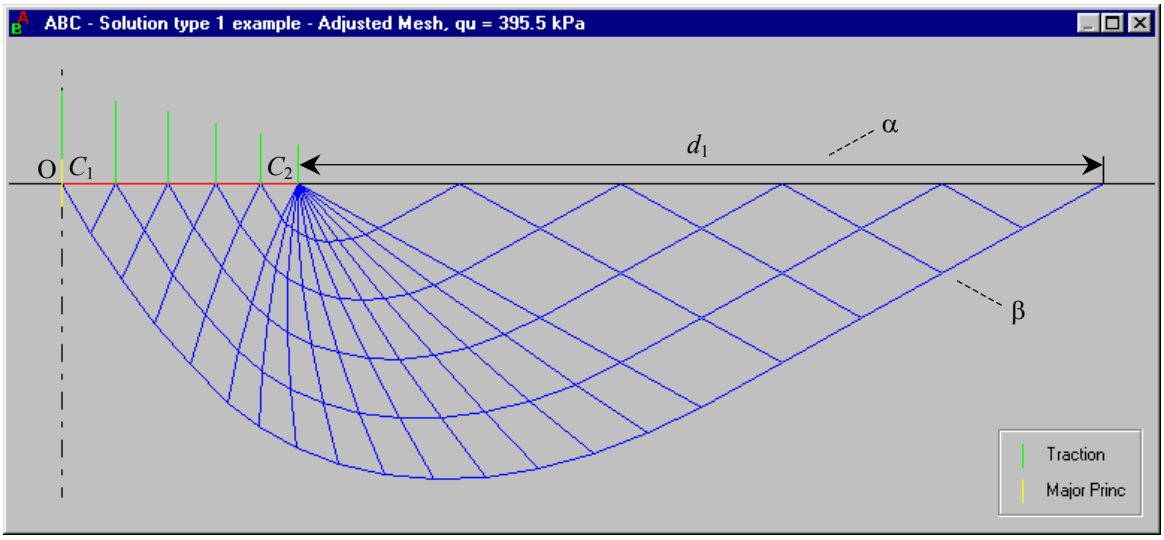


(b) Partway through construction

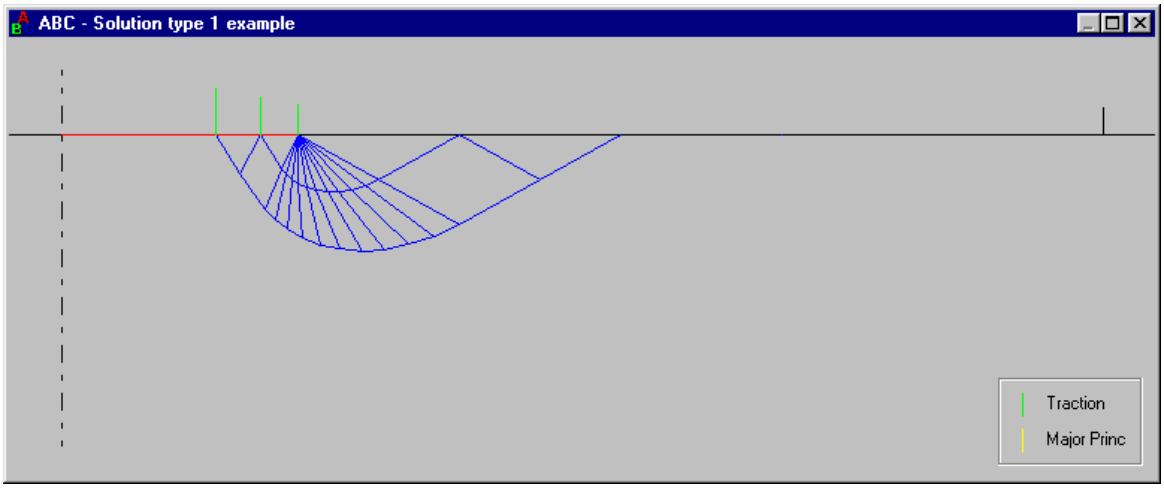


(c) CalcAB

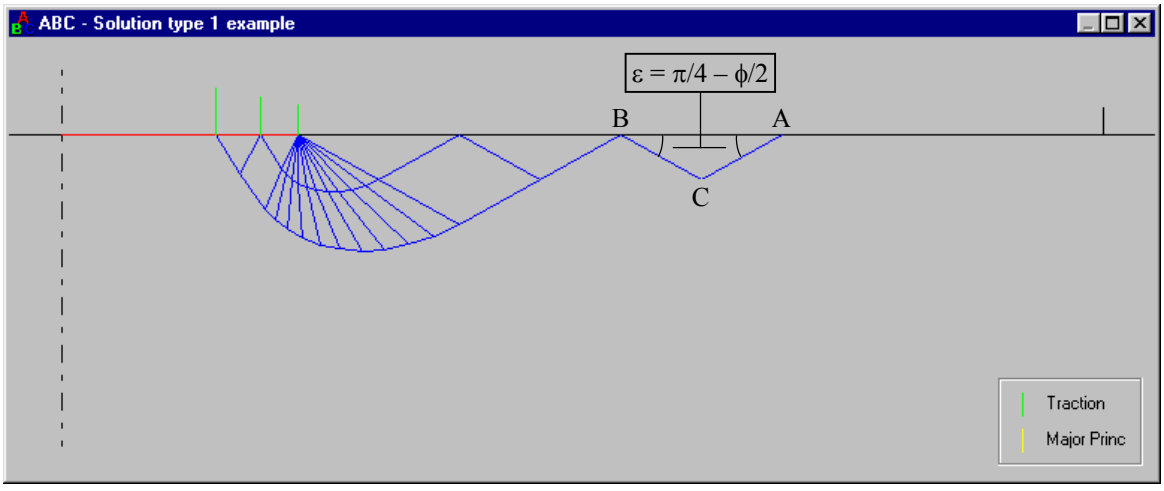

(d) CalcAB

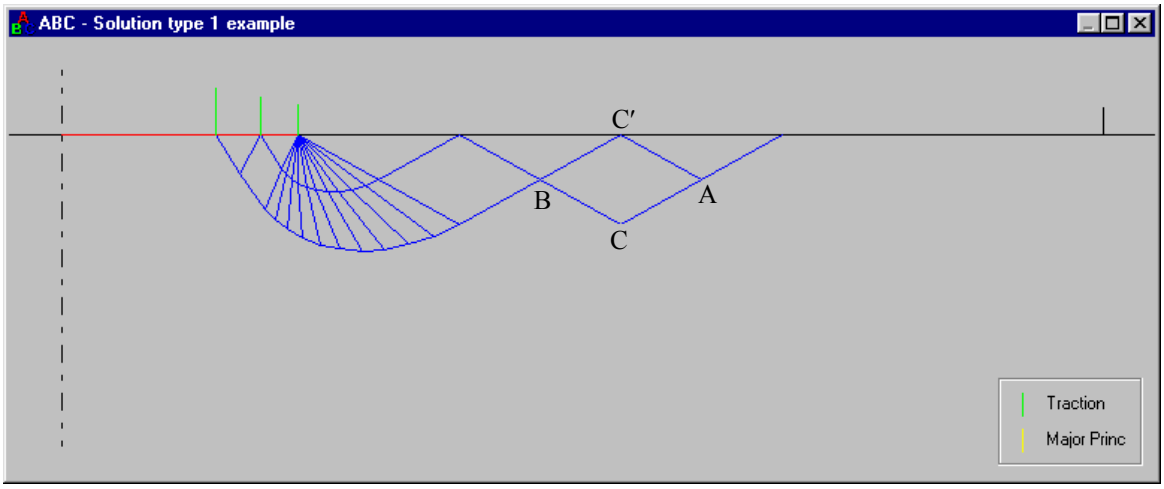


(e) CalcAB

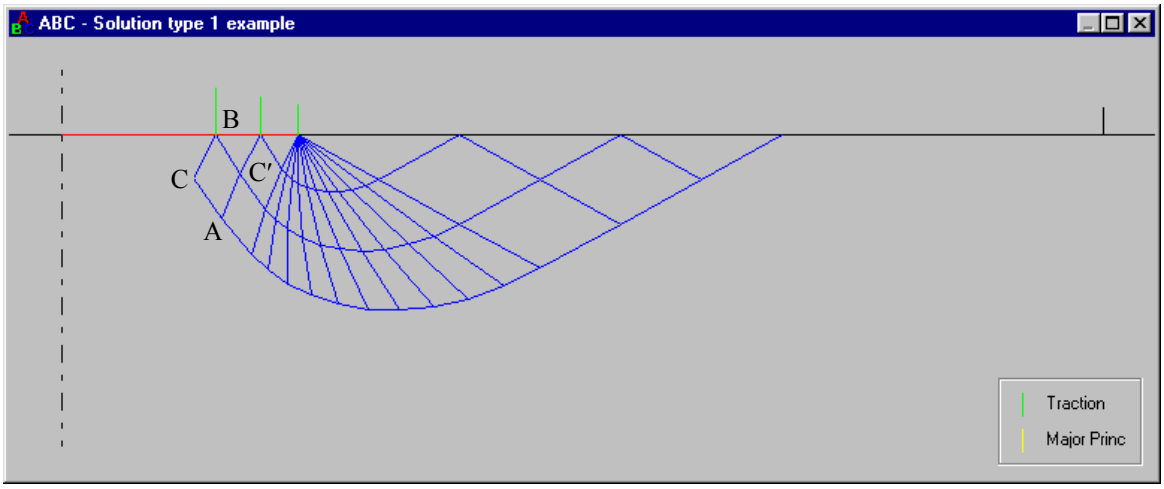


(f) CalcA

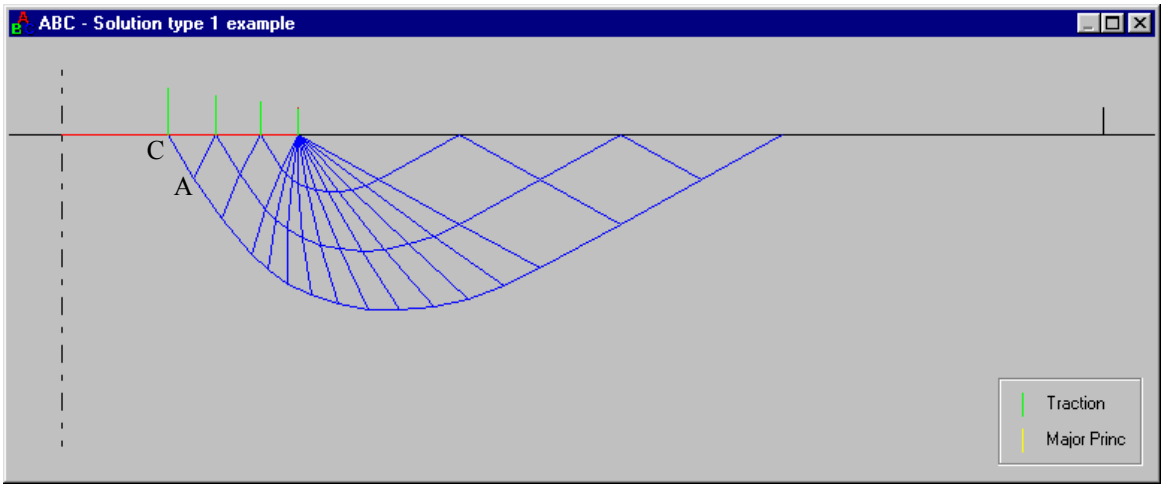


**Figure 2.6** Solution type 1, showing (a) completed mesh; (b)-(f) construction procedure

previous section. Referring to Figure 2.6c, let A denote the first point of the current (i.e. new) α characteristic, and B the first point of the previous α characteristic. The coordinates of A are easily established, while the values of σ and θ at A are obtained from equations (2.10); these are of course identical to σ and θ at B. Propagation of the solution to C, the second point of the current α characteristic, is performed using CalcAB, starting with the following initial approximations:

$$\begin{aligned} \sigma_{\mathrm{C}}^{\mathrm{i}} &= \frac{q + \gamma z_{\mathrm{C}} + c_{\mathrm{C}} \cos\phi}{1 - \sin\phi} \\ \theta_{\mathrm{C}}^{\mathrm{i}} &= \pi/2 \end{aligned} \tag{2.21}$$

where

$$z_{\mathrm{C}} = \frac{x_{\mathrm{A}} - x_{\mathrm{B}}}{2} \cdot \tan\varepsilon \quad \text{and} \quad c_{\mathrm{C}} = c_0 + k z_{\mathrm{C}}$$

The first of equations (2.21) is derived from a passive Mohr's circle construction similar to that in Figure 2.2, but with $c = c_{\mathrm{C}}$ and $\sigma_3 = q + \gamma z_{\mathrm{C}}$. These special initial approximations are actually exact in plane strain, and they provide reasonable starting values in axial symmetry. Figure 2.6d shows the next application of CalcAB. The second point of the current α characteristic (the point C just calculated) is now used as A, and the second point of the previous α characteristic is now used as B. The first point of the previous α characteristic is now available as a known solution point C′ diagonally opposite C (cf. Figure 2.4), so the initial approximations $\sigma_{\mathrm{C}}^{\mathrm{i}}$ and $\theta_{\mathrm{C}}^{\mathrm{i}}$ can be determined from the linear extrapolation equations (2.15). CalcAB is applied in a similar fashion until all of the points on the previous α characteristic have been used up; this is the situation shown in Figure 2.6e. The current α characteristic is then completed by stepping it onto the footing, using a single application of CalcA – see Figures 2.5 and 2.6f. Further α characteristics, in this case only two more, are added until the mesh is complete. The method for choosing $d_1$ correctly, such that the final α characteristic intersects the footing at $x = 0$, is discussed in Section 2.9.

The α characteristic used to initiate the construction is degenerate in the sense that all of its solution points have the same $(x, z)$ coordinates, namely $(B/2, 0)$. Equally spaced θ values are assigned to these solution points, varying from $\pi/2$ at the start of the characteristic to 0 at the end (see equations (2.10) and (2.11s)), and the corresponding σ values can then be worked out. Because $\mathrm{d}x = \mathrm{d}z = 0$ for each of the degenerate α segments between successive solution points, equation (2.5α) simplifies to

$$\mathrm{d}\sigma + \frac{2R}{\cos\phi}\mathrm{d}\theta = 0 \tag{2.22}$$

where $R = c\cos\phi + \sigma\sin\phi$. This same simplification applies to equation (2.8α) in axial symmetry. Now $c = c_0$ because $z = 0$, so

$$\mathrm{d}\sigma + 2\left(c_0 + \sigma\tan\phi\right)\mathrm{d}\theta = 0 \tag{2.23}$$

which after separating variables can readily be integrated to give:

$$\begin{aligned} \sigma &= \sigma_{\text{passive}} + 2c_0\left(\theta_{\text{passive}} - \theta\right) && \text{if } \phi = 0 \\ \sigma &= \left(c_0\cot\phi + \sigma_{\text{passive}}\right) e^{2\tan\phi\left(\theta_{\text{passive}} - \theta\right)} - c_0\cot\phi && \text{if } \phi > 0 \end{aligned} \tag{2.24}$$

Equations (2.24) allow the solution $[x, z, \sigma, \theta]$ at every point on the degenerate α characteristic to be determined analytically, thus providing a 'base' α characteristic from which the rest of the mesh can be built up numerically in the manner described above. Note that the fixed quantities $\sigma_{\text{passive}}$ and $\theta_{\text{passive}}$ are given by equation (2.10).

*2.5.2 Rough footings (solution types 2 and 3)*

When constructing the stress field for a rough footing problem, the symmetry requirement that $\theta = 0$ when $x = 0$ (major principal stress direction = vertical on $z$ axis) means that the fully-mobilised roughness condition of equation (2.11r) and Figure 2.3b cannot apply over the whole of the soil–footing interface. Instead there are two possibilities, and these are shown schematically in Figure 2.7. In solution type 2, full roughness is not mobilised at any point of the interface: no $\alpha$ characteristics progress to the footing, so no $\beta$ characteristics become tangential to it. In solution type 3, full roughness is mobilised on part, but not all, of the interface: there is a defined region $C_2C_3$ (away from the axis of symmetry) where the $\alpha$ characteristics do progress to the footing, spawning $\beta$ characteristics that originate tangentially, as per Figure 2.3b. In both of the rough footing solution types, the bearing capacity can be found without extending the stress field into the blank 'false head' region $OC_1C_2$. As mentioned in Section 1.2, however, an admissible extension into this region (as well as into the soil outside the mesh) is one of the formalities that would need to be completed in order to establish the calculated bearing capacity as a strict (rather than incomplete) lower bound solution.

In many respects, the procedure for constructing a type 2 mesh of characteristics (Figure 2.7a) is similar to that already described for solution type 1, but there are two major differences. First, when establishing the degenerate $\alpha$ characteristic, the final value of $\theta$ is now an angle lying somewhere between the extremes defined by equations (2.11s) and (2.11r). In practice it is simpler to specify the fan aperture $\Theta$, which must (for a valid type 2 solution) lie somewhere between $\pi/2$ and $3\pi/4 + \phi/2$. Second, while the remaining $\alpha$ characteristics are initiated and extended using CalcAB in exactly the same way as before, they are not stepped onto the footing using CalcA. As shown in Figure 2.7a, each new $\alpha$ characteristic is simply terminated in mid-soil when all of the solution points on the previous $\alpha$ characteristic have been exhausted.

In a type 3 solution (Figure 2.7b), the first step in constructing the mesh is to establish the degenerate $\alpha$ characteristic using the rough footing equation (2.11r) to determine the final value of $\theta$. The construction then proceeds in two distinct phases. The first $\alpha$ characteristics to be added, up to and including the one on the $d_1 - d_2$ boundary, resemble those of solution type 1 in that they are stepped onto the footing with a final application of CalcA (noting however that $\theta_{\text{footing}}$ is now obtained from equation (2.11r) rather than (2.11s)). The remaining $\alpha$ characteristics resemble those of solution type 2 – they are terminated in mid-soil without being stepped onto the footing.

The solution type that is applicable to a particular rough footing problem depends on the geometry (plane strain or axial symmetry), the friction angle $\phi$, and the dimensionless ratio

$$F = \frac{kB + \gamma B \tan\phi}{c_0 + q \tan\phi} \tag{2.25}$$

Indeed, as noted by Salençon & Matar (1982a), these three factors control the form and extent of the whole mesh. (Appendix A shows how the governing equations and boundary conditions can all be recast in terms of $\phi$, $F$ and normalised variables alone.) For a given geometry and friction angle, problems with small values of $F$ have solution type 2, and those with large values of $F$ have solution type 3. When $\phi = 0$, the transition from type 2 to type 3 occurs when $F \approx 1.193$ in plane strain, and $F \approx 0.715$ in axial symmetry. The corresponding thresholds when $\phi = 30°$ are about 10.98 and 5.58.

It should be pointed out that the naming of the solution types in ABC is quite arbitrary – there is no generally accepted terminology. For example Davis & Booker (1971, 1973) emphasise the role of the footing breadth $B$, the soil properties and surcharge being assumed given; they therefore refer to solution types 2 and 3 as "narrow rough footing" and "wide rough footing" solutions. Equation (2.25) confirms that, as expected, these terms are consistent with small and large values of $F$.

(a) Solution type 2 – no α characteristics progress to footing

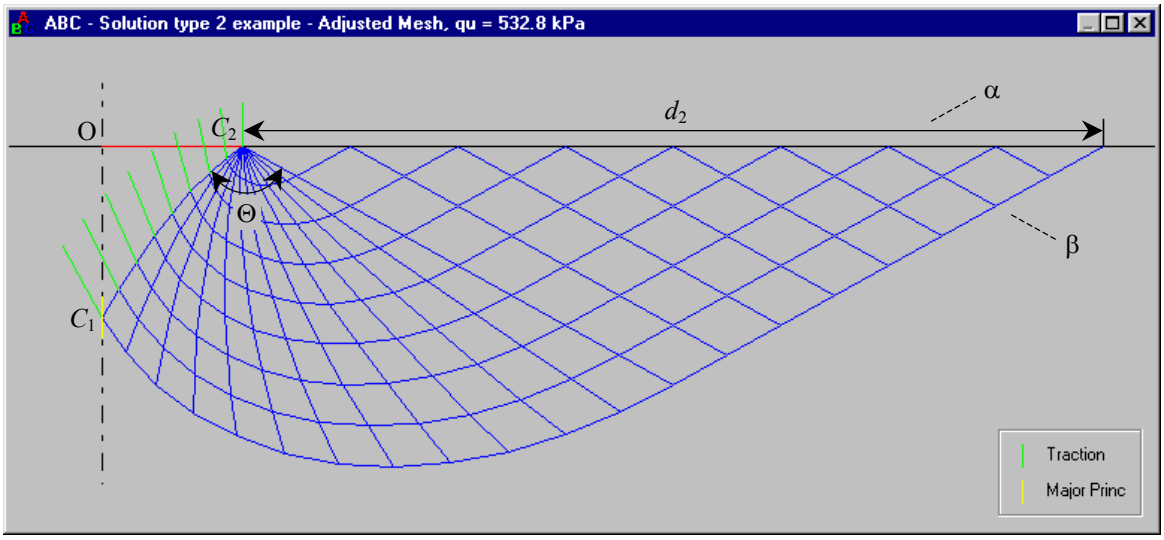


(b) Solution type 3 – some α characteristics progress to footing

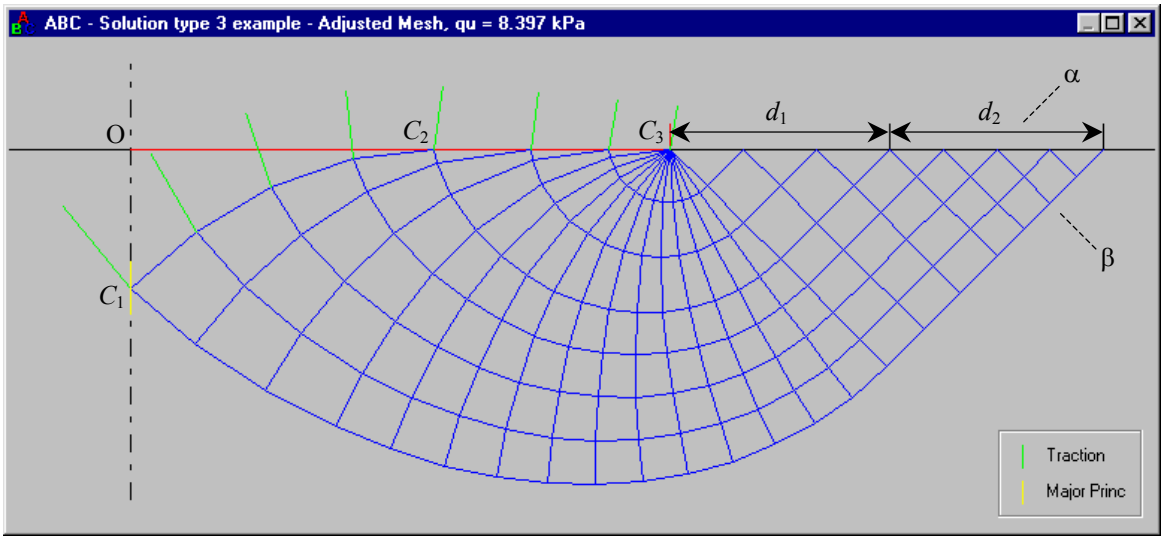


**Figure 2.7** Solution types 2 and 3

### 2.6 Adaptivity

In Figures 2.6 and 2.7, the α characteristics originate at equally spaced intervals along the soil surface. Although this approach is straightforward, it is not always satisfactory. Consider, for example, a smooth strip footing problem with $c_0 = k = 0$, $\phi = 40°$, $\gamma = 20\,\text{kN/m}^3$, $B = 10\,\text{m}$ and $q = 0.1\,\text{kPa}$, such that $F = 2000$ in equation (2.25). Figure 2.8a shows how the use of 20 equally spaced α characteristics gives a mesh in which there is very poor resolution of the stress field near the edge of the footing. In particular, there is a large jump in θ where the first (non-degenerate) α characteristic leaves the fan and steps onto the footing, and this defect is passed 'downstream' to all subsequent α characteristics. Even allowing for the coarseness of the mesh, the calculated bearing capacity is very inaccurate: $q_u = 5.628 \times 10^3$ kPa is 29.6% higher than the converged value of $q_u = 4.344 \times 10^3$ kPa that is obtained (eventually!) when this mesh is refined using **Double Up** (see Section 3.2).

(a) No adaptivity

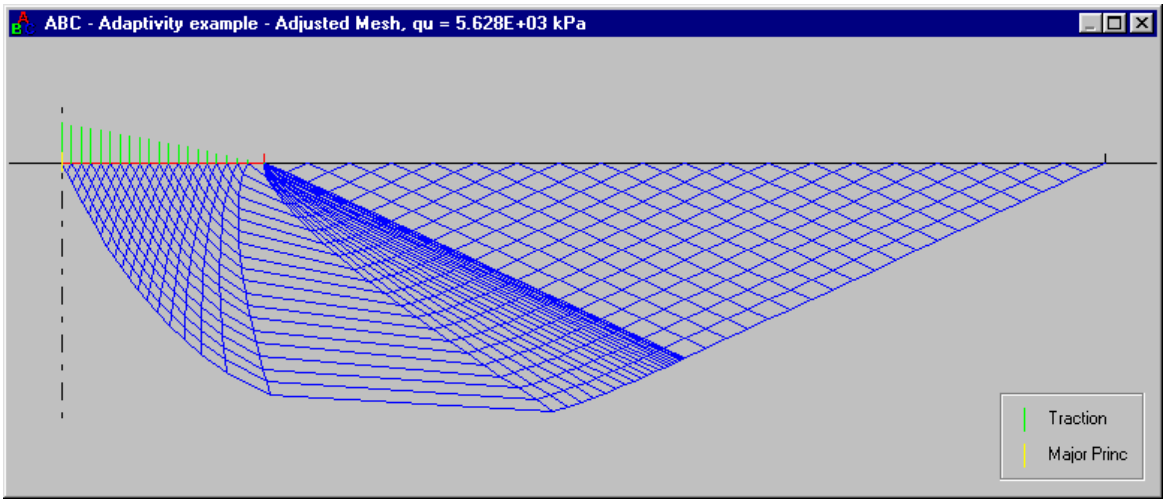


(b) With adaptivity

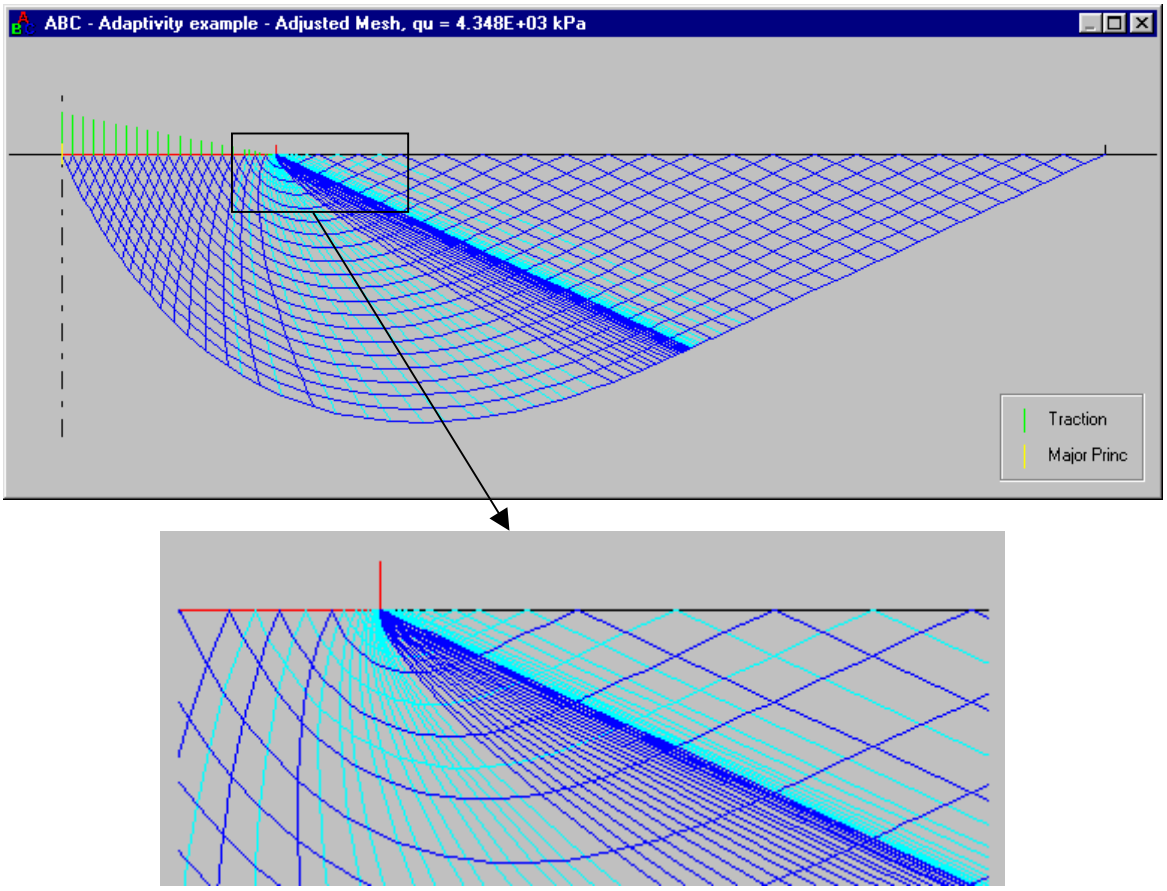


**Figure 2.8** Adaptively-added characteristics

As shown in Figure 2.8b, the quality of the solution can be greatly improved by the tactical insertion of some additional characteristics while the mesh is being constructed. In ABC, a simple recursive subdivision technique (described in more detail below) is used to restrict the jump in θ that can occur

when an α characteristic is stepped onto the footing (i.e. when CalcA is applied). In this example, 15 additional α characteristics have been generated adaptively. These give better resolution of the stress field near the edge of the footing, which in turn leads to better resolution in the 'downstream' region of the mesh that was previously sparse – the extra β characteristics spawned by the extra α characteristics greatly improve the concentration of solution points in this area. As might be expected from a qualitative comparison of Figures 2.8a and 2.8b, the use of adaptivity also gives a dramatic improvement in the accuracy of the calculated bearing capacity: $q_u = 4.348\times10^3$ kPa is just 0.1% above the converged solution obtained with a very fine mesh. This is an excellent result for a mesh with just 35 α characteristics[2]. When the adaptive mesh is refined, only a few applications of **Double Up** are needed for the bearing capacity to stabilise at $q_u = 4.344\times10^3$ kPa.

There is another compelling reason for avoiding a large jump in θ when stepping an α characteristic onto the footing, and this is related to the finite difference approximation employed in CalcA. In plane strain, for example, when equation (2.18) is solved for $\sigma_C$ the result is:

$$\sigma_C = \frac{\sigma_A - \left(\frac{R_A}{\cos\phi} + c_C\right)(\theta_C - \theta_A) + (-\gamma\tan\phi - k)(x_C - x_A) + \gamma(z_C - z_A)}{1 + \tan\phi(\theta_C - \theta_A)} \tag{2.26}$$

This expression is exact when $\theta_A = \theta_C$ $(= \theta_{footing})$, in which case the α segment AC is straight. At the other extreme, the expression becomes singular when $\theta_A - \theta_C = \cot\phi$. To preserve a reasonable degree of accuracy in the finite difference approximation, the jump in θ is restricted according to

$$\theta_A - \theta_C \le \mathrm{MIN}\left(f_{jump}\cdot\cot\phi, \Delta\theta_{lim}\right) \tag{2.27}$$

where $f_{jump}$ and $\Delta\theta_{lim}$ are empirically chosen constants. The values $f_{jump} = 0.1$ and $\Delta\theta_{lim} = \pi/2$ have been found to be suitable in practice; in this case the cutoff $\Delta\theta_{lim}$ governs when φ is less than about 3.6°. The same values are used in both plane strain and axial symmetry.

When stepping an α characteristic onto the footing, CalcA is only invoked if equation (2.27) is satisfied. If the proposed jump in θ is too large, the construction of the current α characteristic is abandoned and a new attempt is made, halving the interval along the soil surface and adding two new equally spaced α characteristics. This strategy is applied recursively. It transpires, however, that if $F = \infty$ in equation (2.25) and φ is greater than a certain threshold (this depends on the footing roughness and the number of fan divisions adopted), no amount of recursive subdivision will allow equation (2.27) to be satisfied. To avoid this numerical difficulty, the maximum value of $F$ is restricted to $10^{12}$ (see Section 3.1). Although this precludes a direct solution of the '$N_\gamma$ problem' in its pure form ($c_0 = k = 0$, $\phi > 0$, $\gamma > 0$, $q = 0$, such that $F = \infty$), the value of $N_\gamma$ for a particular combination of geometry, roughness and friction angle can nevertheless be evaluated to any desired precision by adopting a sufficiently large value of $F$ (which reduces to $\gamma B/q$ in the special case of a cohesionless soil). Experience has shown that to evaluate an $N_\gamma$ factor correct to $n$ significant digits using ABC, a choice of parameters such that $F = 10^{n+2}$ is usually adequate (and $F = 10^{n+3}$ is certainly adequate). Examples are given in Sections 3.3.2, 4.2.7, 4.2.8, 4.3.7 and 4.3.8.

### 2.7 Bias

For any given friction angle φ, bearing capacity analyses using the method of characteristics (or any other numerical method) become progressively more difficult as the dimensionless ratio $F$ in equation (2.25) increases. When φ is greater than about 1°, adaptively-added characteristics can be introduced

[2] Note that a mesh with 35 *equally spaced* α characteristics only gives a modest improvement on the one with 20 equally spaced α characteristics: $q_u = 5.131\times10^3$ kPa which is still 18.1% too high.

(a) $F = 20$ : $d_1/B = 0.1553$ , $d_2/B = 0.0161$

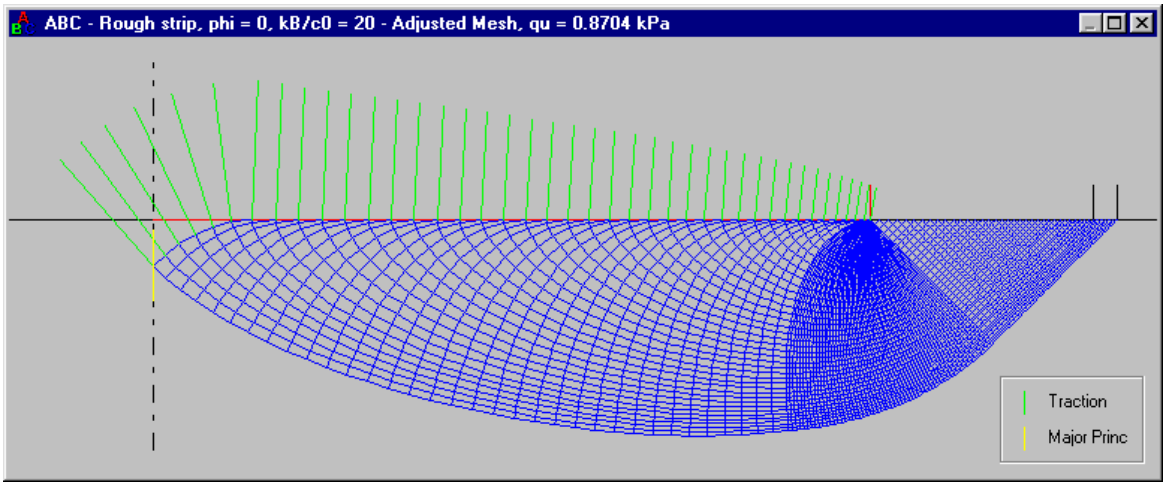


(b) $F = 50$ : $d_1/B = 0.1020$ , $d_2/B = 0.0041$

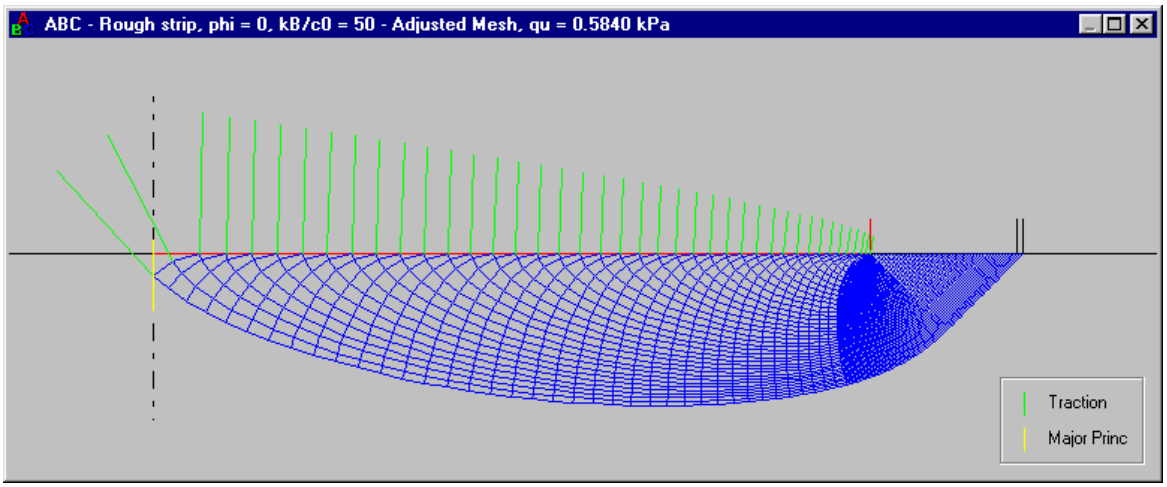


(c) $F = 100$ : $d_1/B = 0.0703$ , $d_2/B = 0.0014$

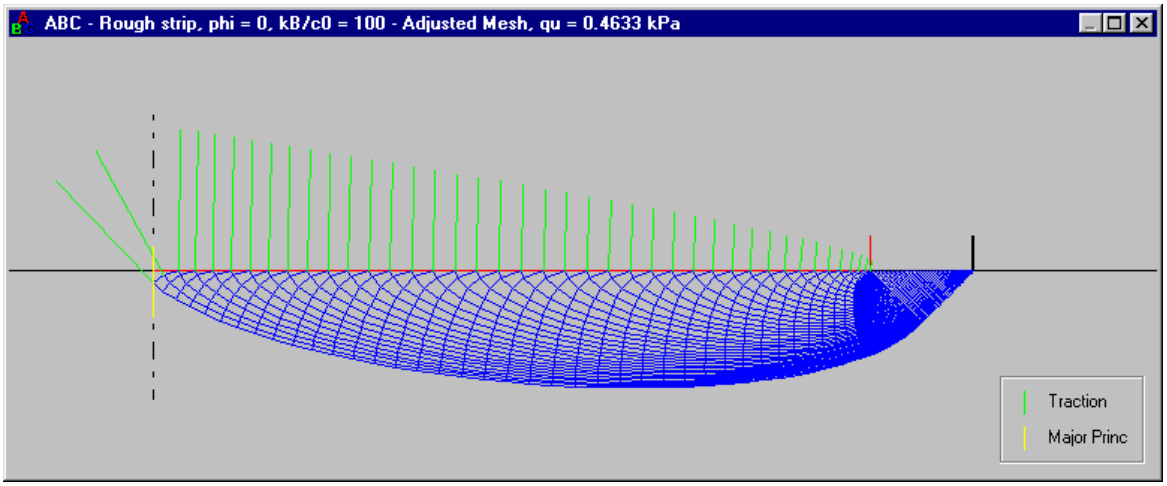


**Figure 2.9** Rough strip footing with $\phi = 0$ and increasing values of $F$ ( $= kB/c_0$ )

to preserve the accuracy and efficiency of the method for large values of *F*, as outlined in the previous section. When $\phi$ is less than about 1°, and in particular when $\phi = 0$, problems of a quite different nature are encountered when *F* becomes large, especially if the footing is rough.

The source of these problems is apparent from Figure 2.9, which shows – for a rough strip footing on purely cohesive soil with $\phi = 0$ – how the mesh of characteristics changes as *F* increases. Note that when $\phi = 0$, *F* reduces to $kB/c_0$, and the form of the mesh is not affected by the unit weight $\gamma$ or the surcharge *q*. These analyses could be reproduced by, for example, fixing $k = 1$ kPa/m, $\phi = 0$, $\gamma = 0$, $B = 1$m and $q = 0$, then choosing suitable values of $c_0$ (0.05, 0.02, 0.01 kPa) to give the desired values of *F* (20, 50, 100). In all cases, solution type 3 is applicable. Figure 2.9 is designed to show that as *F* increases,

- the overall size of the mesh decreases (when $F = \infty$ it degenerates altogether);
- the size of the 'false head' region decreases (again when $F = \infty$ it degenerates altogether).

In terms of the mesh size parameters $d_1$ and $d_2$, although both distances tend to zero as $F \to \infty$, they do so in such a way that the ratio $d_2/d_1$ also tends to zero. The structure of the mesh near the axis of symmetry then becomes extremely sensitive to small variations in $d_1$ and $d_2$, presenting a considerable challenge to both the **Auto Guess** algorithm and the library routine HYBRD that is used to adjust the mesh until it satisfies the symmetry conditions (see Section 2.9)[3].

One way to obtain better resolution near the axis of symmetry is to bias the partitioning of $d_1$ in such a way that the subdivisions near the outside of the mesh are smaller than those near the edge of the footing. This counteracts the tendency of the $\alpha$ characteristics to spread apart as they approach the axis of symmetry, an effect that is most pronounced in axial symmetry when $\phi = 0$ and *F* is large. An example is given in Figure 2.10 (rough circular footing, $\phi = 0$, $F = kB/c_0 = 100$). Figure 2.10a shows the mesh obtained if $d_1$ is partitioned into equal subdivisions. There is poor resolution near the axis of symmetry, and furthermore there is a sharp disparity in size between the final $d_1$ subdivision and the lone $d_2$ subdivision. These factors combine to make the mesh extremely ill-conditioned for the iterative adjustment process described in Section 2.9. Figure 2.10b shows the effect of a simple biasing strategy in which the subdivisions of $d_1$ are arranged in a geometric progression. The result is a mesh with much better resolution near the axis of symmetry, and an inmost cell that is approximately 'square' – a feature that, from a conditioning point of view, is highly desirable in axial symmetry (it is not particularly important in plane strain). A convenient way to specify the degree of bias is via the ratio of the final (i.e. outmost) $d_1$ subdivision to the initial (i.e. inmost) $d_1$ subdivision. In Figure 2.10b this ratio is 0.05; in the plane strain examples of Figure 2.9 the biasing is somewhat milder (ratios 0.5, 0.5, 0.2). When using ABC, the choice of an appropriate bias ratio is handled automatically, as explained in Section 3.3.3.

### 2.8 Sub-subdivisions

When $\phi$ is small (or zero) and *F* is greater than about 100, rough footing problems in both plane strain and axial symmetry have type 3 solutions where $d_2$ can be many orders of magnitude smaller than $d_1$. In these circumstances, the biasing technique described in the previous section is no longer effective on its own – if too many characteristics are concentrated near the perimeter of the mesh, there is a loss of resolution near the edge of the footing.

A more effective approach is to introduce a small number of additional $\alpha$ characteristics as sub-subdivisions of the final (i.e. outmost) $d_1$ subdivision. These can be arranged to provide a smooth transition in spacing between the $d_1$ characteristics and the $d_2$ characteristic(s). To give an example,

[3] Note that in the limiting case of $F = \infty$ there is no need to use ABC at all – there are simple analytical solutions for both strip and circular footings on soil with $\phi = 0$ and $F = \infty$ (see Sections 4.2.5, 4.2.6, 4.3.5 and 4.3.6).

(a) No bias

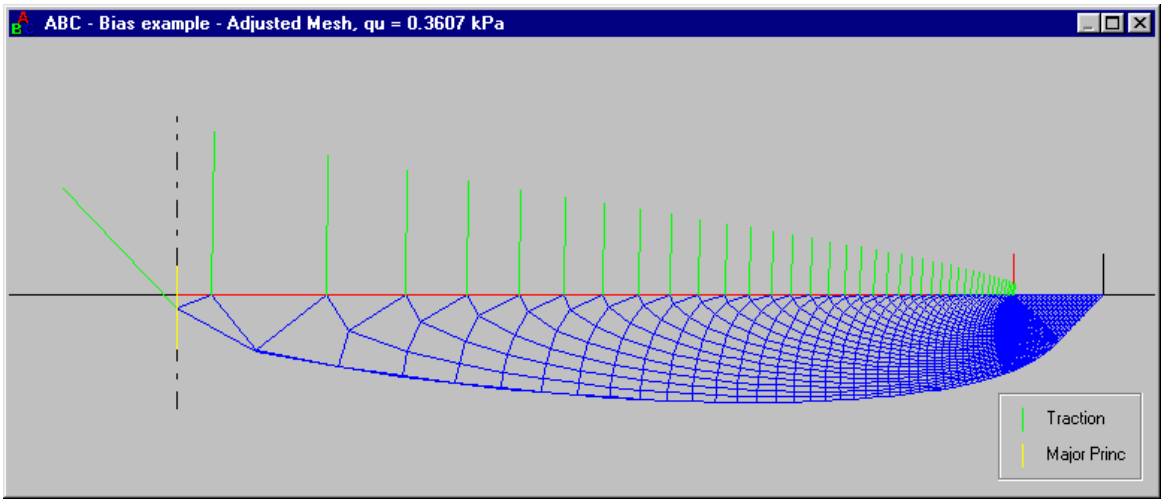


(b) With bias

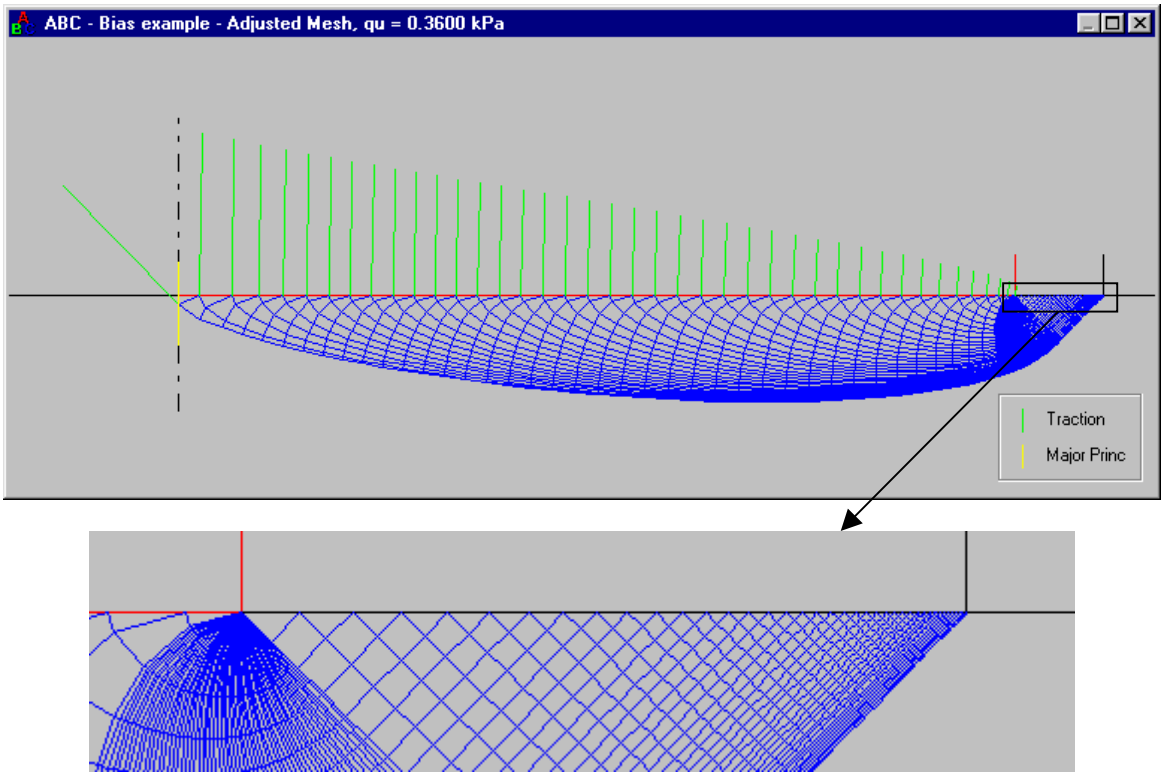


**Figure 2.10** Biasing of $d_1$ subdivisions

consider the problem of a rough circular footing with $\phi = 0$ and $F = kB/c_0 = 500$. Figure 2.11 shows a mesh in which the final $d_1$ subdivision has been partitioned into 6 sub-subdivisions, arranged in a geometric progression to ensure that the size of the final sub-subdivision matches that of the lone $d_2$ subdivision. The use of this special approach allows the problem to be solved with a well-conditioned mesh, even though the 'false head' region is tiny ($d_2$ is over 10000 times smaller than $d_1$). Activation of the sub-subdivision strategy is automatic, as explained in Section 3.3.4.

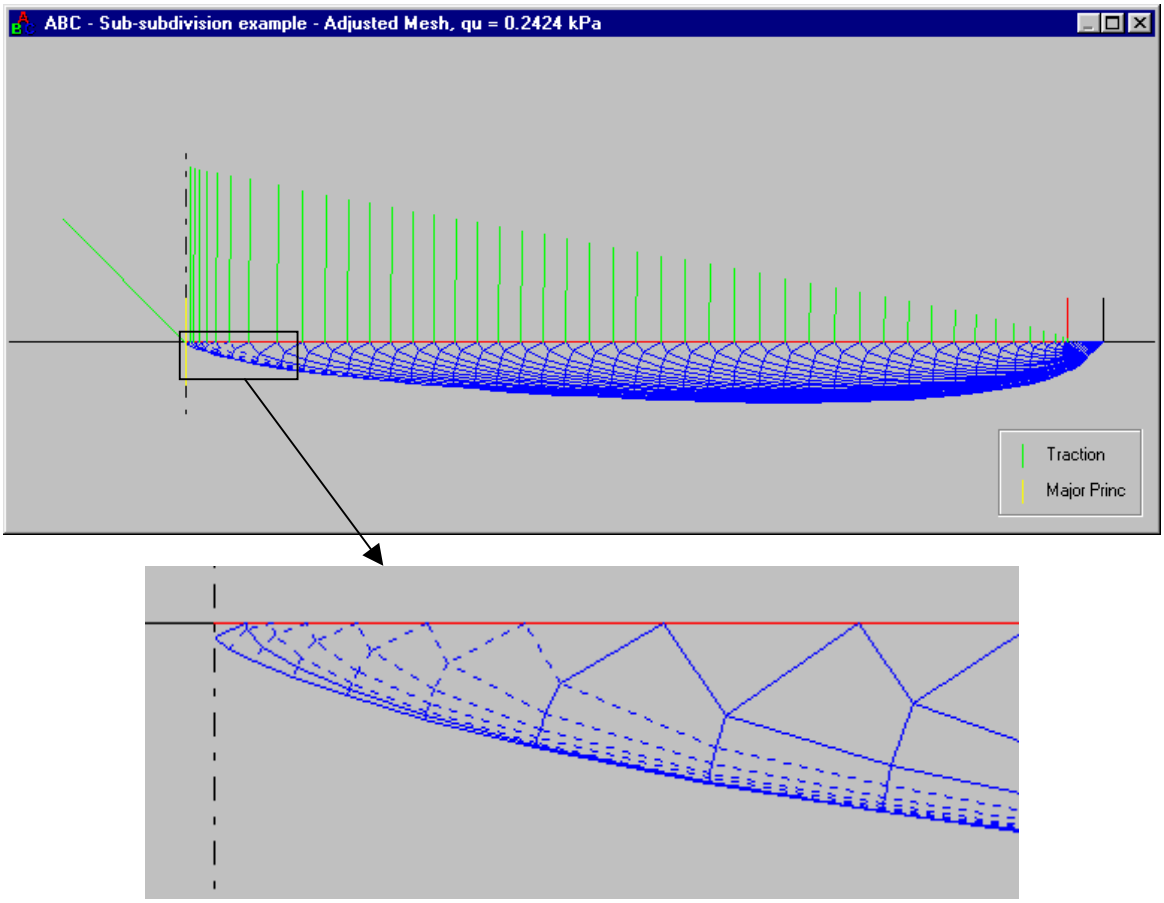


**Figure 2.11** Use of sub-subdivisions when $d_2 << d_1$

### 2.9 Adjustment of mesh size parameters

Once the soil and footing data for a problem have been entered into ABC, the **Auto Guess** facility (Section 3.2) can be used to determine

- the solution type;
- initial estimates of the relevant mesh size parameters ( $d_1$ and/or $d_2$ and/or $\Theta$);
- appropriate subdivision counts for an initial (i.e. fairly coarse) mesh;
- a suitable degree of bias, if any;
- whether sub-subdivisions are required.

These specifications can also be entered manually if desired, though it is anticipated that users will prefer to use **Auto Guess** on most occasions. Various aspects of the algorithm are still being refined, notably the provision of faster initial guesses for difficult rough footing problems where the friction angle $\phi$ and the dimensionless ratio $F$ in equation (2.25) are both large. A description of how **Auto Guess** works will therefore be deferred until the algorithm has stabilised in a future release.

The initial estimates of $d_1$, $d_2$ and $\Theta$ are adjusted using the MINPACK subroutine HYBRD (Moré et al., 1980). This routine implements the hybrid algorithm of Powell (1970), and the source code (in Fortran 77) is freely available from the Netlib repository at www.netlib.org. HYBRD has proven to be extremely robust as a general-purpose code for the solution of nonlinear equations, even when analytical derivatives are unavailable (clearly the case here) or when non-smooth behaviour is

encountered during the iterations (often an issue in axial symmetry – see below). As an indication of its enduring popularity, HYBRD still forms the core of the nonlinear equation solvers in many commercial subroutine libraries, including NAG and IMSL. As already noted, HYBRD is used elsewhere in ABC as a back-up strategy in CalcAB (see Section 2.4).

In a smooth footing problem (solution type 1, Figure 2.6a) there is only one mesh size parameter to be adjusted, namely $d_1$. The adjustment is iterative, and continues until the $x$ coordinate of $C_1$, the inmost solution point of the mesh, is approximately zero. Each iteration involves recalculation of the whole mesh for a different value of $d_1$, and although this is clearly inefficient[4], it is consistent with the approach used for solution types 2 and 3. The adjustment of a type 1 mesh can be viewed as the numerical solution of one nonlinear equation ($x_{\text{misclose}} = 0$) in one unknown ($d_1$). Note that there is no need to enforce explicitly the symmetry requirement that $\theta = 0$ when $x = 0$, since $\theta$ is automatically zero at all solution points on the smooth interface.

In a rough footing problem there are two mesh size parameters to be adjusted, either $d_2$ and $\Theta$ (solution type 2, Figure 2.7a) or $d_1$ and $d_2$ (solution type 3, Figure 2.7b). Again the adjustment is iterative, continuing until the conditions $x = 0$ and $\theta = 0$ are satisfied (approximately) at the inmost solution point $C_1$. Each iteration involves global recalculation of the mesh, and although this is computationally arduous, it does have the advantage of simplicity. (Schemes that use local iteration or interpolation to locate the inmost point are difficult to implement in axial symmetry as meshes that cross into the 'negative radius' region $x < 0$ are vulnerable to numerical instability, and in any case give results that have no physical meaning.) The adjustment of a type 2 or type 3 mesh can be viewed as the numerical solution of two nonlinear equations ($x_{\text{misclose}} = 0$, $\theta_{\text{misclose}} = 0$) in two unknowns.

It is obviously harder to solve a pair of nonlinear equations than a single one, and the degree of nonlinearity is much greater in axial symmetry than it is in plane strain. A further complication in axial symmetry is the need for special procedures to abandon and recover from iterations where the mesh of characteristics, if continued, would have entered the region $x < 0$. All of these factors influence the time that it takes for ABC to reach a converged solution. In crude terms, the relative difficulty of adjusting the mesh size parameters can be summarised as follows:

| | Smooth | Rough |
|---|---|---|
| Strip | Easy | Medium |
| Circular | Medium | Hard |

## 2.10 Calculation of bearing capacity

The bearing capacity is integrated over a curve $C$ that connects the endpoints of the $\alpha$ characteristics. For rough footings (solution types 2 and 3), the weight of the soil within the 'false head' region must be deducted to obtain the net bearing capacity available to the foundation. This is the purpose of the terms involving $\gamma$ in the line integrals

$$\begin{aligned} Q_u &= 2\oint_C \sigma_{zz}\mathrm{d}x - \tau_{xz}\mathrm{d}z - \gamma z\mathrm{d}x && \text{plane strain} \\ Q_u &= 2\pi\oint_C \sigma_{zz}x\mathrm{d}x - \tau_{xz}x\mathrm{d}z - \gamma z x\mathrm{d}x && \text{axial symmetry} \end{aligned} \tag{2.28}$$

Integration is performed using the trapezoidal rule. With the solution $[x, z, \sigma, \theta]$ known at each point on $C$, it is easy to recover the stresses $\sigma_{zz}$ and $\tau_{xz}$ using equations (2.1), (2.2) and (2.3)/(2.6). In

[4] Once $d_1$ is known approximately, it is more efficient to apply the iterative recalculation to just the final (i.e. outmost) $\alpha$ characteristic.

equation (2.28) it is assumed that $C$ is traversed in an outward direction, starting from the axis of symmetry and finishing at the edge of the footing, so that $\mathrm{d}x > 0$ and $\mathrm{d}z \le 0$ for all panels of the trapezoidal integration. To clarify, $C = C_1 \to C_2$ in Figure 2.6a, $C = C_1 \to C_2$ in Figure 2.7a and $C = C_1 \to C_2 \to C_3$ in Figure 2.7b.

At each solution point on $C$, the components of the traction vector $T$ (as plotted in green by ABC) are calculated from

$$\begin{bmatrix} T_x \\ T_z \end{bmatrix} = \begin{bmatrix} \sigma_{xx} & \tau_{xz} \\ \tau_{xz} & \sigma_{zz} \end{bmatrix} \begin{bmatrix} n_x \\ n_z \end{bmatrix} \tag{2.29}$$

where, since compression is positive, $n_x$ and $n_z$ are the components of the unit *inward* normal to the soil beneath $C$. The integrals in equation (2.28) are based on the fact that:

$$\oint_C T_z \mathrm{d}s = \oint_C \left( \tau_{xz} n_x + \sigma_{zz} n_z \right) \mathrm{d}s = \oint_C \sigma_{zz} \mathrm{d}x - \tau_{xz} \mathrm{d}z \tag{2.30}$$

While this is not the only way to calculate the bearing capacity (see, for example, the elegant method of Salençon & Matar, 1982a), it is convenient in ABC because the solution points on $C$ are stored for drawing purposes, and hence are readily available.

### 2.11 Implementation details

| | |
|---|---|
| Front end (abc.exe): | Microsoft Visual Basic v6.0 |
| Back end (abc.dll): | Compaq Visual Fortran v6.6 |
| Tested on: | Microsoft Windows 98, 2000, XP Pro |

Dynamically allocated arrays are used extensively; generally speaking these are allocated in the front end and passed by reference to the back end, where they are filled with data. On returning to the front end, therefore, the arrays are instantly available for drawing the mesh and printing the text output. The use of temporary disk files to transfer the data would be much slower.

In 'full mesh' mode, array space is allocated for every solution point, so that the complete mesh of characteristics can be drawn. In 'outline' mode, memory is conserved by only allocating enough space to hold the longest two $\alpha$ characteristics[5], plus the solution points on curve $C$ (Figures 2.6, 2.7; Section 2.10). When using **Double Up**, the cost of drawing the full mesh quickly becomes prohibitive, so outline mode is automatically activated once a certain (user-defined) number of $\alpha$ characteristics is reached.

During the adjustment of the mesh size parameters (Section 2.9), a callback to the front end is made after each iteration (Etzel & Dickinson, 1999). This is used to display the progress of the solution, and to check whether the user has cancelled the calculation (see Section 3.2).

[5] The mesh is built up using a leapfrogging approach, storing only the current and most recent characteristics.

## 3. USING ABC

### 3.1 Specifying a problem

When the program is started a disclaimer appears, followed by the main form:

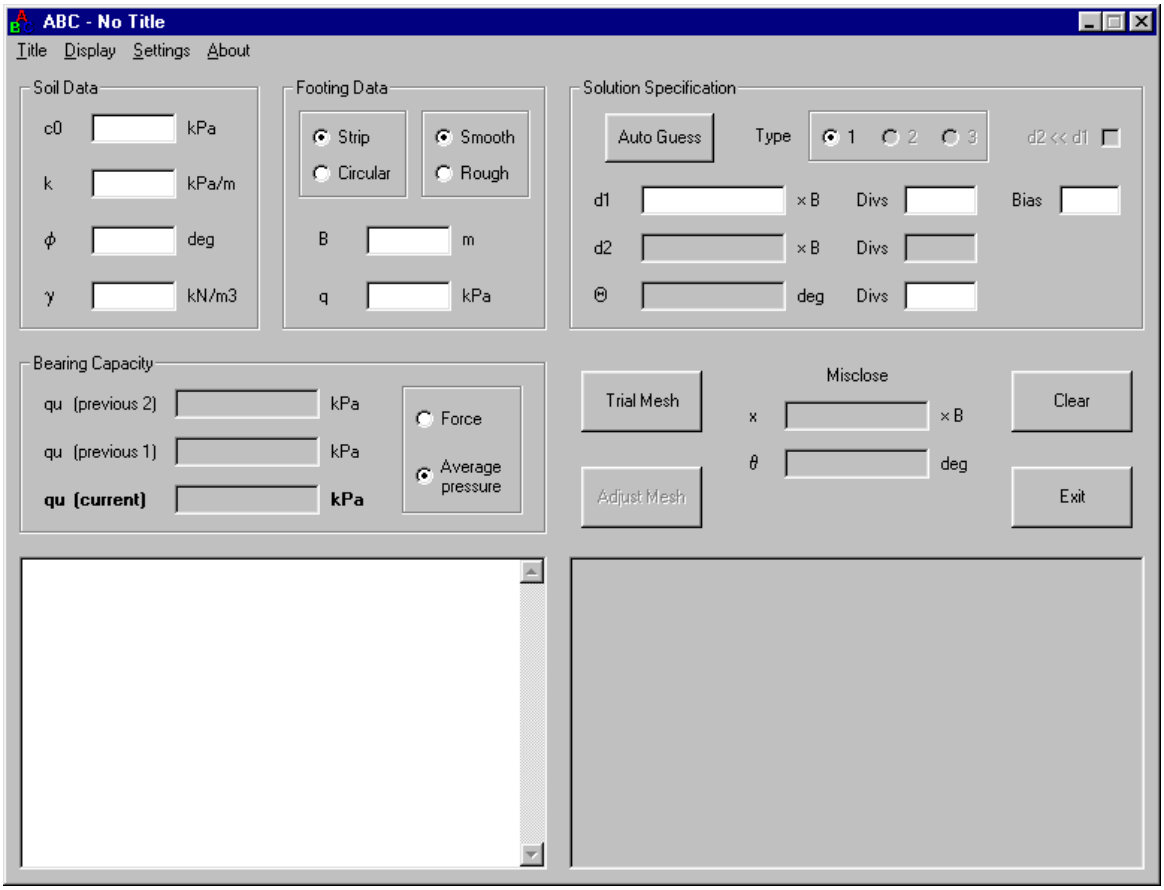


Soil properties are entered in the *Soil Data* frame:

| | | |
|---|---|---|
| $c_0$ | Cohesion at footing level | $\geq 0$ |
| $k$ | Rate of increase of cohesion with depth | $\geq 0$ |
| $\phi$ | Friction angle | $\geq 0$, $\leq 60°$ |
| $\gamma$ | Unit weight | $\geq 0$ |

Footing properties are entered in the *Footing Data* frame:

| | | |
|---|---|---|
| | Geometry – plane strain or axial symmetry | |
| | Roughness – smooth or rough | |
| $B$ | Width of strip, or diameter of circle | $> 0$ |
| $q$ | Surcharge pressure at footing level | $\geq 0$ |

At least one of $c_0$, $k$ and $\phi$ must be non-zero[1]. Also, the dimensionless ratio

$$F = \frac{kB + \gamma B \tan\phi}{c_0 + q\tan\phi} \tag{3.1}$$

[1] Otherwise the soil has no shear strength!

is subject to various restrictions. It must be defined (not $0/0$), and must satisfy:

$$\begin{aligned} F &\le 10^3 \qquad \text{if } \phi < 1° \\ F &\le 10^{12} \qquad \text{if } \phi \ge 1° \end{aligned} \tag{3.2}$$

These restrictions only come into play for certain problems of theoretical interest, such the evaluation of the bearing capacity factor $N_\gamma$; practical problems have $F$ values that fall well within the permitted limits. The reasons for the somewhat arbitrary choices of $10^3$ and $10^{12}$ are discussed later in the chapter (see also Sections 2.6, 2.7 and 2.8).

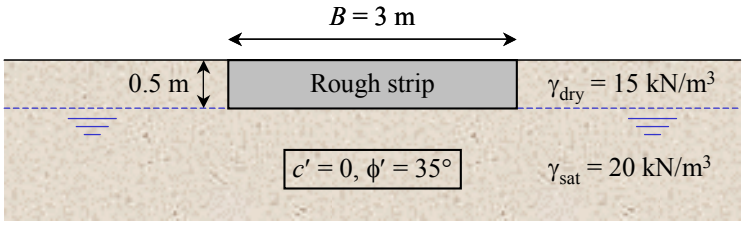


**Figure 3.1** Example problem with self-weight and surcharge

Consider the drained bearing capacity problem shown in Figure 3.1. Drained analysis is performed in terms of effective stresses, so because the soil below footing level is saturated, $\gamma$ must be taken as the *effective* unit weight $\gamma'$. On the other hand the overburden soil is dry, so the effective surcharge is equal to the total surcharge. The numerical data are: $c_0 = k = 0$, $\phi = 35°$, $\gamma = 20 - 9.8 = 10.2$ kN/m$^3$, $B = 3$ m and $q = 15 \times 0.5 = 7.5$ kPa. Since the geometry is plane strain and the footing is rough, the problem is entered into ABC as follows (note that if a field is left blank, that entry is taken to be zero):

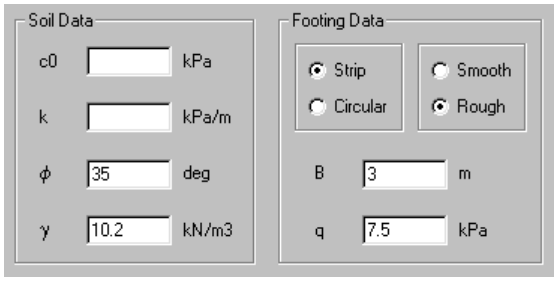


### 3.2 Analysing a problem

The example above will be used to illustrate the usual semi-automated solution procedure. Further examples, including one requiring user intervention, are given in Section 3.3.

Having entered the soil and footing data, clicking on the **Auto Guess** button causes the fields in the *Solution Specification* frame to be filled in automatically:

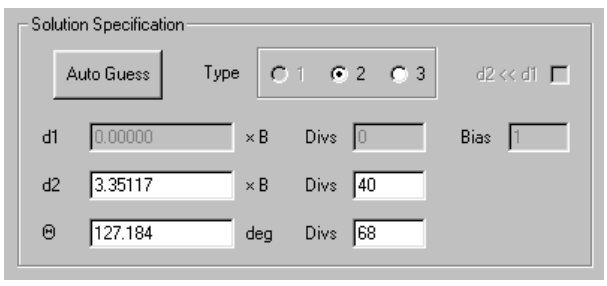

**Auto Guess** has determined that the problem requires a type 2 solution, with estimated values for $d_2$ and Θ as shown (the terminology is defined in Figure 2.7a). All of the fields related to $d_1$ are greyed out, because no α characteristics progress to the footing in solution type 2. The subdivision counts suggested by **Auto Guess** are appropriate for a fairly coarse initial mesh that will subsequently be refined in the manner described below. These counts can of course be overridden, e.g. if producing schematic diagrams like those in Figure 2.7, it is better to use even fewer subdivisions.

The next step is to click on the **Trial Mesh** button, which constructs the initial mesh of characteristics and displays it in the thumbnail drawing window. The main form then looks like:

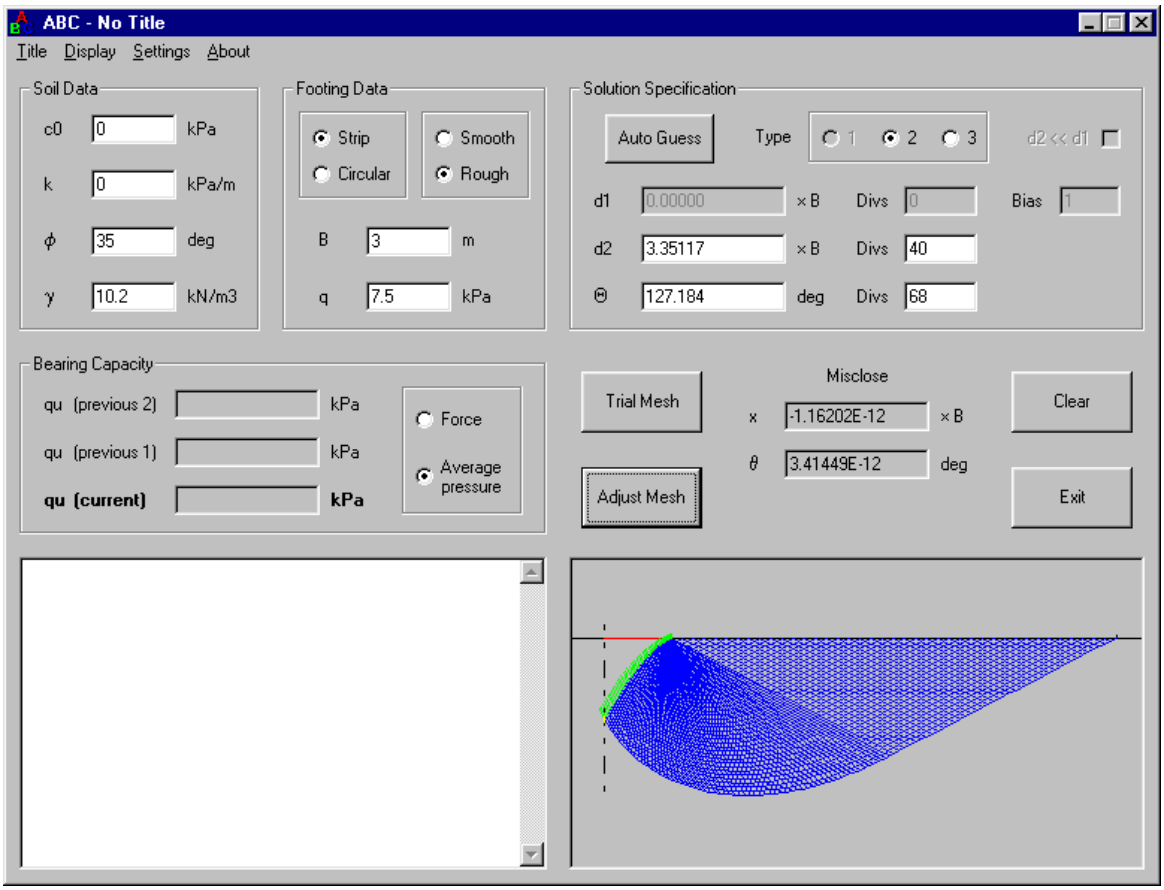


Notice how:

- the $x$ and θ miscloses at the inmost solution point (see Figure 2.1 for the definitions of $x$ and θ) are very small, indicating that the **Auto Guess** estimates of $d_2$ and Θ are accurate;
- no bearing capacity has been calculated;
- no text output has been generated.

Clicking on the **Adjust Mesh** button causes the iterative adjustment of the mesh size parameters (Section 2.9) to commence. After each iteration, the current values of $d_2$, Θ and the two miscloses are displayed, and the thumbnail drawing is updated. For speed, only the outline of the mesh is drawn at each update, but this is sufficient for monitoring the progress of the solution. During the iterations, the **Adjust Mesh** button becomes a **Cancel** button, allowing the calculation to be terminated (at the end of the current iteration) if needed. When the iterative adjustment has finished, the main form should resemble[2]:

[2] Some of the output values (notably the miscloses) may not be identical to those shown, because floating-point arithmetic is processor-dependent. All of the examples in this manual were run on a Pentium III machine.

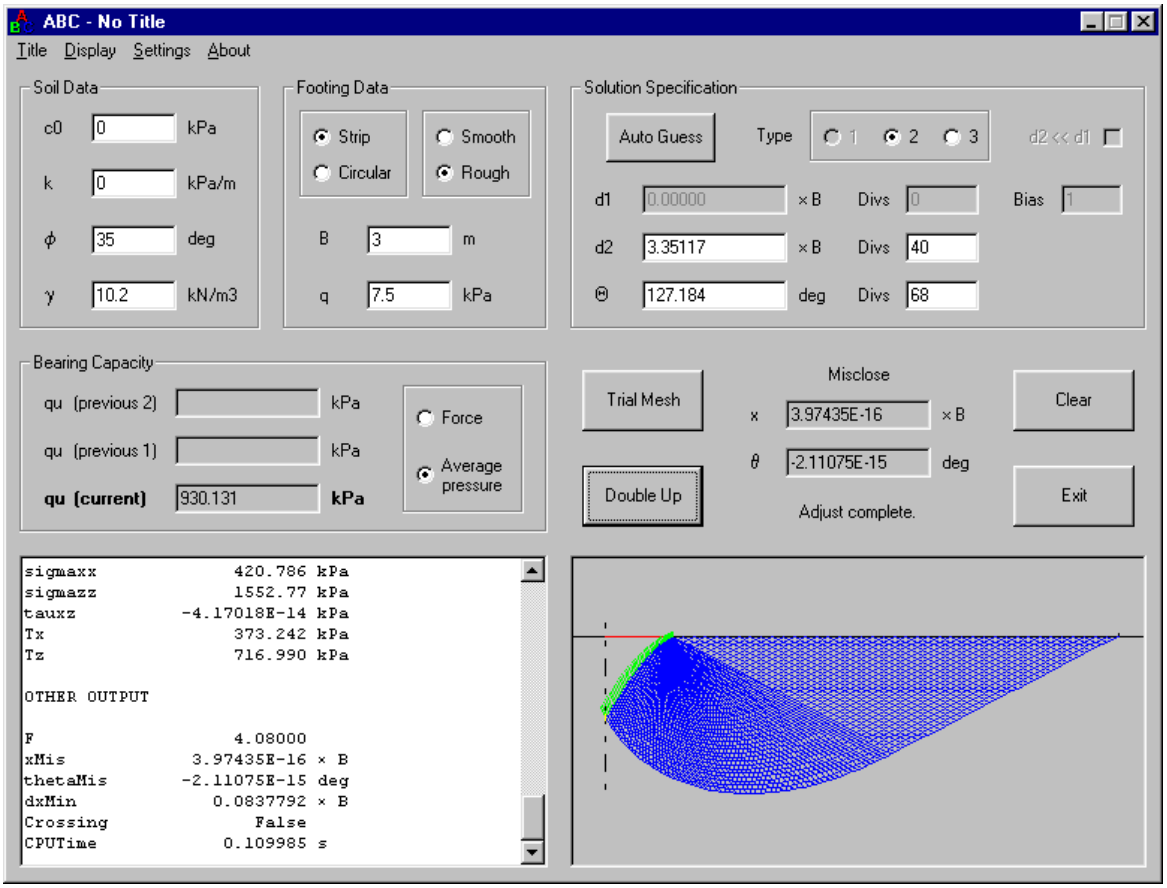


Notice how:

- the *x* and θ miscloses are, to all intents and purposes, zero;
- the bearing capacity has been calculated and displayed;
- text output has been generated.

The thumbnail drawing can be expanded by double-clicking on it, or by right-clicking on it and selecting *Expand*. The expanded drawing initially occupies the full screen, but the window may be resized and repositioned if desired; it will subsequently reappear in the same position. To close the expanded drawing, click on the × control or right-click on the drawing and select *Reduce*. Right-clicking on the drawing (whether thumbnail or expanded) and selecting *Settings* brings up a form that allows certain aspects of the drawing to be customised. For example, unchecking *Inmost solution point only* causes major principal stresses to be plotted throughout the mesh.

By default, the bearing capacity is displayed as an average pressure $q_u$, but it can also be displayed as a force $Q_u$ (per unit run in the case of a strip footing). These modes can be toggled at any time by selecting the appropriate button. The text output can either be viewed *in situ* using the scroll bar, or copied and pasted into another application, should a record of the analysis be required (use the right mouse button to *Select All* and *Copy*). Section 3.5 gives a key to the abbreviations used in the text output. At present there is no facility to save input or output data directly from ABC – in fact the program makes no use of disk files at all, not even temporary scratch files.

The final stage of the solution process is to refine the mesh until the calculated bearing capacity converges. While this can be achieved manually by increasing the subdivision counts in the *Solution Specification* frame and repeating the **Trial Mesh**, **Adjust Mesh** procedure outlined above, it is simpler to make use of the **Double Up** facility. Each time the **Double Up** button is clicked, all active subdivision counts are doubled, and a new adjustment of the active mesh size parameters (in this case

$d_2$ and Θ) begins, taking the converged values from the previous mesh as initial estimates. After two **Double Up**s of the initial solution, the main form looks like:

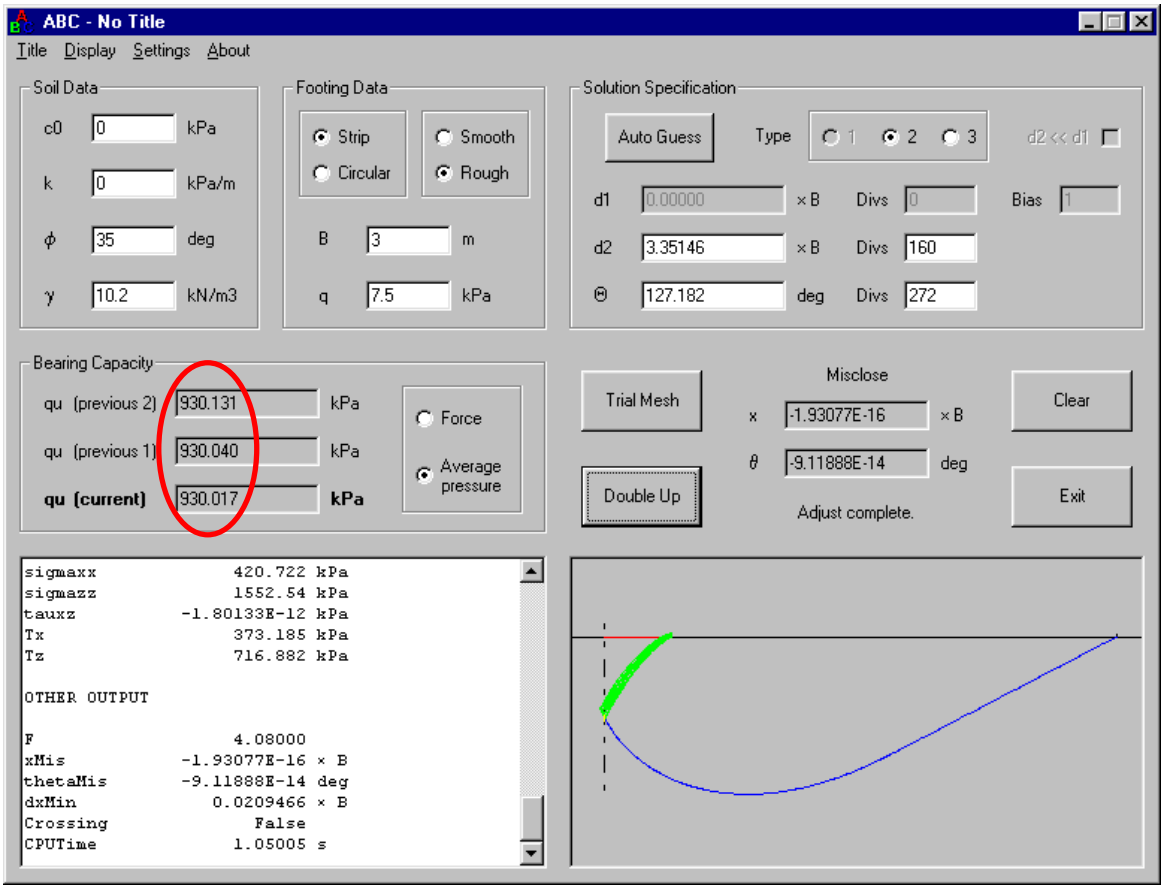


The bearing capacity $q_u$ is evidently converging from above (930.131, 930.040, 930.017 kPa). With further (optional) **Double Up**s the bearing capacity converges to 930.009 kPa, and the mesh size parameters $d_2$ and Θ also approach stable values. Note how, once a specified number of subdivisions has been reached, only the outline of the mesh is stored and drawn – see Sections 2.11 and 3.4.6.

In principle, there is no restriction on the number of **Double Up**s that can be executed. The main practical limit is that each one typically takes three to four times longer than its predecessor, though for most problems the convergence of the calculated bearing capacity is sufficiently rapid that several digits of precision can be achieved within seconds, as in the example above. This is more than adequate for practical purposes, but it is sometimes desirable to obtain results to a higher precision, e.g. in theoretical studies or benchmarking exercises. Another potential limitation when using **Double Up** is that each successive analysis requires more memory, though the allocations required are moderate once the program has entered the 'outline' mode referred to in the previous paragraph.

## 3.3 Further examples

### *3.3.1 Convergence behaviour*

As discussed in Section 2.9, the computational cost of obtaining a converged solution is higher in axial symmetry than in plane strain, and higher for rough footings than for smooth ones. This can be illustrated by re-running the example from the previous section for all four combinations of geometry and roughness. The convergence histories are tabulated below. Each entry shows the calculated bearing capacity $q_u$ (in kPa), with the associated CPU time (in seconds) in brackets.

| | Smooth strip | Rough strip | Smooth circle | Rough circle |
|---|---|---|---|---|
| **Adjust Mesh** | 619.840 (0.1) | 930.131 (0.1) | 838.772 (0.1) | 1449.10 (0.1) |
| **Double Up 1** | 619.711 (0.2) | 930.040 (0.3) | 838.934 (0.6) | 1449.37 (1.2) |
| **Double Up 2** | 619.679 (0.5) | 930.017 (0.8) | 838.986 (1.9) | 1449.46 (3.8) |
| **Double Up 3** | 619.670 (1.9) | 930.011 (2.6) | 839.003 (7.1) | 1449.50 (13.3) |
| **Double Up 4** | 619.668 (7.3) | 930.009 (10.4) | 839.007 (15.8) | 1449.51 (48.6) |
| **Double Up 5** | 619.668 (25.8) | 930.009 (35.2) | 839.009 (51.9) | 1449.51 (102.4) |

The comparative timings for the different classes of problem are reasonably typical. The initial **Adjust Mesh** is always quite fast, but only because most of the necessary work has been done in **Auto Guess**. In all of these examples the bearing capacity converges monotonically, but this is not always the case. Consider the smooth circular footing problem with $B$ modified to 1 m:

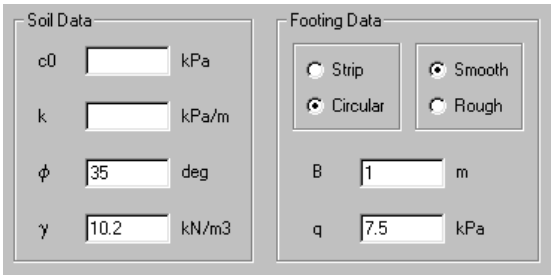


| | |
|---|---|
| **Adjust Mesh** | 597.628 (0.1) |
| **Double Up 1** | 597.598 (0.6) |
| **Double Up 2** | 597.596 (1.9) |
| **Double Up 3** | 597.598 (7.0) |
| **Double Up 4** | 597.598 (15.6) |
| **Double Up 5** | 597.599 (50.5) |

It is clear that if high-precision results are required, a degree of caution is necessary. In particular, even if two successive **Double Up**s give identical bearing capacities, this does not necessarily indicate convergence; this is why the latest *three* bearing capacities are displayed in the main form. Although the **Double Up** process might seem an obvious candidate for Richardson extrapolation (forecasting the final result based on estimates obtained with stepsizes 4$h$, 2$h$ and $h$), this technique can only be applied if the convergence is strictly monotonic, so it is not entirely suitable for use in ABC.

### *3.3.2 Problems requiring adaptivity*

The drained '$N_\gamma$ problem' in Figure 3.2 will be used to illustrate a solution in which additional characteristics are introduced adaptively (see Section 2.6). A literal specification of the input data, i.e.

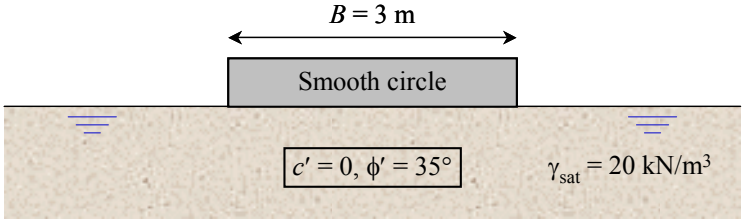


**Figure 3.2** Example problem requiring adaptivity

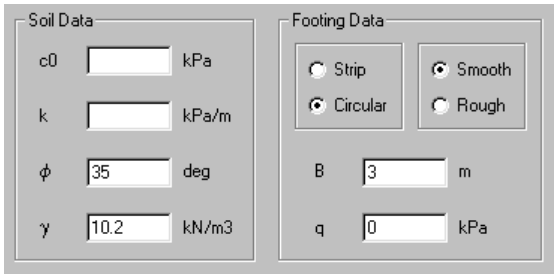


results in an error message when **Auto Guess** is attempted:

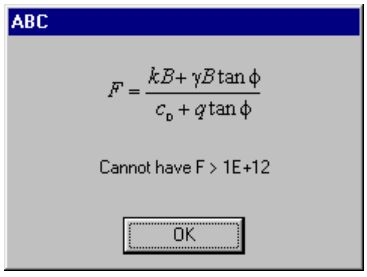


Because $c_0 + q\tan\phi = 0$, the dimensionless ratio $F$ in equation (3.1) is infinite, violating the restriction $F \le 10^{12}$ in equation (3.2b). To analyse the example using ABC it is first necessary to introduce a nominal surcharge, e.g. $q = 10^{-9}$ kPa which gives a large but legal $F = 3.1\times10^{10}$ (alternatively a nominal cohesion $c_0$ can be introduced). This tiny surcharge, corresponding to an embedment of just $10^{-10}$ m in the saturated soil, has a negligible effect on the bearing capacity (this is shown below), but it prevents the potential numerical difficulty described in the final paragraph of Section 2.6.

After revising the entry for $q$ to be 1e-9, clicking on **Auto Guess** and then **Trial Mesh** results in:

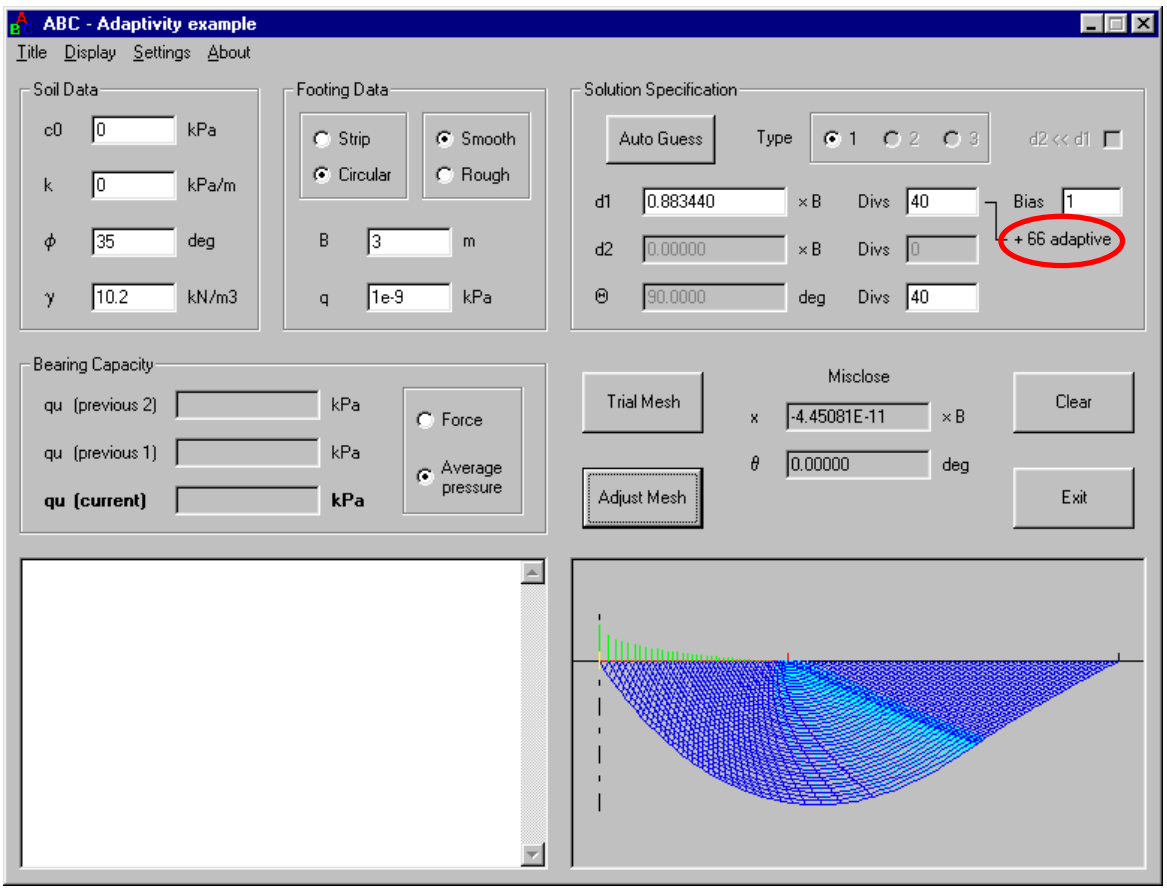

In addition to the 40 main α characteristics, a further 66 have been added adaptively near the edge of the footing (see Figures 2.1 and 2.6a for the distinction between α and β characteristics). The extra α characteristics are drawn in light blue, as are the extra β characteristics that originate from the start and finish of each one. This can be seen more clearly by double-clicking on the thumbnail drawing and inspecting the expanded version:

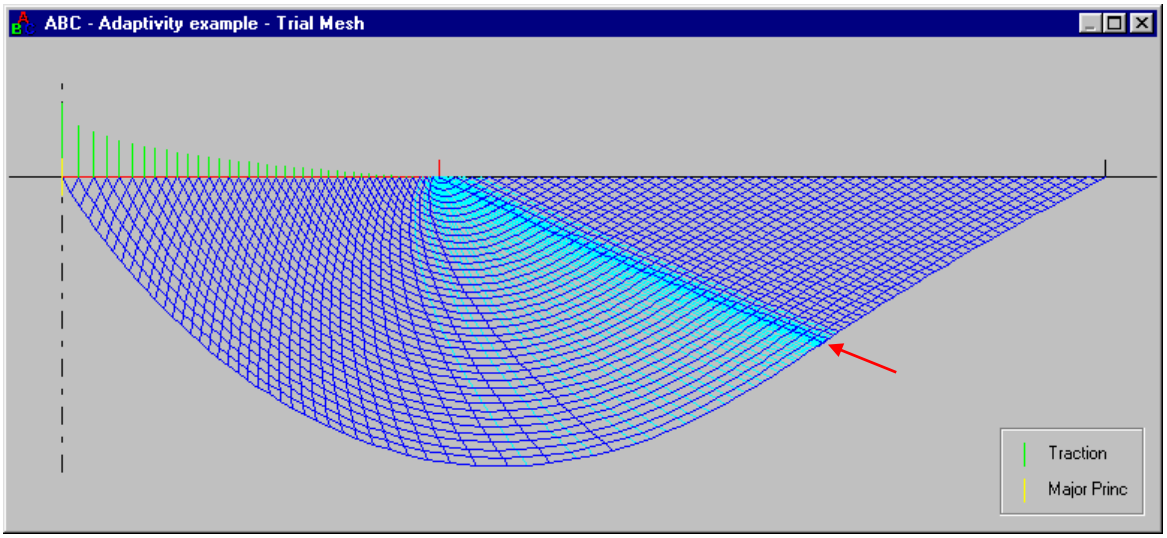


The arrow indicates how the fan zone has (almost, since $F < \infty$) degenerated into a single β characteristic – this is typical of all $N_\gamma$-type problems.

Clicking on **Adjust Mesh** starts the adjustment of $d_1$, after which the bearing capacity is displayed ($q_u = 275.7$ kPa). Each iteration of this initial adjustment involves a fresh adaptive calculation of the mesh. When the solution is refined using **Double Up**, however, the initial pattern of recursive subdivision is 'locked in' and provides the template for all subsequent doublings of the mesh (this can be seen by inspecting the pattern of dark blue and light blue characteristics in successive drawings). The following message is displayed at the start of the **Double Up** sequence:

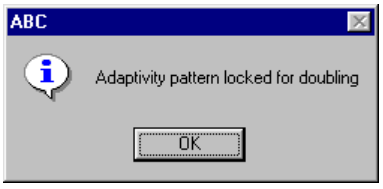


As the mesh is refined, the calculated bearing capacity $q_u$ quickly converges to 275.9 kPa. It is worth recalling from Section 3.3.1 that the corresponding result with an effective surcharge of 7.5 kPa was $q_u = 839.0$ kPa, indicating the profound effect of embedment on the bearing capacity of a footing on cohesionless soil.

It remains to confirm that the artificial surcharge $q = 10^{-9}$ kPa is small enough to have no significant influence on the result. This can be done by repeating the analysis with a larger surcharge, say $q = 10^{-6}$ kPa, such that $F$ (which is just $\gamma B/q$ when $c_0 = k = 0$) has a smaller value of $3.1 \times 10^7$. It is found that the bearing capacity still converges to $q_u = 275.9$ kPa, slightly more quickly than before because the initial mesh prior to doubling contains fewer adaptive α characteristics, 47 as opposed to 66. Even a surcharge of $10^{-3}$ kPa, such that $F = 3.1 \times 10^4$, is perfectly acceptable from a practical point of view, leading to a bearing capacity of $q_u = 276.2$ kPa that is only marginally too high. It should now be clear that the limit of $F \le 10^{12}$ in equation (3.2b) is not particularly restrictive; in fact it is sufficient for an $N_\gamma$ problem to be solved to about 9 correct digits, if desired (see Section 2.6).

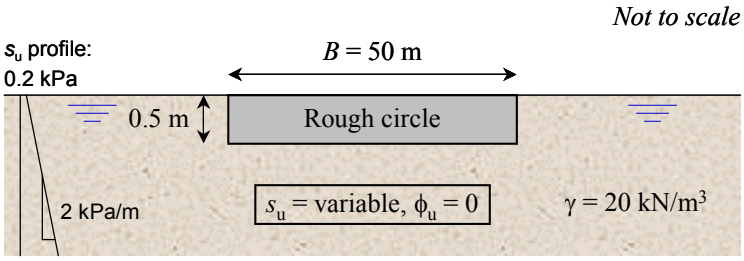


**Figure 3.3** Example problem requiring bias

*3.3.3 Problems requiring bias*

Consider the undrained bearing capacity problem shown in Figure 3.3. Undrained analysis is performed in terms of total stresses, so even though the soil is saturated, γ must be taken as the *total* unit weight[3], and $q$ as the *total* surcharge pressure at footing level, namely $20\times0.5=10$ kPa. As indicated in the figure, the undrained strength $s_u$ increases with depth, and its value at the level of the footing base is $0.2+2\times0.5=1.2$ kPa. The problem is therefore entered as follows:

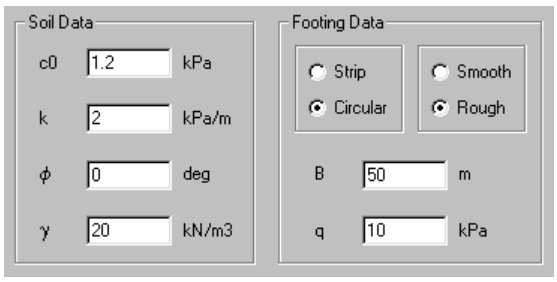


The dimensionless ratio $F$, which reduces to $kB/c_0$ when $\phi=0$, is equal to 83.3. This is well inside the limit of 1000 that applies when $\phi\le1°$ (see equation (3.2a)), but it is large enough to mean that a significant degree of bias – skewing the concentration of α characteristics towards the outside of the mesh – is needed to construct a well-conditioned solution. As discussed in Section 2.7, the simplest method of achieving this effect is to distribute the starting points of the α characteristics in geometric progression, rather than spacing them equally along the free surface. The *Bias* entry in the *Solution Specification* frame sets the ratio of the final (i.e. outmost) to the initial (i.e. inmost) subdivision of $d_1$, from which the parameters for the geometric progression can readily be worked out. If bias is required, a suitable ratio will be chosen by **Auto Guess**, and in this instance 0.1 is proposed:

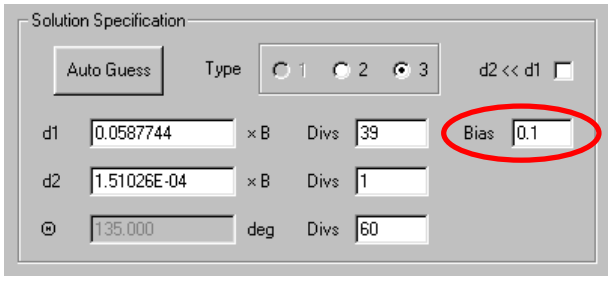


After clicking on **Trial Mesh** and **Adjust Mesh**, the initial solution can be inspected by double-clicking on the thumbnail drawing:

[3] When $\phi=0$ the bearing capacity is independent of γ, but the direct stresses at solution points with $z>0$ will only be calculated correctly if the true value of γ is entered. For example if weightless soil is used, the direct stresses will be low by $\gamma z$ throughout the mesh, and this will affect the plotting and reporting of the stresses.

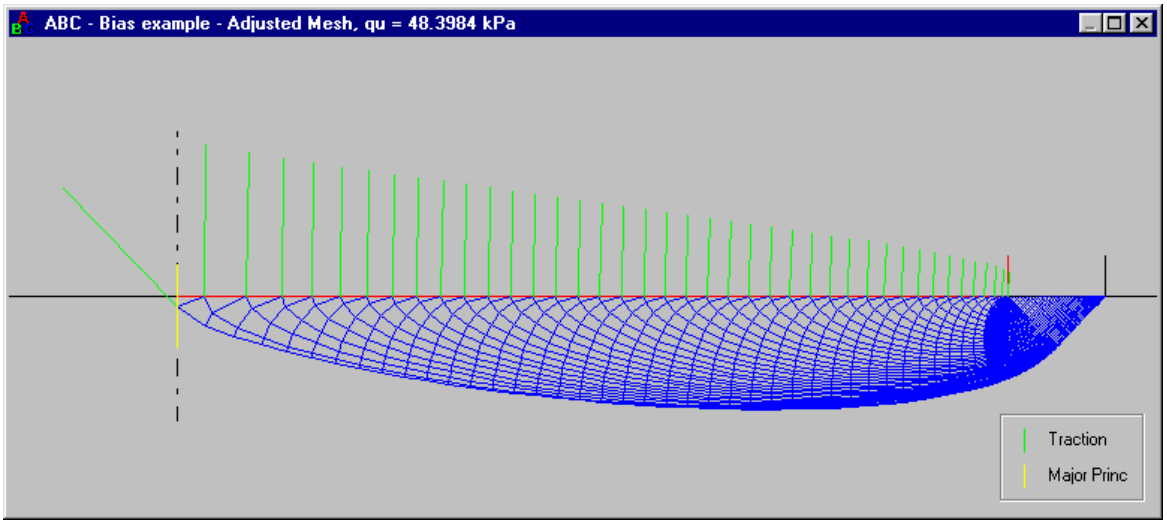


If the recommended *Bias* is overridden with 1, such that the $d_1$ subdivisions are equally spaced, there is much poorer resolution near the axis of symmetry:

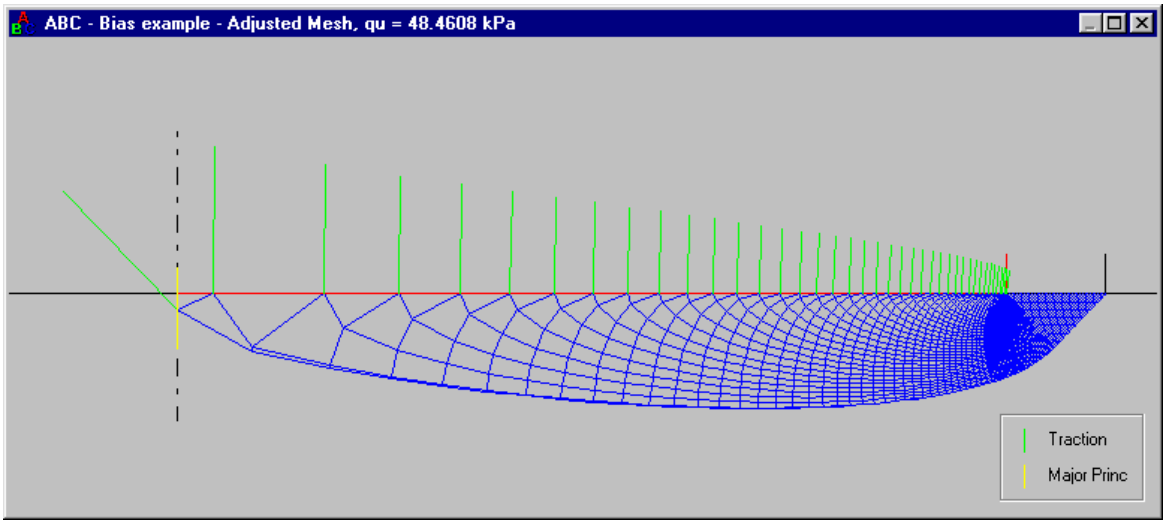


This can lead to problems during the **Adjust Mesh** and **Double Up** stages, in the form of numerical ill-conditioning – see Section 2.7 for a more detailed discussion. In summary, if **Auto Guess** suggests a *Bias* that is less than 1, it is strongly recommended that this value be adopted.

### *3.3.4 Problems requiring sub-subdivisions*

Figure 3.4 shows a modified version of the previous example (the footing diameter *B* is even larger).

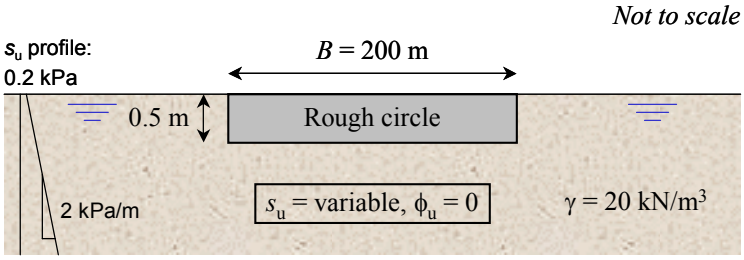


**Figure 3.4** Example problem requiring sub-subdivisions

Although this is not a realistic problem, it serves to illustrate a type 3 solution where $d_2 << d_1$, such that the sub-subdivision technique described in Section 2.8 is needed to maintain adequate resolution near the axis of symmetry. The problem is specified as:

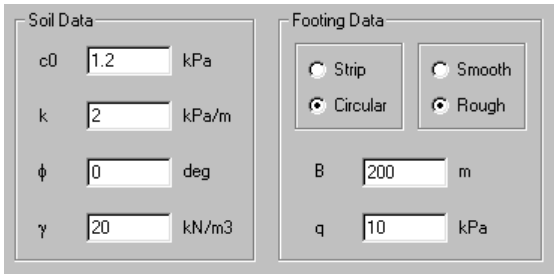


The dimensionless ratio $F$ is now 333.3, well into the range that would be regarded as 'difficult' for a rough circular footing on soil with $\phi = 0$ (see Sections 2.7 and 2.8). The initial solution proposed by **Auto Guess**, which in this instance takes several seconds to perform its calculations, involves both a heavy bias and activation of the sub-subdivision strategy. The latter is indicated by the appearance of a check in the $d_2 << d_1$ box:

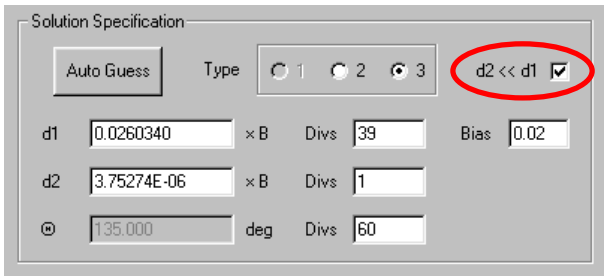


Note that (the estimated value of) $d_2$ is indeed much smaller than $d_1$, by a factor of about 7000, suggesting that the 'false head' region of the type 3 solution ($OC_1C_2$ in Figure 2.7b) will be extremely small. Clicking on **Trial Mesh** and **Adjust Mesh** confirms that this is the case:

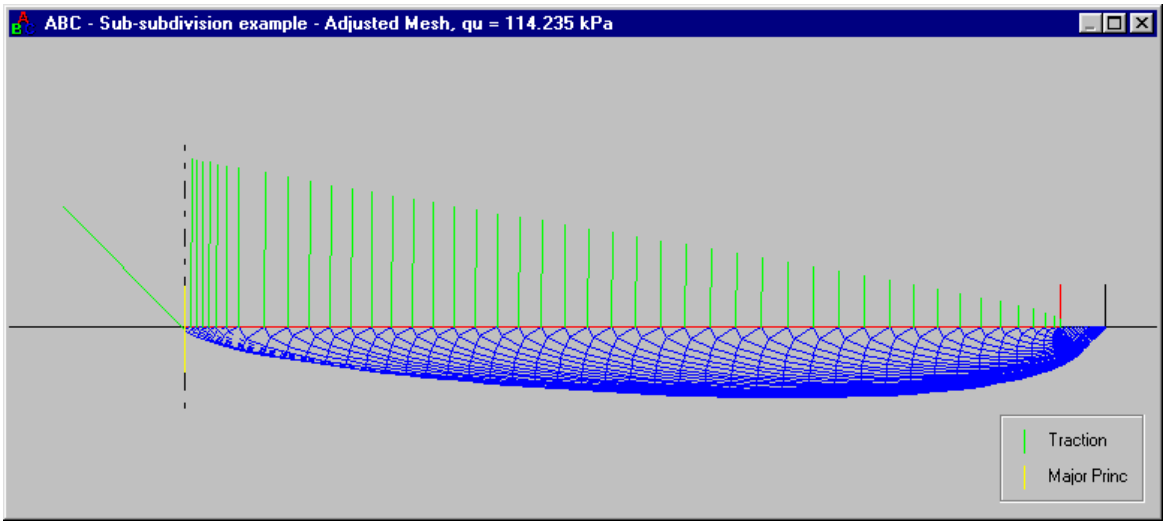


The sub-subdivisions occur in the final (i.e. outmost) $d_1$ subdivision, and are visible as dotted characteristics. As explained in Section 2.8, the spacing of the sub-subdivisions is determined using a local version of the bias technique applied to the main subdivisions of $d_1$. The extra α characteristics spawn extra β characteristics when they reach the footing, giving a mesh that is able to resolve the tiny 'false head' region in a well-conditioned manner. This can be seen more clearly by expanding

the thumbnail drawing, right-clicking on it, selecting *Settings*, making the $x$ range (say) –0.1 to 0.1×$B$, and also unchecking *Show Tractions*:

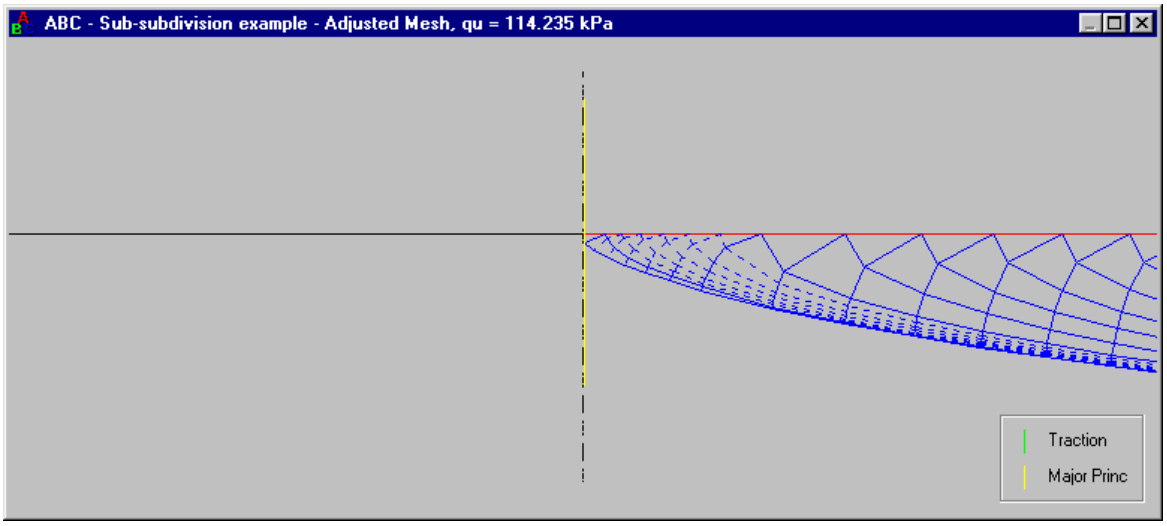


Solutions involving bias and/or sub-subdivisions can be refined as usual using **Double Up**. In this case convergence is quite slow because of the inherent difficulty of the problem (cf. Section 3.3.1):

| | |
|---|---|
| **Adjust Mesh** | 114.235 (0.8) |
| **Double Up 1** | 112.849 (1.6) |
| **Double Up 2** | 112.516 (4.1) |
| **Double Up 3** | 112.418 (14.1) |
| **Double Up 4** | 112.390 (59.3) |
| **Double Up 5** | 112.383 (176.2) |

Rough footing problems where $\phi = 0$ and $F$ ($= kB/c_0$) becomes greater than about 1000 become very difficult to solve, even with the bias and sub-subdivision strategies, and this is the reason for imposing the restriction in equation (3.2a). As with equation (3.2b), however, this limitation is unlikely to be important in practice – witness the outlandish choice of parameters needed to achieve $F = 333.3$ in the example above. It must also be borne in mind that, unlike the '$N_\gamma$ problem' ($\phi > 0$ and $F = \infty$), the limiting undrained problem ($\phi = 0$ and $F = \infty$) can be solved analytically in both plane strain and axial symmetry. For details see Sections 4.2.5, 4.2.6, 4.3.5 and 4.3.6.

### *3.3.5 Problems requiring user intervention*

For most rough footing problems, the choice of the applicable solution type (2 or 3) is clear-cut. Occasionally, however, for problems that fall close to the borderline (see Section 2.5.2), the solution type may need to be changed from 2 to 3 or *vice versa* as the mesh is refined using **Double Up**. To illustrate such a case, consider the following (specially contrived) problem:

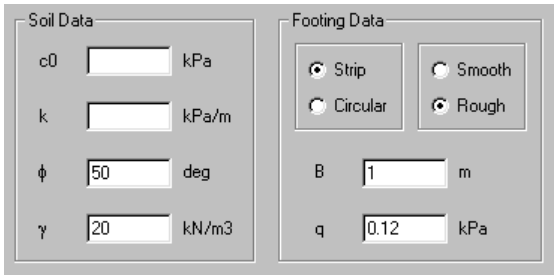

Clicking on **Auto Guess**, **Trial Mesh** and **Adjust Mesh** gives:

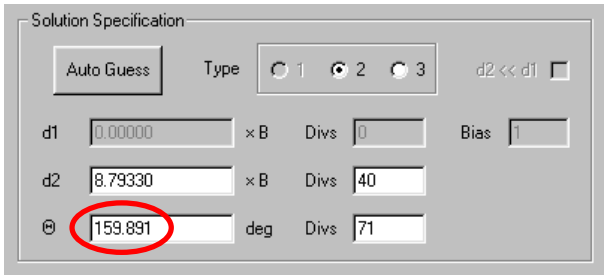


This is a valid type 2 solution, but the fan aperture $\Theta$ is very close to the maximum possible value of 160° (recall from Section 2.5.2 that $\Theta_{max} = 3\pi/4 + \phi/2$). On the first application of **Double Up**, the following mesh size parameters are obtained, accompanied by an advisory message:

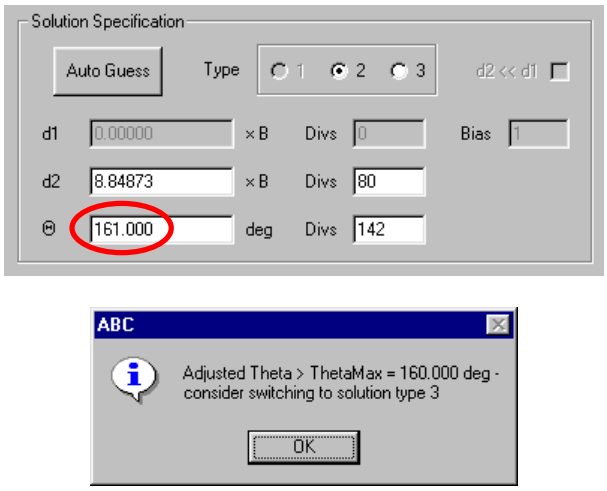


Now that the mesh has been refined and re-adjusted, $\Theta$ exceeds $\Theta_{max}$. In other words, the fan of the type 2 solution has wrapped around so far that, near the edge of the footing, there are solution points that lie just above the surface of the soil. This indicates that the problem actually requires a type 3 solution, with a small value of $d_1$. The situation can be rectified by manually changing the solution type to 3, then editing the data pertaining to $d_1$:

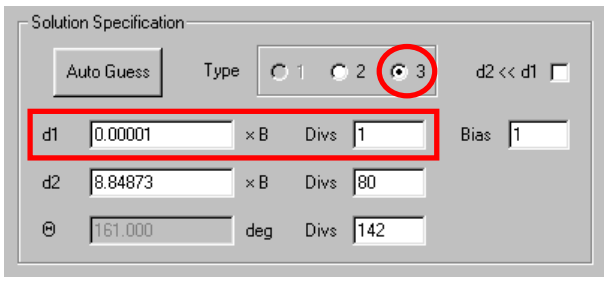


Although it is permissible to use zero as an initial guess for $d_1$, it is generally better (i.e. faster and more stable) to enter a small positive value such as the 0.00001 shown above. It is not permissible to have a zero subdivision count, so this entry should be changed to 1, as shown[4]. All of the other

[4] When $d_1 << d_2$ it is counterproductive to have more than one $d_1$ subdivision, since this results in a mesh with even more elongated cells along the perimeter of the 'false head' region. The presence of such cells near the inside of the mesh can be a source of ill-conditioning, particularly in axial symmetry. This is also the reason that, when **Double Up** is applied to a type 3 solution with $d_1 << d_2$, the subdivision count for $d_1$ remains static until the inmost cell of the mesh has become more or less 'square' (cf. Section 2.7).

entries in the *Solution Specification* frame can be left unchanged. As expected, clicking on **Trial Mesh** and **Adjust Mesh** (without, for once, first clicking on **Auto Guess**!) produces a valid type 3 solution:

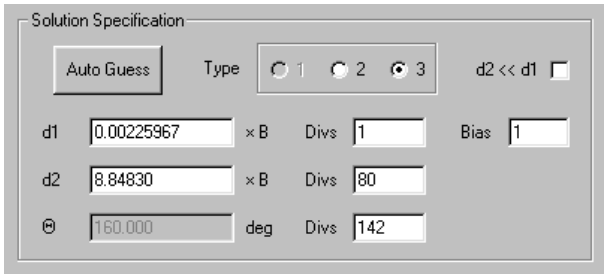


The ensuing **Double Up** sequence confirms that solution type 3 is indeed the correct choice for this problem (the bearing capacity converges to $q_u = 7557$ kPa, and the mesh size parameters converge to $d_1/B = 0.0038$ and $d_2/B = 8.872$).

The complementary situation occurs when a type 3 mesh is adjusted and a negative value of $d_1$ is obtained; this indicates that solution type 2 is in fact the correct choice for the current level of mesh refinement:

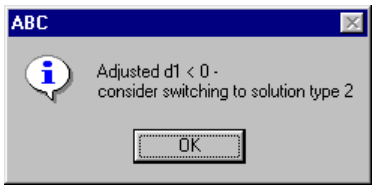


The corrective action required in this case is simpler. The solution type needs to be altered from 3 to 2, but the rest of the fields in the *Solution Specification* frame can be left unchanged prior to embarking on the usual the sequence of **Trial Mesh**, **Adjust Mesh**, **Double Up**, **Double Up**, …

Note that, in either situation, the prompt to change solution type does not have to be followed – it is also possible to continue with the **Double Up** process, ignoring all messages and seeing whether, as refinement continues, the adjusted mesh size parameters do eventually become valid for the current solution type. It is, however, extremely rare to encounter a case where this is necessary to obtain the bearing capacity.

## 3.4 Menu options

### *3.4.1 Title*

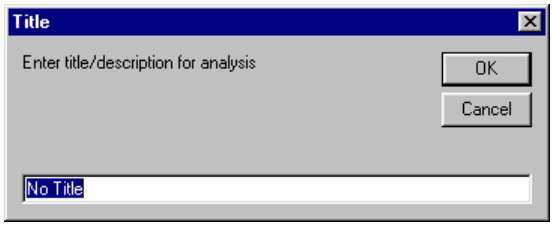


The text entered here appears in the title bars of the main ABC form and the expanded drawing window, and at the head of the text output (Section 3.5).

### *3.4.2 Display/Units, Display/Precision*

These options are self-explanatory. The defaults are Metric, and 6 significant figures.

### *3.4.3 Settings/Adjust*

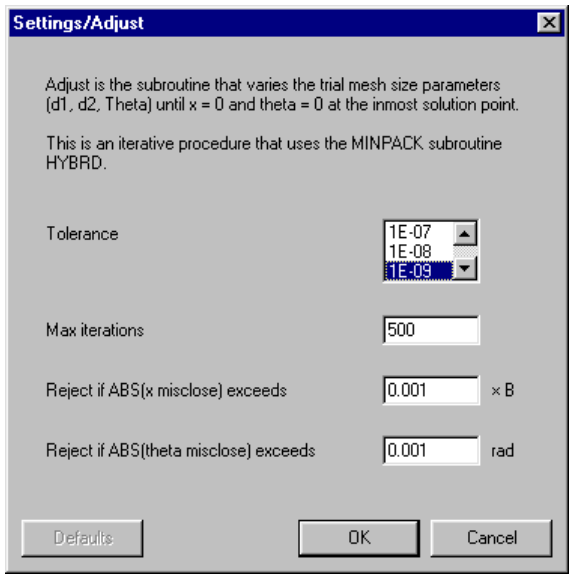


The first two settings control the MINPACK subroutine HYBRD that is used to adjust the mesh size parameters $d_1$, $d_2$ and $\Theta$ (see Section 2.9). The convergence criterion in HYBRD is based purely on relative error – for further details see Moré et al. (1980) or the source code at www.netlib.org.

- *Tol*: default = $10^{-9}$, min = $10^{-12}$, max = $10^{-6}$
- *MaxIt*: default = 500, min = 50, max = 5000

The other two settings are used to confirm that a newly-adjusted mesh appears to be sensible. These checks are required because of a bug in HYBRD that sometimes causes it to abandon the iterations and report successful convergence, when in fact it has not converged properly. This only tends to happen if the initial estimates of the mesh size parameters are very poor, or if the chosen solution type for a rough footing problem is incorrect (Section 3.3.5). A simple 'reality check' on the final values of $x_{\text{misclose}}$ and $\theta_{\text{misclose}}$ allows any such misbehaviour to be detected.

- Acceptable $|x_{\text{misclose}}|$: default = $0.001 \times B$, min = $0^+$, max = n/a
- Acceptable $|\theta_{\text{misclose}}|$: default = 0.001 rad, min = $0^+$, max = n/a

### *3.4.4 Settings/CalcAB*

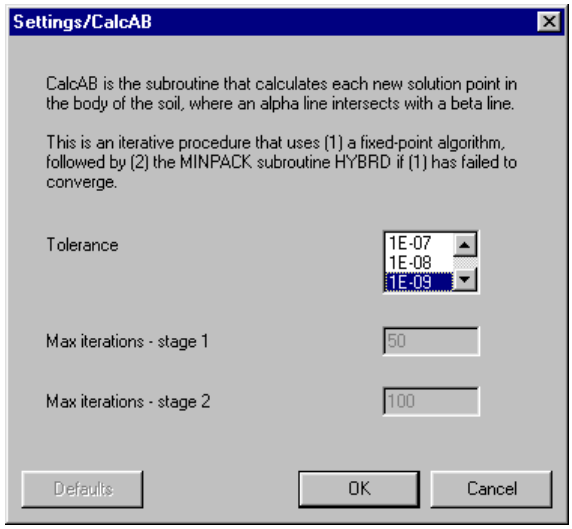

These settings control the behaviour of the subroutine CalcAB described in Section 2.4. Only the convergence tolerance *Tol* can be varied by the user. In general, the calculated bearing capacity is surprisingly insensitive to this tolerance, particularly once a mesh has been through several stages of refinement using **Double Up**. For high-quality work, however, this sensitivity should be explored to confirm that the bearing capacities obtained are indeed accurate to the desired number of significant figures. A reduction in *Tol* leads to a small increase in CPU time, since every call to CalcAB requires a few additional iterations.

- *Tol*: default = $10^{-9}$, min = $10^{-12}$, max = $10^{-6}$

The iteration counts *MaxIt1* (fixed-point iteration stage) and *MaxIt2* (HYBRD stage) are hard-wired to suitable values that have been determined empirically. Although a single iteration of the fixed-point algorithm is much faster than a single iteration of HYBRD, the fixed-point method sometimes requires many more iterations to reach convergence (e.g. when close to the *z* axis in axial symmetry). CalcAB therefore spends a maximum of 50 iterations in the fixed-point loop before switching to HYBRD, which is quadratically convergent in the neighbourhood of a solution. If this back-up strategy fails to converge within 100 iterations, a fatal error is notified (see Section 3.6.3).

### *3.4.5 Settings/Drawing*

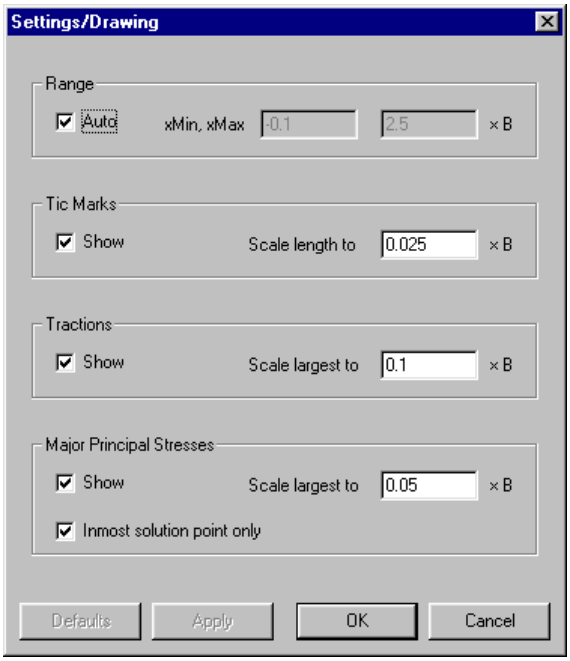


As already noted, this form can also be accessed by right-clicking on the drawing itself (whether thumbnail or expanded). The settings are all self-explanatory, and their effects are best explored by experimentation.

When producing a series of drawings that are related, it can be useful to uncheck *Auto* and set *xMin* and *xMax* manually to ensure that the plots all have a common *x* range. Once the various drawings have been copied and pasted into a word processor or spreadsheet[5], they can then be stacked vertically to facilitate comparison. Figure 2.9 was created in this way.

To show major principal stresses for the whole mesh, the default setting *Inmost solution point only* must be unchecked. Often some trial-and-error adjustment of the default scale factor will then be necessary as well, during which it is convenient to use **Apply** rather than **OK**.

[5] Use Alt-PrtSc to copy an image of the active window to the clipboard, then Ctrl-V to paste it.

*3.4.6 Settings/Misc*

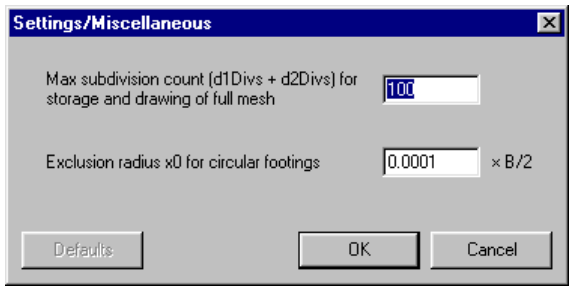


The first setting determines the threshold at which the calculation and drawing procedures switch from 'full mesh' mode to 'outline' mode, in order to conserve memory and save drawing time (see Section 2.11). The transition is based on the total number of α characteristics, excluding the degenerate characteristic at the edge of the footing, and any that have been added adaptively.

- *MaxDivsFullMesh*: default = 100, min = 0, max = 1000

The second setting is only applicable in axial symmetry, and is ignored in plane strain. It allows the goal of the mesh adjustment (Section 2.9) to be altered from "$x = 0$ and $\theta = 0$ at the inmost solution point" to "$x = x_0$ and $\theta = 0$ at the inmost solution point". Setting $x_0$ to some small fraction of the footing radius $B/2$, say $10^{-4}$ or $10^{-3}$, has the desirable effect of accelerating the adjustment process, and is particularly effective when attempting to solve difficult circular footing problems such as the one considered in Section 3.3.4. Not only is the singularity at $x = 0$ specifically excluded, but there are fewer iterations involving trial meshes that, if continued, would cross the axis of symmetry into the physically meaningless – and numerically capricious – region of 'negative radius' (see Sections 2.2.2 and 2.9).

In terms of the calculated bearing capacity, an analysis with $x_0 > 0$ will give a lower converged value of $q_u$ or $Q_u$ than an analysis with $x_0 = 0$, so the exclusion procedure is conservative[6]. If $x_0$ is small, the error in the bearing capacity will be even smaller because the fraction of the total *area* being excluded is proportional to $x_0^2$, though it must also be noted that in circular footing problems the bearing pressure is invariably higher near the axis of symmetry than at the edge of the footing. Experience has shown that the default value of $x_0 = 10^{-4} \times B/2$ has an utterly negligible influence on the calculated bearing capacity (of the order of $10^{-7}$). Unsurprisingly, however, the mesh size parameters $d_1$, $d_2$ and $\Theta$ are affected more 'directly', with errors of order $10^{-4}$. For high-quality work in axial symmetry, the sensitivity of the results to the choice of $x_0$ can always be examined by overriding the default value. Although it is permissible to set $x_0 = 0$, this can have a detrimental effect on the rate at which **Adjust Mesh** and **Double Up** converge in certain more difficult problems, as mentioned above.

- $x_0$ : default = $0.0001 \times B/2$, min = 0, max = $1^- \times B/2$

*3.4.7 About*

This displays information including the version number, the address of the ABC homepage, and the email address of the author. Comments, bug reports, requests for future enhancements, etc. are always welcome.

[6] Note that, regardless of the value of $x_0$, the average pressure $q_u$ is always calculated with respect to the gross footing area $\pi B^2/4$.

### 3.5 Text Output

The text output that appears after a successful **Adjust Mesh** or **Double Up** contains an echo of the input and a summary of the results. Relevant sections of this manual are indicated on the right.

| | | | |
|---|---|---|---|
| ABC - Analysis of Bearing Capacity | | | |
| Version 1.0 Build 1 | | version number | 3.4.7 |
| TITLE | | | |
| Example problem | | title/description | 3.4.1 |
| SOIL DATA | | | |
| c0 | 0.00000 kPa | $c_0$ | 2.1, 3.1 |
| k | 0.00000 kPa/m | $k$ | 2.1, 3.1 |
| phi | 35.0000 deg | $\phi$ | 2.1, 3.1 |
| gamma | 20.0000 kN/m3 | $\gamma$ | 2.2, 3.1 |
| FOOTING DATA | | | |
| Geometry | Circular | geometry: strip or circular | 2.2, 3.1 |
| Interface | Rough | roughness: smooth or rough | 2.3.2, 3.1 |
| B | 1.00000 m | $B$ | 2.5, 3.1 |
| q | 0.100000 kPa | $q$ | 2.3.1, 3.1 |
| SOLUTION SPECIFICATION | | | |
| SolnType | 3 | solution type | 2.5, 3.2 |
| d1 | 0.183240 × B | $d_1$ | 2.5, 3.2 |
| d1Divs | 9 | $d_1$ subdivisions (main) | 2.5, 3.2 |
| d1Divs+ | 3 | $d_1$ subdivisions (adaptive) | 2.6, 3.3.2 |
| d1Bias | 1.00000 | $d_1$ bias ratio | 2.7, 3.3.3 |
| d2 | 1.39782 × B | $d_2$ | 2.5, 3.2 |
| d2Divs | 31 | $d_2$ subdivisions | 2.5, 3.2 |
| Theta | 152.500 deg | $\Theta$ | 2.5, 3.2 |
| ThetaDivs | 68 | $\Theta$ subdivisions | 2.5, 3.2 |
| Adaptivity | On | adaptivity: on or 'locked' | 2.6, 3.3.2 |
| d2 << d1 | Off | sub-subdivisions: on or off | 2.8, 3.3.4 |
| SETTINGS | | | |
| AdjustTol | 1.00000E-09 | *Tol* for Adjust | 2.9, 3.4.3 |
| CalcABTol | 1.00000E-09 | *Tol* for CalcAB | 2.4, 3.4.4 |
| x0 | 1.00000E-04 × B/2 | $x_0$ | 3.4.6 |
| BEARING CAPACITY | | | |
| Qu | 345.518 kN | $Q_u$ | 2.10, 3.2, 3.4.6 |
| qu | 439.927 kPa | $q_u$ | 2.10, 3.2, 3.4.6 |

| | | | |
|---|---|---|---|
| EDGE OF FOOTING | | solution point at end of degenerate α char. | |
| x | 0.500000 × B | $x$ | 2.1, 2.2 |
| z | 0.00000 × B | $z$ | 2.1, 2.2 |
| sigma | 9.74856 kPa | σ | 2.1, 2.2 |
| theta | -62.5000 deg | θ | 2.1, 2.2 |
| sigmaxx | 12.9557 kPa | $\sigma_{xx}$ | 2.2 |
| sigmazz | 6.54138 kPa | $\sigma_{zz}$ | 2.2 |
| tauxz | -4.58033 kPa | $\tau_{xz}$ | 2.2 |
| Tx | -4.58033 kPa | $T_x$ | 2.10 |
| Tz | 6.54138 kPa | $T_z$ | 2.10 |
| INMOST POINT | | solution point at end of final α char. | |
| x | 5.00000E-05 × B | $x$ | 2.1, 2.2 |
| z | 0.384399 × B | $z$ | 2.1, 2.2 |
| sigma | 2052.30 kPa | σ | 2.1, 2.2 |
| theta | -3.88687E-10 deg | θ | 2.1, 2.2 |
| sigmaxx | 875.151 kPa | $\sigma_{xx}$ | 2.2 |
| sigmazz | 3229.46 kPa | $\sigma_{zz}$ | 2.2 |
| tauxz | -1.59713E-08 kPa | $\tau_{xz}$ | 2.2 |
| Tx | 776.268 kPa | $T_x$ | 2.10 |
| Tz | 1491.20 kPa | $T_z$ | 2.10 |
| OTHER OUTPUT | | | |
| F | 200.000 | $F$ | 2.5, 3.1 |
| xMis | 4.91820E-12 × B | $x_{\text{misclose}}$ | 2.9, 3.2, 3.4.3 |
| thetaMis | -3.88687E-10 deg | $\theta_{\text{misclose}}$ | 2.9, 3.2, 3.4.3 |
| dxMin | 0.00508999 × B | smallest $d_1$ or $d_2$ subdivision | |
| Crossing | False | crossing β characteristics | 1.2, 3.6.2 |
| CPUTime | 0.269989 s | CPU time (excl. drawing) | 3.3.1, 3.3.4 |

## 3.6 Messages

### *3.6.1 Advisory messages*


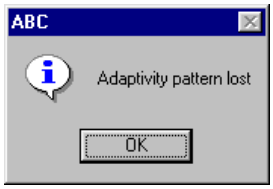


The first message is issued when **Double Up** is first applied to a mesh containing adaptively-added characteristics (see Section 3.3.2). This is a reminder that, during the ensuing **Double Up** sequence, it not permissible to perform any manual editing of the $d_1$, $d_2$ or Θ subdivision counts. If any such edits are made, the second message is issued, indicating that the next **Trial Mesh** will be a fresh adaptive calculation (Sections 2.6, 3.3.2).

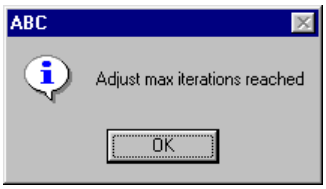


Assuming that progress towards the solution appears to be satisfactory, the adjustment can be resumed with a new batch of iterations by clicking on **Adjust Mesh**. If the message is received regularly, the value of *MaxIt* in *Settings/Adjust* (Section 3.4.3) should be increased.

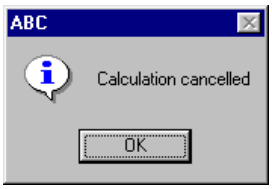


If the adjustment was cancelled accidentally, it can be resumed by clicking on **Adjust Mesh**.


To prevent overflow problems with the Visual Basic drawing routines, meshes with unrealistic dimensions (perhaps arising because of numerical difficulties during an adjustment) are not drawn.

*3.6.2 Warning messages*

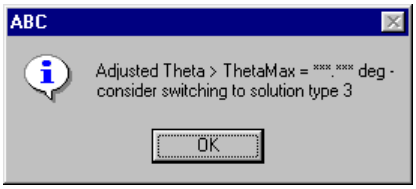


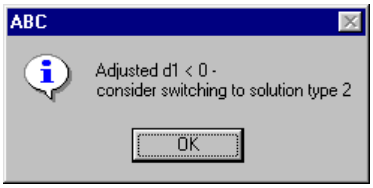


User intervention may be required – Section 3.3.5 gives details of how to proceed in each case.


The mesh contains crossing β characteristics, indicating that a stress discontinuity (analogous to a shock wave) should have been introduced while the mesh was being constructed, to maintain the admissibility of the solution. These calculations are not performed in the current version of ABC. Although they will be implemented in future, it is worth pointing out that crossing characteristics only arise in a fairly small class of circular footing problems (see Sections 4.3.3, 4.3.4, 4.3.11).

Furthermore, if the area of crossing is localised, the error in the calculated bearing capacity may not be too serious (Houlsby, 1982). Certainly it appears that many previous researchers, including Cox et al. (1961), Cox (1962), Salençon & Matar (1982a) and Bolton & Lau (1993), have turned a blind eye to the occurrence of crossing characteristics in their meshes, if indeed they were aware of it at all.

*3.6.3 Error messages*


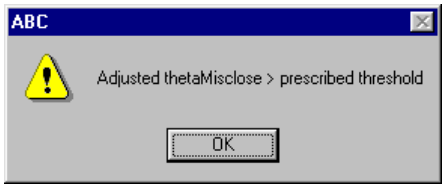


The thresholds referred to are those prescribed in *Settings/Adjust* (Section 3.4.3). If there is no obvious problem visible in the drawing, it is usually worth clicking on **Adjust Mesh** to restart the adjustment. If problems persist, perturb one or more of the mesh size parameters ($d_1$, $d_2$, $\Theta$) before clicking again on **Trial Mesh**, **Adjust Mesh**, etc. If the footing is rough, these messages may indicate a need to change from solution type 2 to solution type 3, or *vice versa* – see Section 3.3.5.

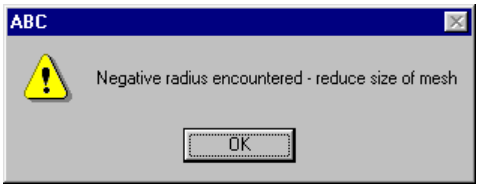


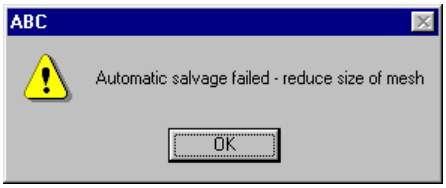


These errors only arise in circular footing problems. They indicate that if construction of the current mesh were to continue, it would cross into the forbidden region $x < 0$. Reduce one or more of the mesh size parameters ($d_1$, $d_2$, $\Theta$) before clicking again on **Trial Mesh**, **Adjust Mesh**, etc.


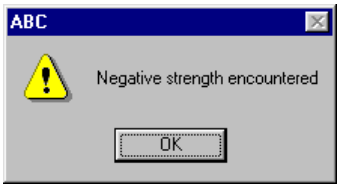


These errors usually indicate convergence difficulties near the axis of symmetry in a circular footing problem. In this case, reduce one or more of the mesh size parameters ($d_1$, $d_2$, $\Theta$) before clicking again on **Trial Mesh**, **Adjust Mesh**, etc. If the cause of the error is elsewhere, it should be apparent from the drawing of the mesh. There may be a need to change solution types – see Section 3.3.5.


This is an error issued by the MINPACK subroutine HYBRD (see Section 2.9). If there is no obvious problem visible in the drawing, it is usually worth clicking on **Adjust Mesh** to restart the adjustment.

If problems persist, perturb one or more of the mesh size parameters ( $d_1$ , $d_2$ , $\Theta$) before clicking again on **Trial Mesh**, **Adjust Mesh**, etc. If the footing is rough, this message may indicate a need to change from solution type 2 to solution type 3, or *vice versa* – see Section 3.3.5.


This is another error issued by the MINPACK subroutine HYBRD (Section 2.9). In *Settings/Adjust* (Section 3.4.3), *Tol* cannot be set to anything smaller than $10^{-12}$, so it is unlikely that this message will ever be received.


During an adaptive **Trial Mesh** or **Adjust Mesh** (see Sections 2.6, 3.3.2), the standard allocation of adaptive α characteristics has been exceeded. This error should not arise under normal conditions, i.e. if **Trial Mesh** has been preceded by **Auto Guess**.

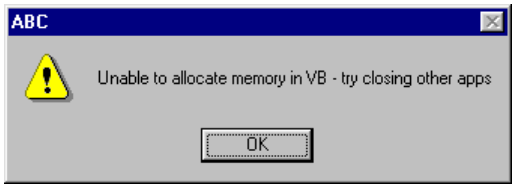



An attempt to allocate array space in the front end (Visual Basic) or the back end (Fortran DLL) has failed. Closing other applications may free up sufficient memory to allow the calculation to proceed. The larger the value of *MaxDivsFullMesh* in *Settings/Misc* (Section 3.4.6), the more likely it is that one of these errors will be received. Once the calculation of the mesh has switched to 'outline' mode (see Sections 2.11, 3.4.6), it is unlikely that insufficient memory will be a problem.

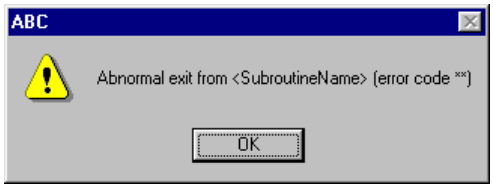


If a message like this is received, please report it (see the *About* menu) and the circumstances in which it arose.

# 4. VALIDATION

## 4.1 Introduction

In this chapter, ABC is tested on a wide range of bearing capacity problems. Closed-form analytical solutions are invaluable for this purpose, but they are only available for certain special combinations of the geometry (plane strain or axial symmetry), the friction angle $\phi$, and the dimensionless ratio

$$F = \frac{kB + \gamma B \tan\phi}{c_0 + q \tan\phi} \tag{4.1}$$

The situation is summarised in the following table:

| $\phi$ | $F$ | Analytical solution? | | Relevant sections | |
|---|---|---|---|---|---|
| | | Plane strain | Axial symm. | Plane strain | Axial symm. |
| 0 | 0 | Yes | No | *4.2.1, 4.2.2* | *4.3.1, 4.3.2* |
| general | 0 | Yes | No | *4.2.3, 4.2.4* | *4.3.3, 4.3.4* |
| 0 | $\infty$ | Yes | Yes | *4.2.5, 4.2.6* | *4.3.5, 4.3.6* |
| general | $\infty$ | No | No | *4.2.7, 4.2.8* | *4.3.7, 4.3.8* |
| 0 | general | No | No | *4.2.9, 4.2.10* | *4.3.9, 4.3.10* |
| general | general | No | No | *4.2.11, 4.2.12* | *4.3.11, 4.3.12* |

For problems where there is no analytical solution, the only comparisons that can be made are with numerical solutions obtained by other researchers. It should be noted, however, that many previous studies of bearing capacity using the method of characteristics do not appear to have incorporated any systematic approach to mesh refinement, so the results obtained in these studies are not necessarily correct to the quoted number of significant figures. It is disappointing that attention to this aspect of the solution process seems to have declined over the years, despite the enormous advances in computing power that have taken place. Cox et al. (1961) state that their bearing capacities "were computed for successively smaller mesh sizes, and the final values … are believed to be accurate to the number of figures given". This was, however, a painstaking process using the computers then available. According to Cox (1962), it took 120 hours (5 days) of running time on the R.A.R.D.E. digital computer AMOS to obtain just 32 bearing capacity factors to a precision of (in most cases) 3 significant figures. When running ABC on a typical present-day PC, this whole series of analyses – including systematic mesh refinements using **Double Up** – can be completed in a matter of minutes (confirming, incidentally, that Cox's results are exemplary; see Sections 4.2.11 and 4.3.11[1]). Among the more recent studies, some researchers have adopted fixed numbers of $\alpha$ and $\beta$ characteristics for a whole series of analyses, while others make no mention at all of the subdivision counts employed (apart from perhaps giving a picture of a typical mesh). Certain results obtained in these studies appear to be suspect, though in some cases inadequate mesh refinement is compounded by other problems. These issues are discussed in more detail below, as they arise.

In this chapter, all of the bearing capacities obtained using ABC are converged values that are believed to be correct to the quoted 4-digit precision. The user can repeat any of these analyses by following the standard procedure of entering the data, followed by

**Auto Guess**, **Trial Mesh**, **Adjust Mesh**, **Double Up**, **Double Up**, …

[1] Note, however, that these analyses (smooth footings only; $F_{max} \approx 17$) are quite straightforward by comparison with (say) a series of analyses to evaluate $N_\gamma$ factors for a rough circular footing.

### 4.2 Plane strain

*4.2.1 Smooth strip footing on homogeneous, undrained clay ($k = 0$, $\phi = 0$)*

The bearing capacity is independent of $\gamma$ and is given by the analytical expression:

$$q_u = c_0 N_c + q \quad \text{where} \quad N_c = 2 + \pi$$

This result, due to Hencky (1923), is obtained from a type 1 solution in which

$$d_1 / B = 1/2$$

Consider a specific example with $c_0 = 15\,\text{kPa}$, $k = 0$, $\phi = 0$, $\gamma = 18\,\text{kN/m}^3$, $B = 2.5\,\text{m}$ and $q = 10\,\text{kPa}$. The bearing capacity is $q_u = 87.12\,\text{kPa}$. Results from ABC:

| | $q_u$ (kPa) | $d_1/B$ |
|---|---|---|
| **Adjust Mesh** | 87.12 | 0.5000 |
| **Double Up 1** | 87.12 | 0.5000 |
| **Double Up 2** | 87.12 | 0.5000 |

The correct $q_u$ is calculated immediately, without any need for mesh refinement. This is because the $\alpha$ characteristics in the fan zone are circular arcs, so the treatment of each curved segment as a chord does not introduce any error. (Even the coarsest possible solution, with subdivision counts of 1 and 1, gives the correct result.)

Initial mesh of characteristics:

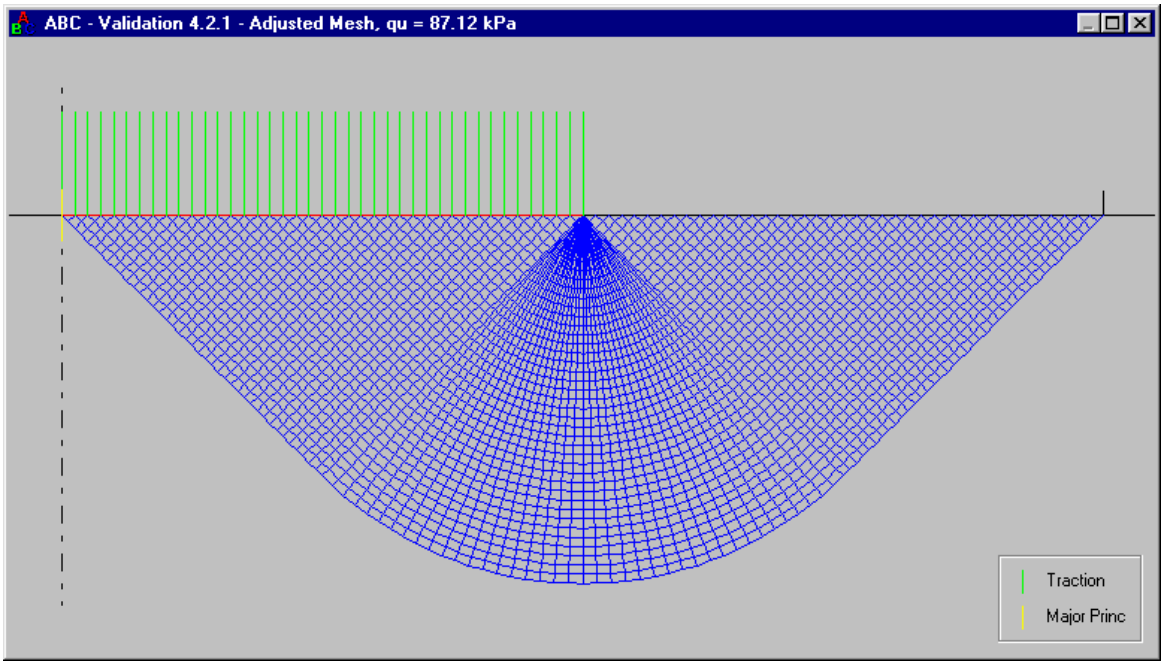

*4.2.2 Rough strip footing on homogeneous, undrained clay ($k = 0$, $\phi = 0$)*

The bearing capacity is independent of $\gamma$ and is given, as for the smooth case, by:

$$q_u = c_0 N_c + q \quad \text{where} \quad N_c = 2 + \pi$$

This result, due to Prandtl (1921), is obtained from a type 2 solution in which

$$d_2/B = 1 \quad \text{and} \quad \Theta = \pi/2$$

Consider a specific example with $c_0 = 15\,\text{kPa}$, $k = 0$, $\phi = 0$, $\gamma = 18\,\text{kN/m}^3$, $B = 2.5\,\text{m}$ and $q = 10\,\text{kPa}$. The bearing capacity is $q_u = 87.12\,\text{kPa}$. Results from ABC:

| | $q_u$ (kPa) | $d_2/B$ | $\Theta$ (°) |
|---|---|---|---|
| **Adjust Mesh** | 87.12 | 1.000 | 90.00 |
| **Double Up 1** | 87.12 | 1.000 | 90.00 |
| **Double Up 2** | 87.12 | 1.000 | 90.00 |

The correct $q_u$ is calculated immediately, without any need for mesh refinement. This is because the $\alpha$ characteristics in the fan zone are circular arcs, so the treatment of each curved segment as a chord does not introduce any error. (Even the coarsest possible solution, with subdivision counts of 1 and 1, gives the correct result.)

Initial mesh of characteristics:

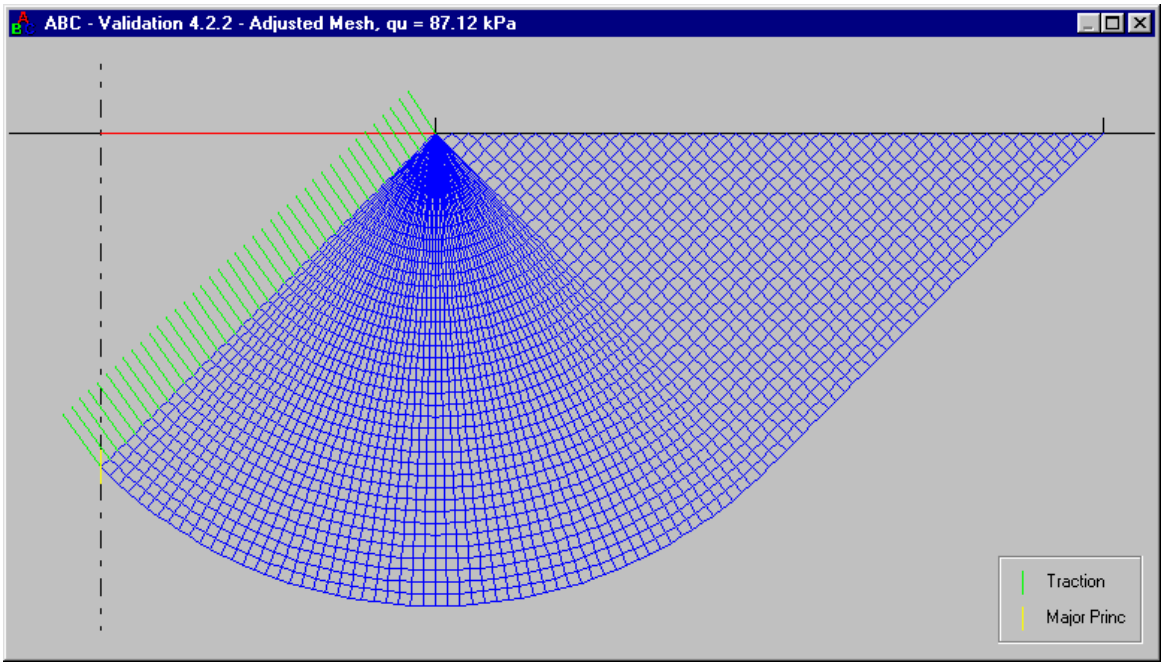

*4.2.3 Smooth strip footing on homogeneous, weightless, cohesive-frictional soil ($k = 0$, $\gamma = 0$)*

The bearing capacity is given by the analytical expression:

$$q_u = c_0 N_c + q N_q \quad \text{where} \quad \begin{cases} N_c = \left(N_q - 1\right)\cot\phi \\ N_q = e^{\pi\tan\phi}\tan^2\left(\pi/4 + \phi/2\right) \end{cases}$$

This result, due to Hencky (1923), is obtained from a type 1 solution in which

$$d_1/B = \sqrt{N_q}/2$$

Consider a specific example with $c_0 = 5$ kPa, $k = 0$, $\phi = 38°$, $\gamma = 0$, $B = 2.5$ m and $q = 10$ kPa. The bearing capacity is $q_u = 796.1$ kPa, and $\sqrt{N_q}/2 = 3.498$. Results from ABC:

| | $q_u$ (kPa) | $d_1/B$ |
|---|---|---|
| **Adjust Mesh** | 796.7 | 3.498 |
| **Double Up 1** | 796.2 | 3.498 |
| **Double Up 2** | 796.1 | 3.498 |
| **Double Up 3** | 796.1 | 3.498 |
| **Double Up 4** | 796.1 | 3.498 |

The correct $q_u$ is not calculated immediately; this is because the α characteristics in the fan zone are logarithmic spirals, so the treatment of each curved segment as a chord introduces a small error. As the mesh is refined, however, the approximate solution converges to the analytical one.

Initial mesh of characteristics:

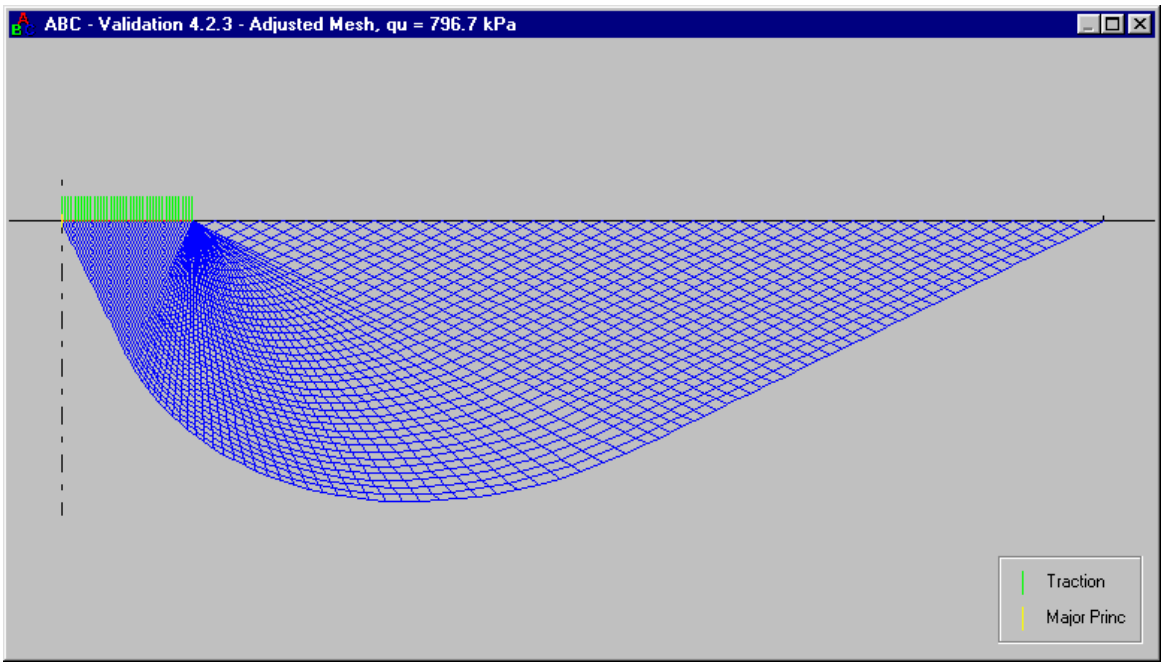

*4.2.4 Rough strip footing on homogeneous, weightless, cohesive-frictional soil ($k = 0$, $\gamma = 0$)*

The bearing capacity is given, as for the smooth case, by:

$$q_u = c_0 N_c + q N_q \quad \text{where} \quad \begin{cases} N_c = \left(N_q - 1\right)\cot\phi \\ N_q = e^{\pi\tan\phi}\tan^2\left(\pi/4 + \phi/2\right) \end{cases}$$

This result, due to Prandtl (1921), is obtained from a type 2 solution in which

$$d_2/B = \sqrt{N_q} \quad \text{and} \quad \Theta = \pi/2$$

Consider a specific example with $c_0 = 5$ kPa, $k = 0$, $\phi = 38°$, $\gamma = 0$, $B = 2.5$ m and $q = 10$ kPa. The bearing capacity is $q_u = 796.1$ kPa, and $\sqrt{N_q} = 6.995$. Results from ABC:

| | $q_u$ (kPa) | $d_2/B$ | $\Theta$ (°) |
|---|---|---|---|
| **Adjust Mesh** | 796.3 | 6.996 | 90.00 |
| **Double Up 1** | 796.1 | 6.995 | 90.00 |
| **Double Up 2** | 796.1 | 6.995 | 90.00 |
| **Double Up 3** | 796.1 | 6.995 | 90.00 |

The correct $q_u$ is not calculated immediately; this is because the α characteristics in the fan zone are logarithmic spirals, so the treatment of each curved segment as a chord introduces a small error. As the mesh is refined, however, the approximate solution converges to the analytical one. Compared with the smooth case (Section 4.2.3), fewer **Double Up**s are required because the initial number of fan divisions selected by **Auto Guess** is greater.

Initial mesh of characteristics:

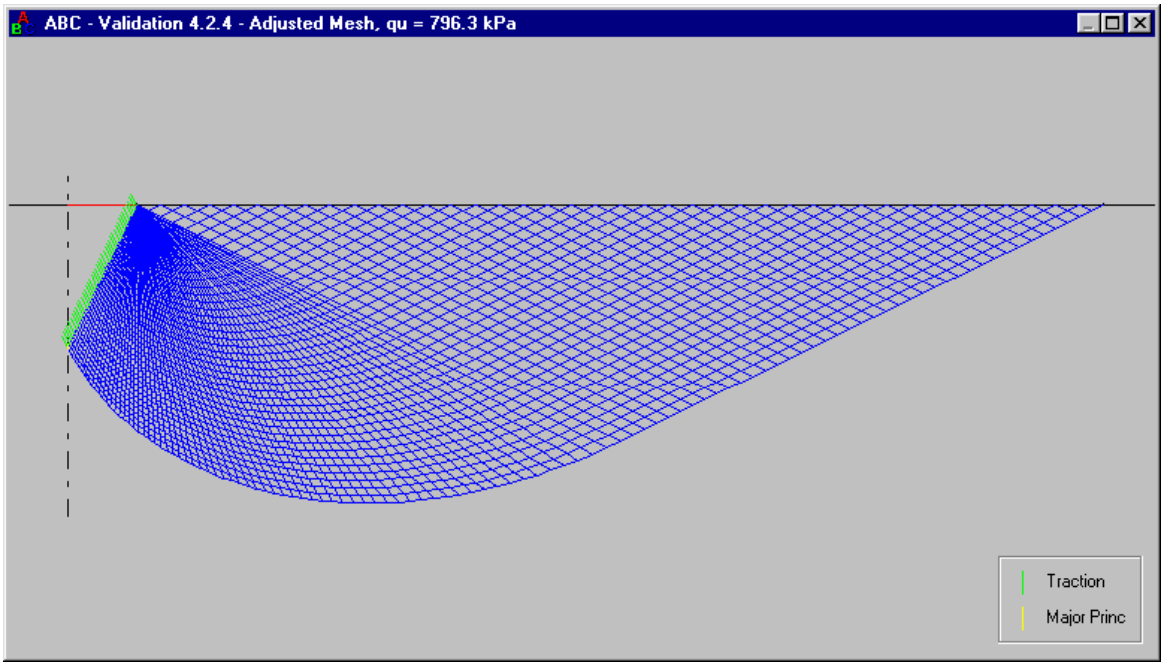

*4.2.5 Smooth strip footing on normally consolidated, undrained clay ($c_0 = 0$, $\phi = 0$)*

The bearing capacity is independent of $\gamma$ and is given by the analytical expression:

$$q_u = kB/4 + q$$

This result, due to Davis & Booker (1973), is obtained from a type 1 solution in which

$$d_1 = 0$$

As discussed in Section 2.7, this problem cannot be solved directly (i.e. with $c_0 = 0$) using ABC. It is, however, possible to approach the analytical solution in the limit as $kB/c_0 \to \infty$ (subject to the permitted maximum of $10^3$ that applies when $\phi < 1°$). Consider a series of analyses with fixed values of $k = 1$ kPa/m, $\phi = 0$, $\gamma = 0$ (or any other value), $B = 1$ m and $q = 0$, but with various values of $c_0 = 0.1, 0.05, 0.02, 0.01, \ldots$ kPa. Converged results from ABC:

| $kB/c_0$ | $q_u$ (kPa) | $d_1/B$ |
|---|---|---|
| 10 | 1.067 | 0.1752 |
| 20 | 0.7339 | 0.1262 |
| 50 | 0.5007 | 0.0769 |
| 100 | 0.4054 | 0.0509 |
| 200 | 0.3474 | 0.0326 |
| 500 | 0.3031 | 0.0175 |
| 1000 | 0.2836 | 0.0106 |

The results exhibit the expected behaviour (approaching 0.25 kPa and 0). When $kB/c_0 = \infty$ the analytical pressure distribution on the footing is linear with slope $k$, commencing from zero at the footing edge (Davis & Booker, 1973). In the ABC analyses, it is indeed found that this type of pressure distribution is beginning to become apparent when $kB/c_0 = 1000$:

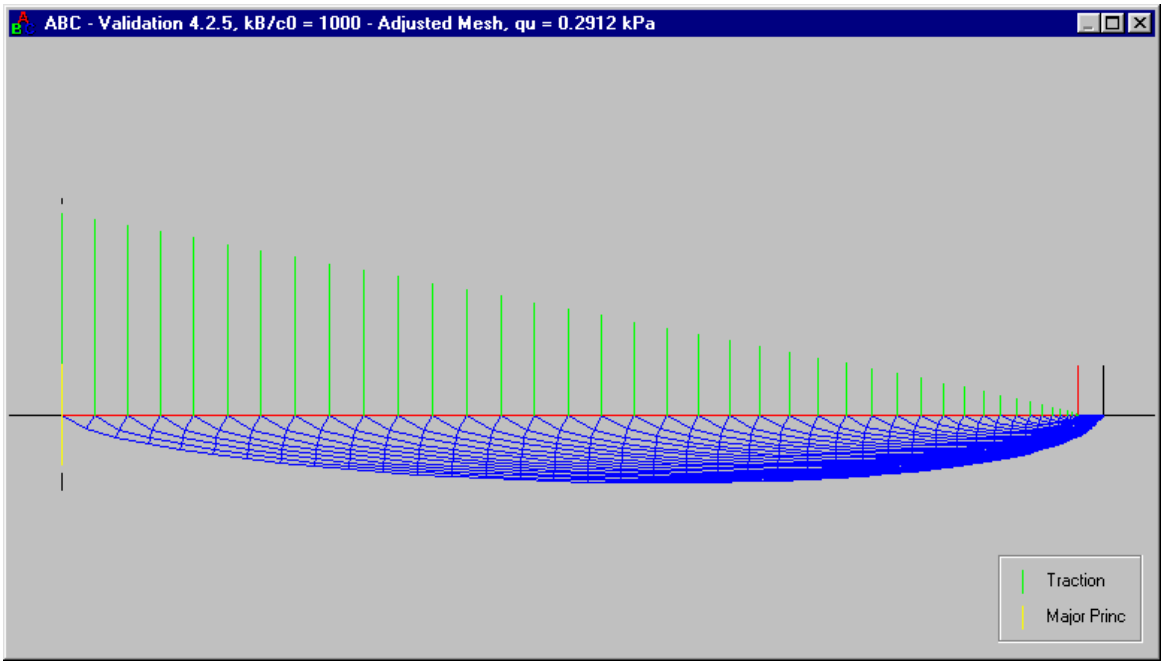

*4.2.6 Rough strip footing on normally consolidated, undrained clay ($c_0 = 0$, $\phi = 0$)*

The bearing capacity is independent of $\gamma$ and is given, as for the smooth case, by:

$$q_u = kB/4 + q$$

This result, due to Davis & Booker (1973), is obtained from a type 3 solution in which

$$d_1 = d_2 = 0$$

As discussed in Section 2.7, this problem cannot be solved directly (i.e. with $c_0 = 0$) using ABC. It is, however, possible to approach the analytical solution in the limit as $kB/c_0 \to \infty$ (subject to the permitted maximum of $10^3$ that applies when $\phi < 1°$). Consider a series of analyses with fixed values of $k = 1$ kPa/m, $\phi = 0$, $\gamma = 0$ (or any other value), $B = 1$ m and $q = 0$, but with various values of $c_0 = 0.1, 0.05, 0.02, 0.01, \ldots$ kPa. Converged results from ABC:

| $kB/c_0$ | $q_u$ (kPa) | $d_1/B$ | $d_2/B$ |
|---|---|---|---|
| 10 | 1.266 | 0.1967 | 0.0423 |
| 20 | 0.8701 | 0.1553 | 0.0161 |
| 50 | 0.5830 | 0.1020 | 0.0041 |
| 100 | 0.4616 | 0.0703 | 0.0013 |
| 200 | 0.3857 | 0.0467 | 0.0004 |
| 500 | 0.3259 | 0.0260 | 0.0001 |
| 1000 | 0.2990 | 0.0162 | 0.0000 |

The results exhibit the expected behaviour (approaching 0.25 kPa, 0 and 0). When $kB/c_0 = \infty$ the 'false head' region vanishes and the analytical pressure distribution on the footing is linear with slope *k*, commencing from zero at the footing edge (Davis & Booker, 1973). In the ABC analyses, it is indeed found that the 'false head' becomes smaller as $kB/c_0$ increases (the ratio $d_2/d_1 \to 0$), and the distinctive linear pressure distribution is beginning to become apparent when $kB/c_0 = 1000$:

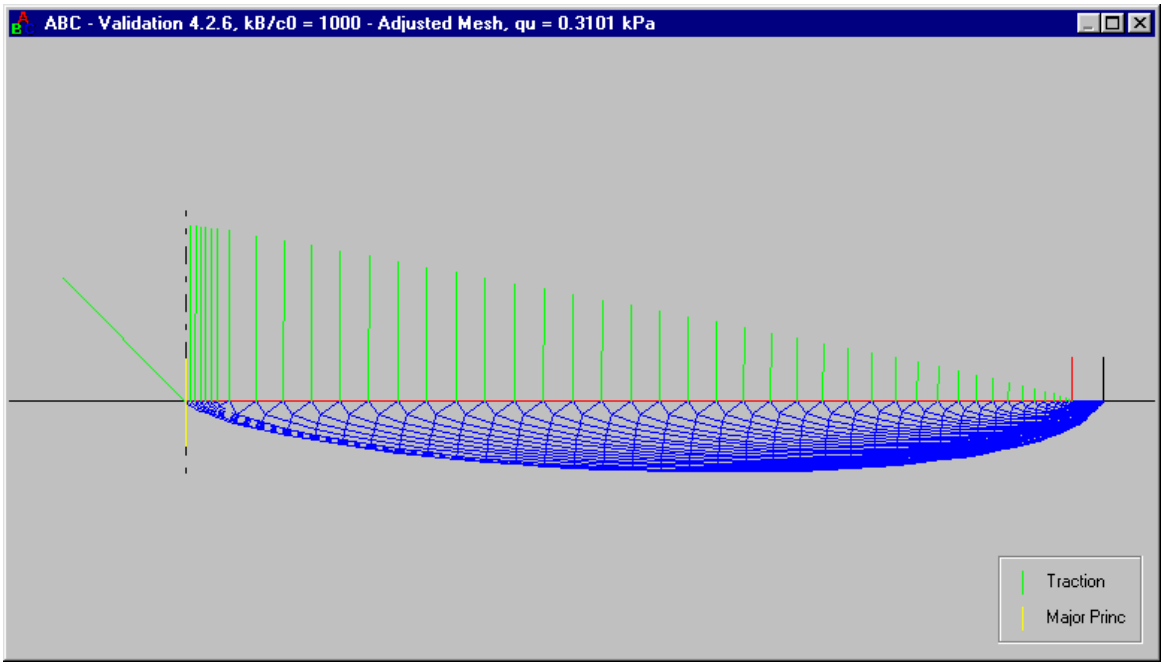

*4.2.7 Smooth strip footing on sand with no surcharge ($c_0 = k = 0$, $q = 0$)*

The bearing capacity is given by:

$$q_u = \gamma B N_\gamma / 2 \quad \text{where} \quad N_\gamma = f(\phi)$$

The factor of $1/2$ is traditional. This problem has been studied previously by Sokolovskii (1965), Hansen & Christensen (1969), Davis & Booker (1971) and Bolton & Lau (1993), among others.

As discussed in Sections 2.6 and 3.3.2, the $N_\gamma$ problem cannot be solved directly (i.e. with $q = 0$) using ABC. It is, however, possible to approach the no-surcharge condition in the limit as $\gamma B/q \to \infty$ (subject to the permitted maxima of $10^{12}$ when $\phi \geq 1°$ and $10^3$ when $\phi < 1°$). It is convenient to fix $c_0 = k = 0$, $\gamma = 1\,\text{kN/m}^3$, $B = 2\,\text{m}$ and let $q \to 0$; the average bearing pressure $q_u$ then corresponds directly to the bearing capacity factor $N_\gamma$. The analyses below were performed with $q = 10^{-9}$ kPa, giving $\gamma B/q = 2 \times 10^9$ which is ample for evaluating $N_\gamma$ to 4-digit precision (in fact it is ample for 6-digit precision). Converged results from ABC, with numerical results from other studies:

| $\phi$ (°) | $N_\gamma$ | | |
|---|---|---|---|
| | ABC | Sok. (1965)[2] | B. & L. (1993) |
| 5 | 0.08446 | 0.085 | 0.09 |
| 10 | 0.2809 | 0.28 | 0.29 |
| 15 | 0.6991 | 0.70 | 0.71 |
| 20 | 1.579 | 1.58 | 1.60 |
| 25 | 3.461 | 3.46 | 3.51 |
| 30 | 7.653 | 7.65 | 7.74 |
| 35 | 17.58 | 17.6 | 17.8 |
| 40 | 43.19 | 43.25 | 44 |
| 45 | 117.6 | — | 120 |
| 50 | 372.0 | — | 389 |

The ABC $N_\gamma$ values show very close agreement with those of Sokolovskii (1965). Most of the Bolton & Lau (1993) results are slightly high, and this could be because

- they used a relatively large surcharge, giving a $\gamma B/q$ value of just 2000;
- their analyses were performed with fixed numbers of $\alpha$ and $\beta$ characteristics (no mesh refinement was performed).

Unfortunately the $N_\gamma$ values of Hansen & Christensen (1969) and Davis & Booker (1971) are only presented in chart form, but they agree with ABC to within curve-reading accuracy.

The initial mesh of characteristics for $\phi = 30°$ is shown at the top of the next page but one.

[2] Converted from the values of $2N_\gamma$ that appear in the original.

*4.2.8 Rough strip footing on sand with no surcharge ($c_0 = k = 0$, $q = 0$)*

The bearing capacity is given by:

$$q_u = \gamma B N_\gamma / 2 \quad \text{where} \quad N_\gamma = f(\phi)$$

The factor of $1/2$ is traditional. This problem has been studied previously by Lundgren & Mortensen (1953), Caquot & Kerisel (1953), Hansen & Christensen (1969), Davis & Booker (1971), Salençon & Matar (1982a) and Bolton & Lau (1993), among others.

As discussed in Sections 2.6 and 3.3.2, the $N_\gamma$ problem cannot be solved directly (i.e. with $q = 0$) using ABC. It is, however, possible to approach the no-surcharge condition in the limit as $\gamma B/q \to \infty$ (subject to the permitted maxima of $10^{12}$ when $\phi \geq 1°$ and $10^3$ when $\phi < 1°$). It is convenient to fix $c_0 = k = 0$, $\gamma = 1\,\text{kN/m}^3$, $B = 2\,\text{m}$ and let $q \to 0$; the average bearing pressure $q_u$ then corresponds directly to the bearing capacity factor $N_\gamma$. The analyses below were performed with $q = 10^{-9}$ kPa, giving $\gamma B/q = 2 \times 10^9$ which is ample for evaluating $N_\gamma$ to 4-digit precision (in fact it is ample for 6-digit precision). Converged results from ABC, with numerical results from other studies:

| $\phi$ (°) | $N_\gamma$ | | | |
|---|---|---|---|---|
| | ABC | C. & K. (1953) | S. & M. (1982a)[3] | B. & L. (1993) |
| 5 | 0.1134 | — | — | 0.62 |
| 10 | 0.4332 | 1.604 | 0.434 | 1.71 |
| 15 | 1.181 | 2.98 | — | 3.17 |
| 20 | 2.839 | 5.69 | 2.84 | 5.97 |
| 25 | 6.491 | 11.22 | 6.491 | 11.6 |
| 30 | 14.75 | 22.69 | 14.75 | 23.6 |
| 35 | 34.48 | 49.1 | 34.46 | 51.0 |
| 40 | 85.57 | 114.0 | 85.513 | 121 |
| 45 | 234.2 | 300 | 234.01 | 324 |
| 50 | 742.9 | — | — | 1052 |

The ABC $N_\gamma$ values show very close agreement with those of Salençon & Matar (1982a). There is also close agreement with the one-off result presented by Lundgren & Mortensen (1953), namely $N_\gamma = 14.8$ for $\phi = 30°$. On the other hand, the results of both Caquot & Kerisel (1953) and Bolton & Lau (1993) are very high; in fact most of their proposed $N_\gamma$ values can be categorically ruled out because they lie above the strict upper bound solutions of Michalowski (1997), Ukritchon et al. (2003) and others. Although the comments made in Section 4.2.7 are equally applicable here, Bolton & Lau's (1993) results for the rough case are based on an incorrect treatment of the 'false head' region, and this is likely to be a more serious source of error. Coincidentally, the results of Caquot & Kerisel (1953) suffer from the same problem; see Lundgren (1953) and Martin (2004) for further details.

Unfortunately the $N_\gamma$ values of Hansen & Christensen (1969) and Davis & Booker (1971) are only presented in chart form, but they agree with ABC to within curve-reading accuracy.

The initial mesh of characteristics for $\phi = 30°$ is shown at the bottom of the next page.

[3] Converted from the values of $N_\gamma \cdot \cot\phi$ that appear in the original.

*Smooth strip footing on sand with no surcharge*

Initial mesh of characteristics for $\phi = 30°$ (note adaptively-added characteristics):

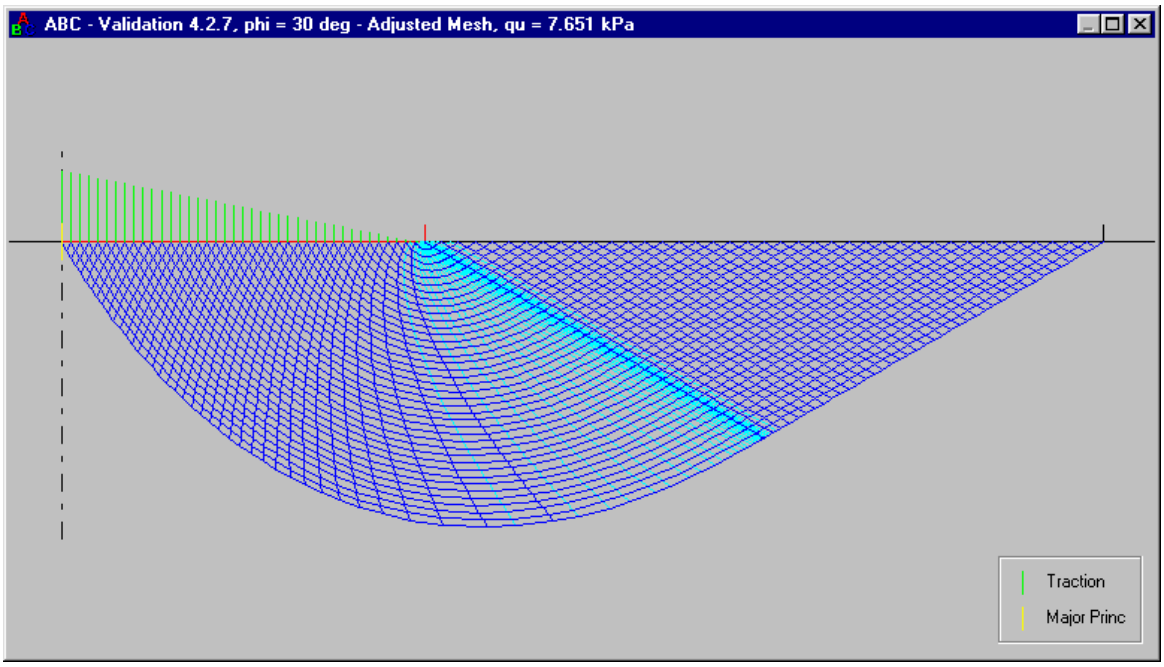


*Rough strip footing on sand with no surcharge*

Initial mesh of characteristics for $\phi = 30°$ (note adaptively-added characteristics):

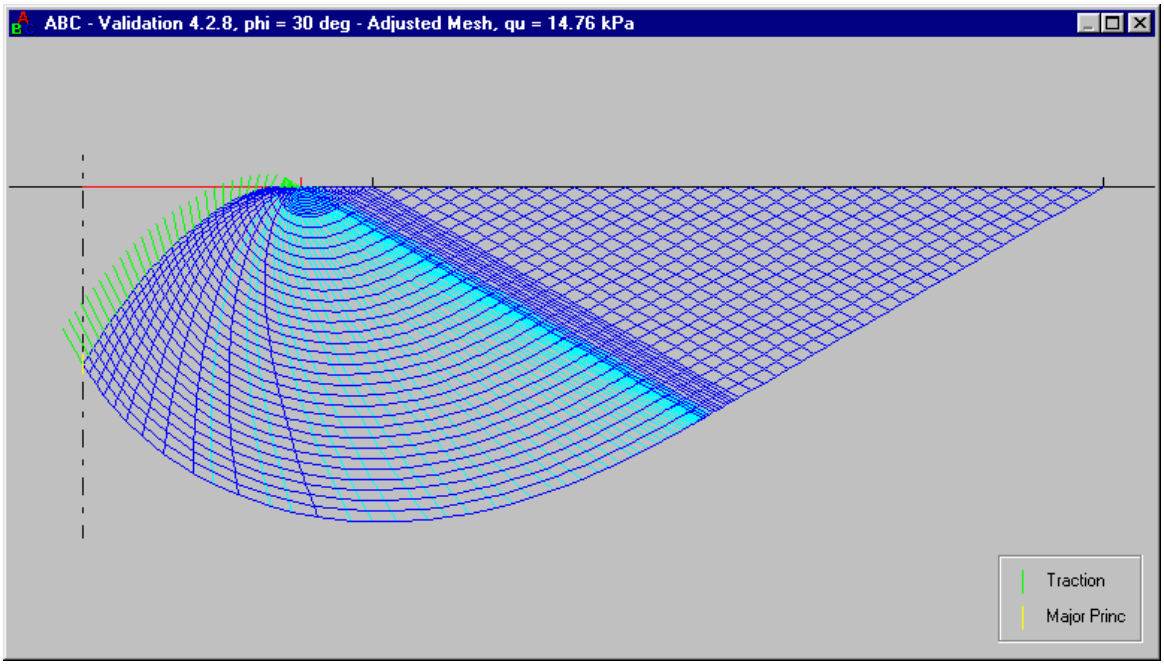

*4.2.9 Smooth strip footing on non-homogeneous, undrained clay ($\phi = 0$)*

The bearing capacity is independent of $\gamma$ and is given by:

$$q_u = c_0 N_c + q \quad \text{where} \quad N_c = f\left(kB/c_0\right)$$

This problem has been studied previously by Davis & Booker (1973), Houlsby & Wroth (1983) and Tani & Craig (1995).

It is convenient to fix $c_0 = 1\,\text{kPa}$, $\phi = 0$, $\gamma = 0$ (or any other value), $B = 1\,\text{m}$ and $q = 0$, then choose $k$ to give the desired $kB/c_0$; the average bearing pressure $q_u$ then corresponds directly to the bearing capacity factor $N_c$. Converged results from ABC, with numerical results from other studies:

| $kB/c_0$ | $N_c$ | | |
|---|---|---|---|
| | ABC | H. & W. (1983) | T. & C. (1995) |
| 0 | 5.142 | 5.14 | 5.14 |
| 1 | 5.982 | — | — |
| 2 | 6.661 | 6.66 | 6.66 |
| 4 | 7.819 | 7.82 | 7.82 |
| 6 | 8.839 | 8.84 | 8.84 |
| 8 | 9.781 | 9.78 | — |
| 10 | 10.67 | 10.67 | 10.67 |

There is perfect agreement between ABC and the other results.

Unfortunately the results of Davis & Booker (1973) are only presented in chart form, but they agree with ABC to within curve-reading accuracy.

Initial mesh of characteristics for $kB/c_0 = 6$:

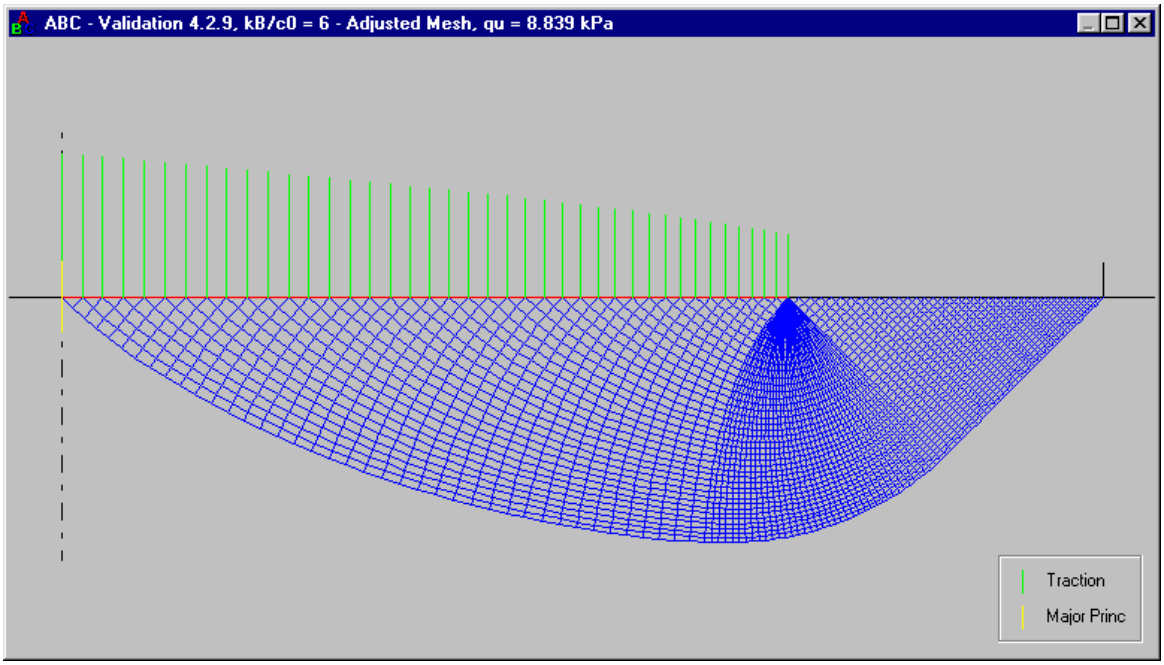

*4.2.10 Rough strip footing on non-homogeneous, undrained clay ($\phi = 0$)*

The bearing capacity is independent of $\gamma$ and is given by:

$$q_u = c_0 N_c + q \quad \text{where} \quad N_c = f\left(kB/c_0\right)$$

This problem has been studied previously by Davis & Booker (1973), Salençon & Matar (1982a), Houlsby & Wroth (1983) and Tani & Craig (1995).

It is convenient to fix $c_0 = 1\,\text{kPa}$, $\phi = 0$, $\gamma = 0$ (or any other value), $B = 1\,\text{m}$ and $q = 0$, then choose $k$ to give the desired $kB/c_0$; the average bearing pressure $q_u$ then corresponds directly to the bearing capacity factor $N_c$. Converged results from ABC, with numerical results from other studies:

| $kB/c_0$ | $N_c$ | | |
|---|---|---|---|
| | ABC | H. & W. (1983) | T. & C. (1995) |
| 0 | 5.142 | 5.14 | 5.14 |
| 1 | 6.609 | — | 6.84 |
| 2 | 7.597 | 7.57 | 7.75 |
| 4 | 9.130 | 9.08 | 9.23 |
| 6 | 10.42 | 10.37 | 10.49 |
| 8 | 11.58 | 11.52 | — |
| 10 | 12.66 | 12.67 | 12.73 |

In general there is close agreement between ABC and the other results. For small $kB/c_0$ the results of Tani & Craig (1995) are a little high, but their procedure for integrating the stresses acting on the 'false head' is suspect (Martin & Randolph, 2001).

Unfortunately the results of Davis & Booker (1973) and Salençon & Matar (1982a) are only presented in chart form, but they agree with ABC to within curve-reading accuracy.

Initial mesh of characteristics for $kB/c_0 = 6$:

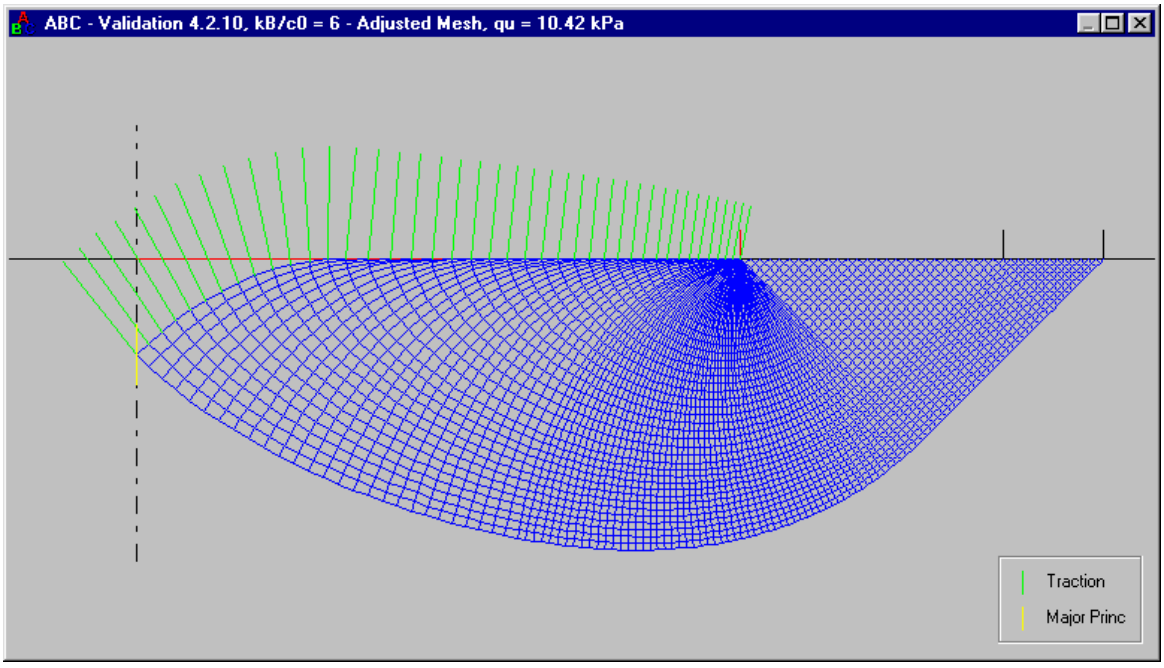

*4.2.11 Smooth strip footing on general cohesive-frictional soil*

Cox (1962) considered a series of problems involving a smooth strip footing on a general *c*-ϕ-γ soil. He defined a "relative cohesion" $c^*$ which in the present notation is equivalent to $c_0 + q\tan\phi$, the term that appears in the denominator of *F* in equation (4.1). To characterise the relative importance of self-weight and cohesion/surcharge, he used a dimensionless ratio

$$G = \frac{\gamma B/2}{c^*}$$

Since Cox was only concerned with homogeneous soil ($k = 0$), there is a simple relationship between his *G* the dimensionless ratio *F* used here, namely $F = 2G\tan\phi$.

In Cox (1962) the results are presented as average bearing pressures, normalised with respect to $c^*$:

TABLE 2. VALUES OF THE MEAN YIELD-POINT PRESSURE $p_2/c^*$ FOR DIE INDENTATION

| $\phi$ \ $G$ | 0 | $10^{-2}$ | $10^{-1}$ | 1 | 10 |
|---|---|---|---|---|---|
| 0° | 5·14 | 5·14 | 5·14 | 5·14 | 5·14 |
| 10° | 8·34 | 8·35 | 8·42 | 9·02 | 13·6 |
| 20° | 14·83 | 14·87 | 15·2 | 17·9 | 37·8 |
| 30° | 30·14 | 30·29 | 31·6 | 42·9 | 127 |
| 40° | 75·31 | 76·13 | 83·0 | 139 | 574 |

To reproduce these analyses in ABC it is convenient to fix $c_0 = 1\,\text{kPa}$, $k = 0$, $B = 2\,\text{m}$ and $q = 0$; the unit weight γ then corresponds directly to *G*, and the average bearing pressure $q_u$ corresponds directly to the normalised pressure in Cox's table. Converged results from ABC:

| ϕ (°) | *G* | | | | |
|---|---|---|---|---|---|
| | 0 | $10^{-2}$ | $10^{-1}$ | 1 | 10 |
| 0 | 5.142 | 5.142 | 5.142 | 5.142 | 5.142 |
| 10 | 8.345 | 8.352 | 8.417 | 9.020 | 13.56 |
| 20 | 14.83 | 14.87 | 15.17 | 17.89 | 37.76 |
| 30 | 30.14 | 30.29 | 31.61 | 42.87 | 126.7 |
| 40 | 75.31 | 76.13 | 83.05 | 139.0 | 573.3 |

There is very close agreement between the two sets of results. The results in the first row ($\phi = 0$) the first column ($G = 0$) of each table can of course be obtained analytically (see Sections 4.2.1 and 4.2.3), but the other 16 entries can only be obtained numerically.

*4.2.12 Rough strip footing on general cohesive-frictional soil*

Salençon & Matar (1982b) considered a series of problems involving a rough strip footing on a general *c*-ϕ-γ soil. The parameters for these problems, including the dimensionless ratio *F* defined in equation (4.1), were as follows:

| Problem[4] | $c_0$ (kPa) | $k$ (kPa/m) | ϕ (°) | γ (kN/m$^3$) | $B$ (m) | $q$ (kPa) | $F$ |
|---|---|---|---|---|---|---|---|
| A4 | 1 | 2.5 | 0 | 16 | 4 | 0 | 10 |
| A5 | 1 | 2.5 | 4 | 16 | 4 | 0 | 14.48 |
| A6 | 1 | 2.5 | 10 | 16 | 4 | 0 | 21.28 |
| B1 | 0 | 0.6 | 0 | 16 | 40 | 0 | ∞ |
| B2 | 0 | 0.6 | 4 | 16 | 40 | 0 | ∞ |
| B3 | 0 | 0.6 | 10 | 16 | 40 | 0 | ∞ |
| C | 16 | 0 | 30 | 18 | 4 | 18 | 1.575 |

The A and C problems can be solved without difficulty, but the B problems require special treatment because $F = \infty$. For problem B1, $\phi = 0$ and $F = \infty$ so the analytical solution $q_u = kB/4 + q$ is applicable (see Section 4.2.6). Problems B2 and B3 also have $F = \infty$, but now $\phi > 0$ so the situation is analogous to that of the '$N_\gamma$ problem' considered in Section 4.2.8. To solve these problems using ABC it is first necessary to introduce a nominal $c_0$ (or a nominal $q$) to make $F$ very large, but not greater than the permitted maximum of $10^{12}$ that applies when $\phi \geq 1°$. The analyses below were performed with $c_0 = 10^{-9}$ kPa, giving $F$ values of $6.9 \times 10^{10}$ for problem B2 and $1.4 \times 10^{11}$ for B3. Converged results from ABC, with numerical results from Salençon & Matar (1982b):

| Problem | $q_u$ (kPa) | |
|---|---|---|
| | ABC | S. & M. (1982b) |
| A4 | 12.66 | 12.6 |
| A5 | 20.91 | 20.3 |
| A6 | 44.99 | 44.9 |
| B1 | 6† | 6† |
| B2 | 38.64 | 38.5 |
| B3 | 168.1 | 168.3 |
| C | $1.626 \times 10^3$ | $1.61 \times 10^3$ |
| | † analytical | † analytical |

There is very close agreement between the two sets of results. Note that exact agreement would not be expected because Salençon & Matar (1982b) used the method of characteristics to produce a series of charts in terms of ϕ and (in the present notation) *F*. Their results for the example problems were based on factors read back from these charts, and not on a direct solution of each problem using the method of characteristics, as is done in ABC.

[4] Problems A1 to A3 involved a soil layer of limited depth.

### 4.3 Axial Symmetry

*4.3.1 Smooth circular footing on homogeneous, undrained clay ($k = 0$, $\phi = 0$)*

The bearing capacity is independent of $\gamma$ and is given by:

$$q_u = c_0 N_c + q \quad \text{where} \quad N_c = 5.69$$

Shield (1955) was the first to obtain this (numerical) result, with a type 1 solution in which

$$d_1 / B = 0.29$$

It is convenient to fix $c_0 = 1\,\text{kPa}$, $k = 0$, $\phi = 0$, $\gamma = 0$ (or any other value), $B = 1\,\text{m}$ (or any other value) and $q = 0$; the average bearing pressure $q_u$ then corresponds directly to the bearing capacity factor $N_c$. Results from ABC:

| | $N_c$ | $d_1/B$ |
|---|---|---|
| **Adjust Mesh** | 5.689 | 0.2872 |
| **Double Up 1** | 5.689 | 0.2872 |
| **Double Up 2** | 5.689 | 0.2871 |

The ABC values agree with those of Shield (1955).

Initial mesh of characteristics:

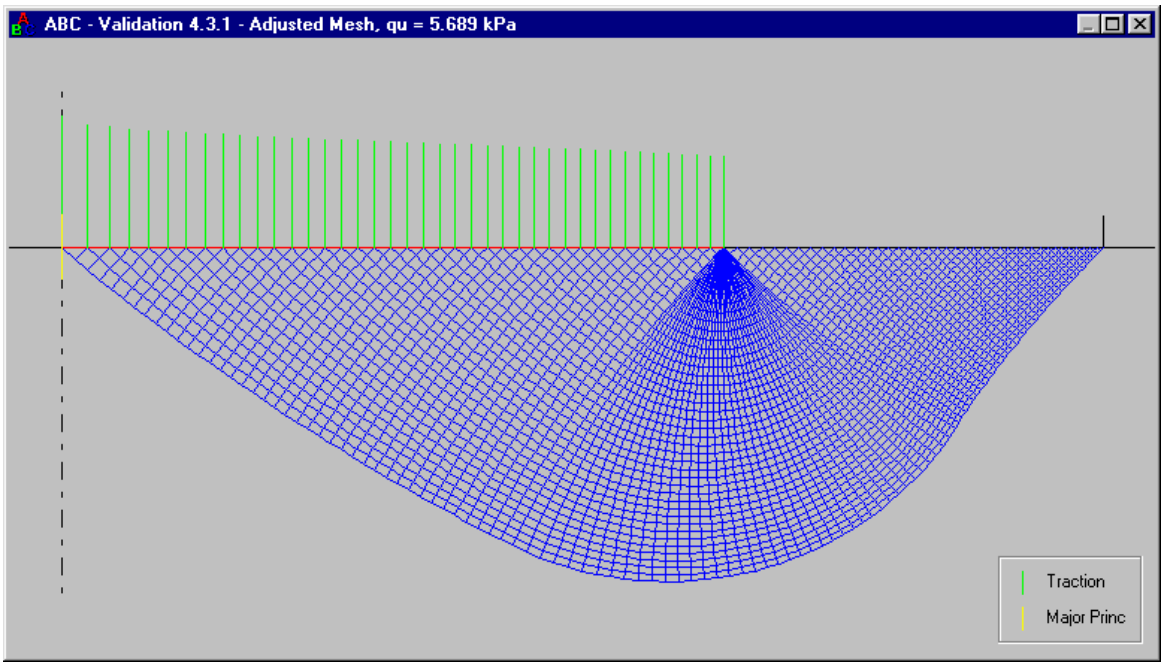

*4.3.2 Rough circular footing on homogeneous, undrained clay ($k = 0$, $\phi = 0$)*

The bearing capacity is independent of $\gamma$ and is given by:

$$q_u = c_0 N_c + q \quad \text{where} \quad N_c = 6.05$$

Eason & Shield (1960) were the first to obtain this (numerical) result, with a type 2 solution in which

$$d_2/B = 0.44 \quad \text{and} \quad \Theta = 116°$$

It is convenient to fix $c_0 = 1\,\text{kPa}$, $k = 0$, $\phi = 0$, $\gamma = 0$ (or any other value), $B = 1\,\text{m}$ (or any other value) and $q = 0$; the average bearing pressure $q_u$ then corresponds directly to the bearing capacity factor $N_c$. Results from ABC:

| | $N_c$ | $d_2/B$ | $\Theta$ (°) |
|---|---|---|---|
| **Adjust Mesh** | 6.047 | 0.4405 | 116.1 |
| **Double Up 1** | 6.048 | 0.4401 | 116.1 |
| **Double Up 2** | 6.048 | 0.4400 | 116.1 |
| **Double Up 3** | 6.048 | 0.4399 | 116.1 |

The ABC values agree with those of Eason & Shield (1960).

Initial mesh of characteristics:

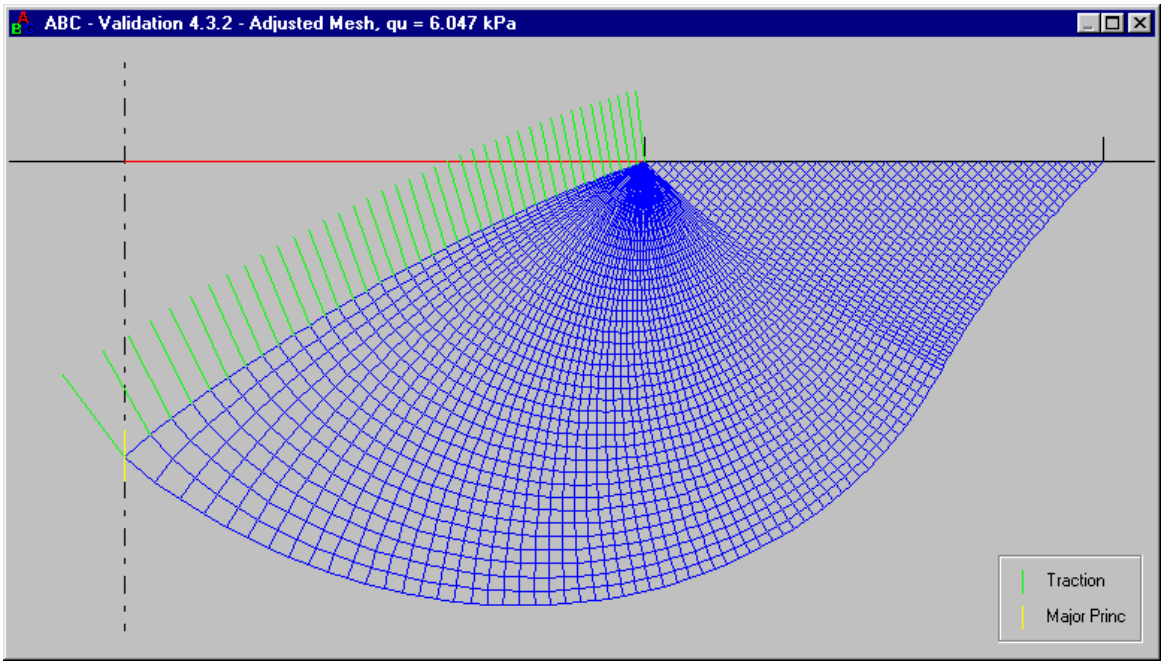

*4.3.3 Smooth circular footing on homogeneous, weightless, cohesive-frictional soil ($k=0$, $\gamma=0$)*

The bearing capacity is given by:

$$q_u = c_0 N_c + q N_q \quad \text{where} \quad \begin{cases} N_c = \left(N_q - 1\right)\cot\phi \\ N_q = f\left(\phi\right) \end{cases}$$

This problem has been studied previously by Cox et al. (1961) and Bolton & Lau (1993).

It is convenient to fix $c_0 = 0$, $k = 0$, $\gamma = 0$, $B = 1\,\text{m}$ (or any other value) and $q = 1\,\text{kPa}$; the average bearing pressure $q_u$ then corresponds directly to the bearing capacity factor $N_q$. Converged results from ABC, with numerical results from other studies:

| $\phi$ (°) | $N_q$ | | |
|---|---|---|---|
| | ABC | C. et al. (1961)[5] | B. & L. (1993) |
| 5 | 1.650 | 1.65 | 1.65 |
| 10 | 2.761 | 2.76 | 2.80 |
| 15 | 4.718 | 4.72 | 4.70 |
| 20 | 8.307 | 8.32 | 8.30 |
| 25 | 15.23 | 15.2 | 15.2 |
| 30 | 29.45 | 29.5 | 29.5 |
| 35 | 61.11* | 61.1 | 61.0 |
| 40 | 139.2* | 139 | 140 |
| 45 | 359.1* | — | 359 |
| 50 | $1.099\times10^3$ * | — | 1103 |

There is very close agreement between ABC and the other results. The solutions for higher friction angles, indicated by *, involve crossing β characteristics (see Section 3.6.2).

Initial mesh of characteristics for $\phi = 30°$:

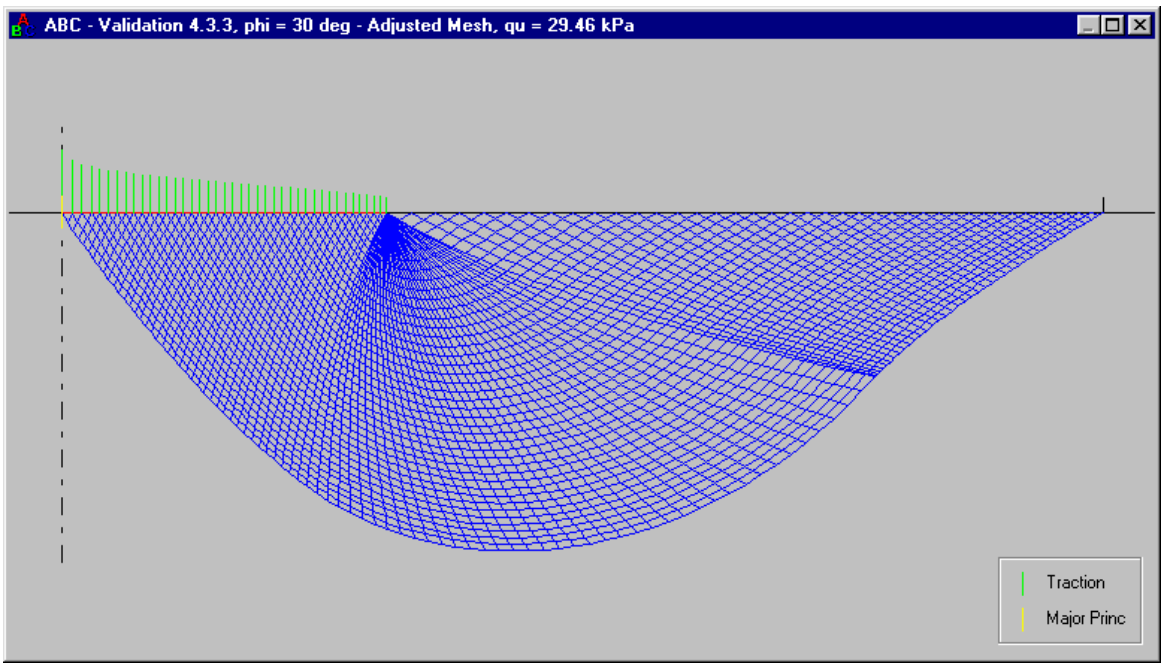


[5] Converted from the values of $N_c$ that appear in the original.

*4.3.4 Rough circular footing on homogeneous, weightless, cohesive-frictional soil ($k=0$, $\gamma=0$)*

The bearing capacity is given by:

$$q_u = c_0 N_c + q N_q \quad \text{where} \quad \begin{cases} N_c = \left(N_q - 1\right)\cot\phi \\ N_q = f\left(\phi\right) \end{cases}$$

This problem has been studied previously by Bolton & Lau (1993) and, indirectly, by Salençon & Matar (1982a).

It is convenient to fix $c_0 = 0$, $k = 0$, $\gamma = 0$, $B = 1\,\text{m}$ (or any other value) and $q = 1\,\text{kPa}$; the average bearing pressure $q_u$ then corresponds directly to the bearing capacity factor $N_q$. Converged results from ABC, with numerical results from Bolton & Lau (1993):

| $\phi$ (°) | $N_q$ | |
|---|---|---|
| | ABC | B. & L. (1993) |
| 5 | 1.705 | 1.65 |
| 10 | 2.955 | 2.80 |
| 15 | 5.246 | 4.70 |
| 20 | 9.618 | 8.30 |
| 25 | 18.40* | 15.2 |
| 30 | 37.21* | 29.5 |
| 35 | 80.81* | 61.0 |
| 40 | 192.7* | 140 |
| 45 | 520.6* | 359 |
| 50 | $1.666\times10^3$ * | 1103 |

ABC predicts $N_q$ values that are greater than those for the smooth case (Section 4.3.3), whereas Bolton & Lau (1993) envisage that roughness has no effect; this is discussed below. The solutions for higher friction angles, indicated by *, involve crossing β characteristics (see Section 3.6.2).

Initial mesh of characteristics for $\phi = 30°$ (note crossing β characteristics):

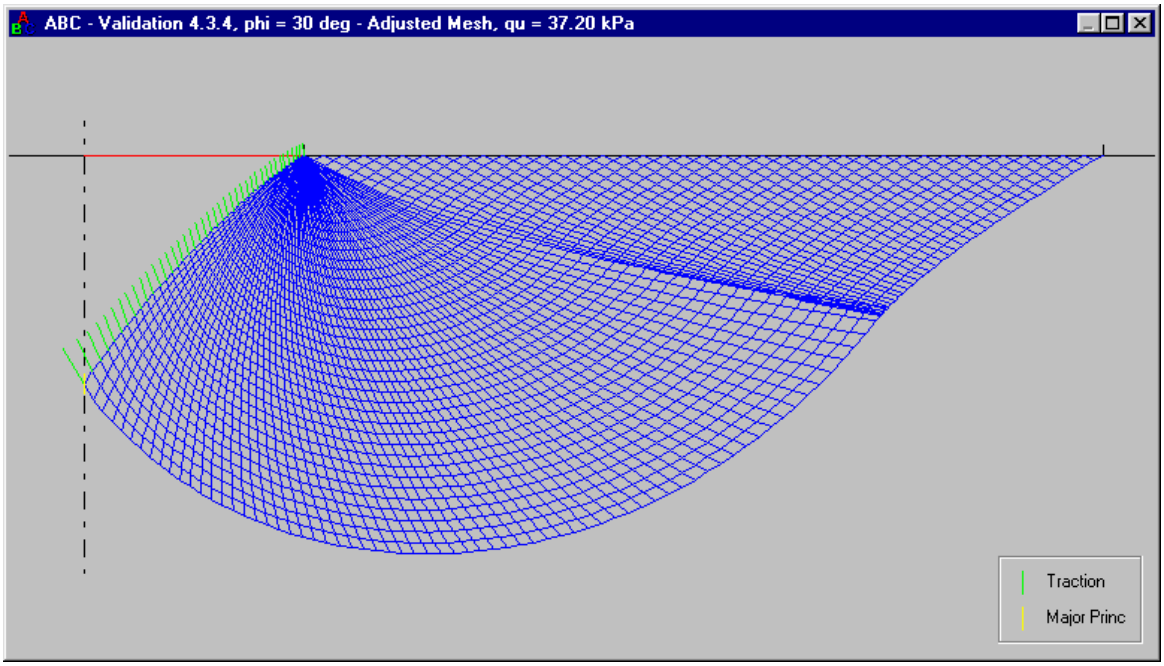

The discrepancy between ABC and Bolton & Lau (1993) can be resolved by seeking a third opinion from Salençon & Matar (1982a), who take the alternative (and totally equivalent) view that the bearing capacity for this problem is given by:

$$q_u = c_0 N_c + q N_q \quad \text{where} \quad \begin{cases} N_c = f(\phi) \\ N_q = N_c \tan\phi + 1 \end{cases}$$

Salençon & Matar define a shape factor

$$\nu = N_{c,\text{circular}} / N_{c,\text{strip}}$$

but unfortunately they do not give numerical results for either ν or $N_{c,\text{circular}}$, just a plot of ν as a function of ϕ. This is shown below, together with the corresponding curves obtained from ABC and from Bolton & Lau (1993).

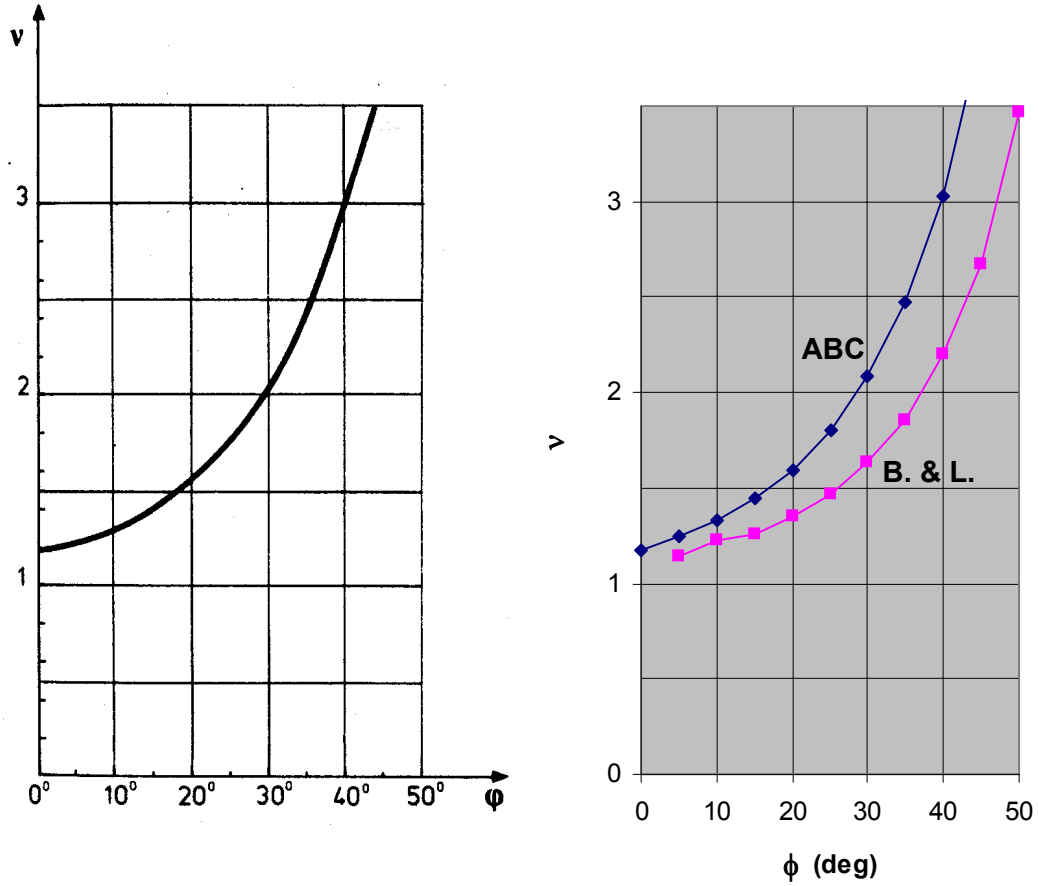


The comparison with Salençon & Matar (1982a) confirms, albeit indirectly, that the ABC-derived values of $N_q$ should be preferred to those of Bolton & Lau (1993) in the table above.

*4.3.5 Smooth circular footing on normally consolidated, undrained clay ($c_0 = 0$, $\phi = 0$)*

The bearing capacity is independent of $\gamma$ and is given by the analytical expression:

$$q_u = kB/6 + q$$

This result, due to Salençon & Matar (1982a), is obtained from a type 1 solution in which

$$d_1 = 0$$

As discussed in Section 2.7, this problem cannot be solved directly (i.e. with $c_0 = 0$) using ABC. It is, however, possible to approach the analytical solution in the limit as $kB/c_0 \to \infty$ (subject to the permitted maximum of $10^3$ that applies when $\phi < 1°$). Consider a series of analyses with fixed values of $k = 1$ kPa/m, $\phi = 0$, $\gamma = 0$ (or any other value), $B = 1$ m and $q = 0$, but with various values of $c_0 = 0.1, 0.05, 0.02, 0.01, \ldots$ kPa. Converged results from ABC:

| $kB/c_0$ | $q_u$ (kPa) | $d_1/B$ |
|---|---|---|
| 10 | 0.9642 | 0.1233 |
| 20 | 0.6287 | 0.0913 |
| 50 | 0.4013 | 0.0573 |
| 100 | 0.3111 | 0.0384 |
| 200 | 0.2572 | 0.0249 |
| 500 | 0.2165 | 0.0134 |
| 1000 | 0.1987 | 0.0081 |

The results exhibit the expected behaviour (approaching 0.1667 kPa and 0). When $kB/c_0 = \infty$ the analytical pressure distribution on the footing is linear with slope $k$, commencing from zero at the footing edge (Salençon & Matar, 1982a). In the ABC analyses, it is indeed found that this type of pressure distribution is beginning to become apparent when $kB/c_0 = 1000$:

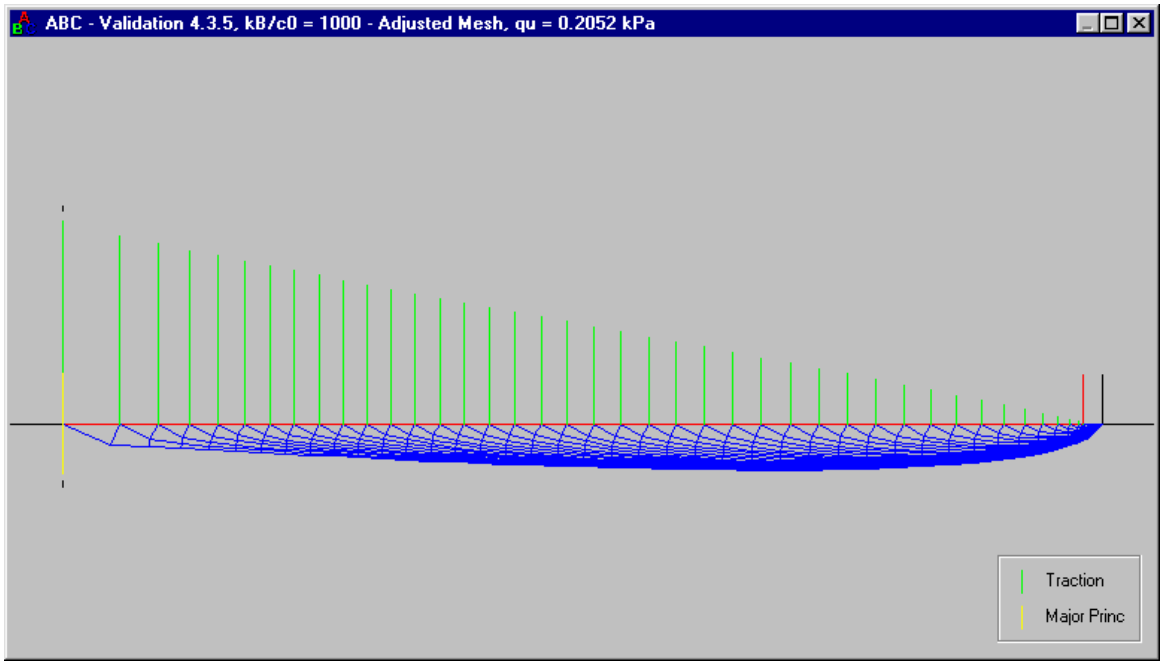

*4.3.6 Rough circular footing on normally consolidated, undrained clay ($c_0 = 0$, $\phi = 0$)*

The bearing capacity is independent of $\gamma$ and is given, as for the smooth case, by:

$$q_u = kB/6 + q$$

This result, due to Salençon & Matar (1982a), is obtained from a type 3 solution in which

$$d_1 = d_2 = 0$$

As discussed in Section 2.7, this problem cannot be solved directly (i.e. with $c_0 = 0$) using ABC. It is, however, possible to approach the analytical solution in the limit as $kB/c_0 \to \infty$ (subject to the permitted maximum of $10^3$ that applies when $\phi < 1°$). Consider a series of analyses with fixed values of $k = 1$ kPa/m, $\phi = 0$, $\gamma = 0$ (or any other value), $B = 1$ m and $q = 0$, but with various values of $c_0 = 0.1, 0.05, 0.02, 0.01, \ldots$ kPa. Converged results from ABC:

| $kB/c_0$ | $q_u$ (kPa) | $d_1/B$ | $d_2/B$ |
|---|---|---|---|
| 10 | 1.137 | 0.1508 | 0.0110 |
| 20 | 0.7447 | 0.1175 | 0.0030 |
| 50 | 0.4708 | 0.0769 | 0.0004 |
| 100 | 0.3586 | 0.0531 | 0.0001 |
| 200 | 0.2897 | 0.0354 | 0.0000 |
| 500 | 0.2361 | 0.0198 | 0.0000 |
| 1000 | 0.2121 | 0.0123 | 0.0000 |

The results exhibit the expected behaviour (approaching 0.1667 kPa, 0 and 0). When $kB/c_0 = \infty$ the 'false head' region vanishes and the analytical pressure distribution on the footing is linear with slope *k*, commencing from zero at the footing edge (Salençon & Matar, 1982a). In the ABC analyses, it is indeed found that the 'false head' becomes smaller as $kB/c_0$ increases (the ratio $d_2/d_1 \to 0$), and the distinctive linear pressure distribution is beginning to become apparent when $kB/c_0 = 1000$:

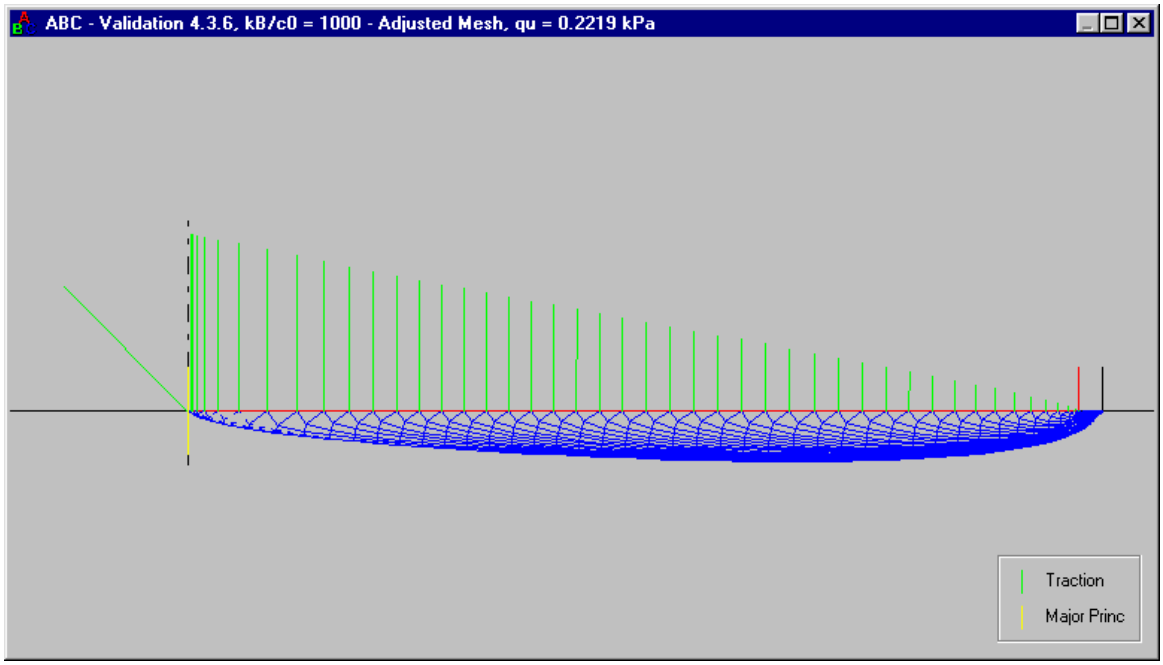

*4.3.7 Smooth circular footing on sand with no surcharge ($c_0 = k = 0$, $q = 0$)*

The bearing capacity is given by:

$$q_u = \gamma B N_\gamma / 2 \quad \text{where} \quad N_\gamma = f(\phi)$$

The factor of $1/2$ is traditional. This problem has been studied previously by Bolton & Lau (1993) and Cassidy & Houlsby (2002).

As discussed in Sections 2.6 and 3.3.2, the $N_\gamma$ problem cannot be solved directly (i.e. with $q = 0$) using ABC. It is, however, possible to approach the no-surcharge condition in the limit as $\gamma B/q \to \infty$ (subject to the permitted maxima of $10^{12}$ when $\phi \geq 1°$ and $10^3$ when $\phi < 1°$). It is convenient to fix $c_0 = k = 0$, $\gamma = 1\,\text{kN/m}^3$, $B = 2\,\text{m}$ and let $q \to 0$; the average bearing pressure $q_u$ then corresponds directly to the bearing capacity factor $N_\gamma$. The analyses below were performed with $q = 10^{-9}$ kPa, giving $\gamma B/q = 2 \times 10^9$ which is ample for evaluating $N_\gamma$ to 4-digit precision (in fact it is ample for 6-digit precision). Converged results from ABC, with numerical results from other studies:

| $\phi$ (°) | $N_\gamma$ | | |
|---|---|---|---|
| | ABC | B. & L. (1993) | C. & H. (2002) |
| 5 | 0.05975 | 0.06 | 0.062 |
| 10 | 0.2059 | 0.21 | 0.200 |
| 15 | 0.5346 | 0.60 | 0.553 |
| 20 | 1.271 | 1.30 | 1.219 |
| 25 | 2.971 | 3.00 | 2.865 |
| 30 | 7.111 | 7.10 | 6.935 |
| 35 | 18.03 | 18.2 | 17.88 |
| 40 | 50.16 | 51 | 50.46 |
| 45 | 159.8 | 160 | 165.1 |
| 50 | 617.8 | 621 | 703.1 |

The ABC $N_\gamma$ values generally agree quite closely with the other results. Most of the Bolton & Lau (1993) results are slightly high, and this could be because

- they used a relatively large surcharge, giving a $\gamma B/q$ value of just 2000;
- their analyses were performed with fixed numbers of $\alpha$ and $\beta$ characteristics (no mesh refinement was performed).

Similarly it seems that Cassidy & Houlsby (2002) did not perform any case-by-case mesh refinement checks. Although most of their results are within a few percent of the converged ABC values, their result for $\phi = 50°$ is high by about 14%.

The initial mesh of characteristics for $\phi = 30°$ is shown at the top of the next page but one.

*4.3.8 Rough circular footing on sand with no surcharge ($c_0 = k = 0$, $q = 0$)*

The bearing capacity is given by:

$$q_u = \gamma B N_\gamma / 2 \quad \text{where} \quad N_\gamma = f(\phi)$$

The factor of $1/2$ is traditional. This problem has been studied previously by Salençon & Matar (1982a), Bolton & Lau (1993) and Cassidy & Houlsby (2002).

As discussed in Sections 2.6 and 3.3.2, the $N_\gamma$ problem cannot be solved directly (i.e. with $q = 0$) using ABC. It is, however, possible to approach the no-surcharge condition in the limit as $\gamma B/q \to \infty$ (subject to the permitted maxima of $10^{12}$ when $\phi \geq 1°$ and $10^3$ when $\phi < 1°$). It is convenient to fix $c_0 = k = 0$, $\gamma = 1\,\text{kN/m}^3$, $B = 2\,\text{m}$ and let $q \to 0$; the average bearing pressure $q_u$ then corresponds directly to the bearing capacity factor $N_\gamma$. The analyses below were performed with $q = 10^{-9}$ kPa, giving $\gamma B/q = 2 \times 10^9$ which is ample for evaluating $N_\gamma$ to 4-digit precision (in fact it is ample for 6-digit precision). Converged results from ABC, with numerical results from other studies:

| $\phi$ (°) | $N_\gamma$ | | | |
|---|---|---|---|---|
| | ABC | S. & M. (1982a)[6] | B. & L. (1993) | C. & H. (2002) |
| 5 | 0.08063 | — | 0.68 | 0.067 |
| 10 | 0.3224 | 0.33 | 1.37 | 0.266 |
| 15 | 0.9323 | — | 2.83 | 0.796 |
| 20 | 2.416 | 2.4 | 6.04 | 2.160 |
| 25 | 6.073 | 6.0 | 13.5 | 5.270 |
| 30 | 15.52 | 15.2 | 31.9 | 14.13 |
| 35 | 41.88 | 41.4 | 82.4 | 42.56 |
| 40 | 123.7 | 121 | 238 | 129.4 |
| 45 | 417.7 | 388 | 803 | 505.0 |
| 50 | $1.710 \times 10^3$ | — | 3403 | 2050.0 |

The ABC $N_\gamma$ values generally agree quite closely with those of Salençon & Matar (1982a), bearing in mind the limited precision of the latter (see footnote). On the other hand the results of Bolton & Lau (1993) are very high, as noted previously by Cassidy & Houlsby (2002). Although the comments made in Section 4.3.7 are equally applicable here, Bolton & Lau's (1993) results for the rough case are based on an incorrect treatment of the 'false head' region, and this is likely to be a more serious source of error. The results of Cassidy & Houlsby (2002) are broadly comparable with the converged ABC values, though unlike the smooth case (Section 4.3.7) there is now a systematic pattern of disagreement, ranging from –17% at small $\phi$ to +20% at large $\phi$.

The initial mesh of characteristics for $\phi = 30°$ is shown at the bottom of the next page.

[6] Converted from the values of $N_\gamma \cdot \cot\phi$ (plane strain) and the shape factor $\nu$ that appear in the original, e.g. for $\phi = 30°$ these values are 25.55 and 1.03, giving $N_\gamma = 25.55 \times \tan(30°) \times 1.03 = 15.2$.

*Smooth circular footing on sand with no surcharge*

Initial mesh of characteristics for $\phi = 30°$ (note adaptively-added characteristics):

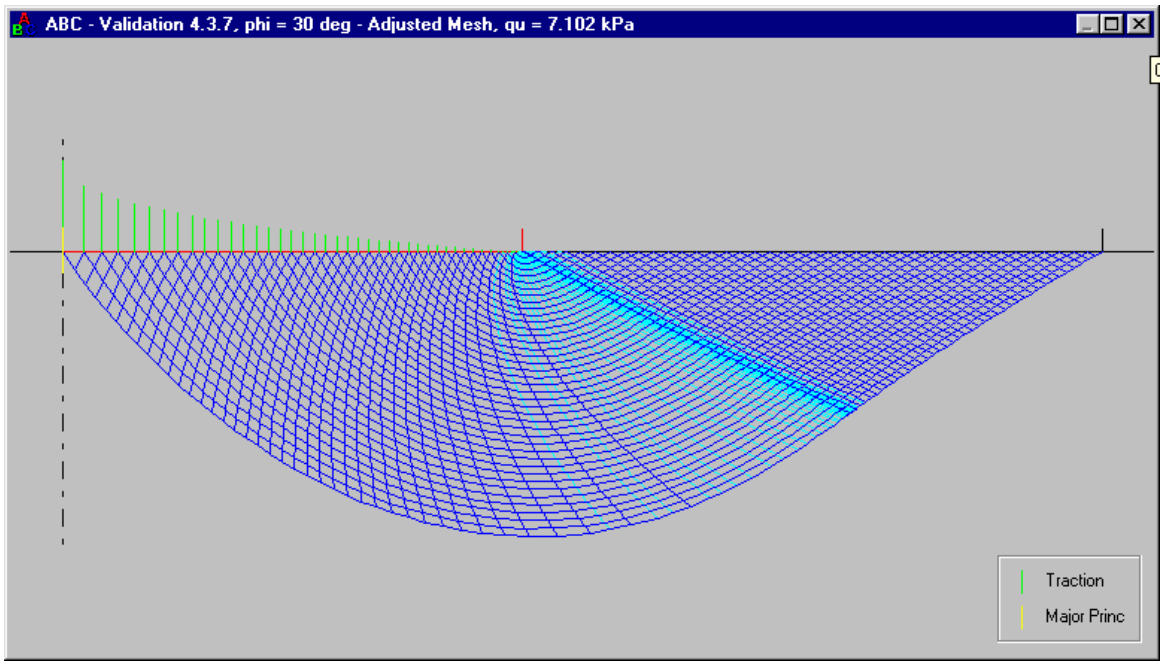


*Rough circular footing on sand with no surcharge*

Initial mesh of characteristics for $\phi = 30°$ (note adaptively-added characteristics):

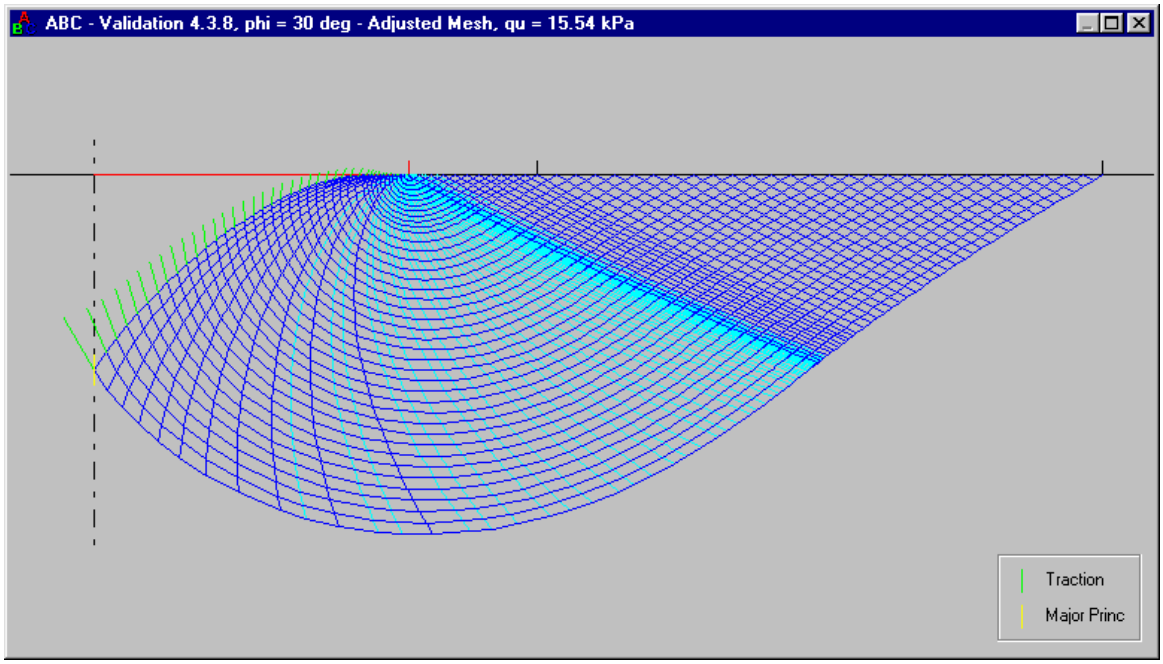

*4.3.9 Smooth circular footing on non-homogeneous, undrained clay ($\phi = 0$)*

The bearing capacity is independent of $\gamma$ and is given by:

$$q_u = c_0 N_c + q \quad \text{where} \quad N_c = f\left(kB/c_0\right)$$

This problem has been studied previously by Houlsby & Wroth (1983), Martin (1994) [see also Houlsby & Martin (2003)] and Tani & Craig (1995).

It is convenient to fix $c_0 = 1\,\text{kPa}$, $\phi = 0$, $\gamma = 0$ (or any other value), $B = 1\,\text{m}$ and $q = 0$, then choose $k$ to give the desired $kB/c_0$; the average bearing pressure $q_u$ then corresponds directly to the bearing capacity factor $N_c$. Converged results from ABC, with numerical results from other studies:

| $kB/c_0$ | $N_c$ | | | |
|---|---|---|---|---|
| | ABC | H. & W. (1983) | Martin (1994) | T. & C. (1995) |
| 0 | 5.689 | 5.69 | 5.69 | 5.69 |
| 1 | 6.246 | — | 6.25 | — |
| 2 | 6.723 | 6.74 | 6.73 | 6.72 |
| 3 | 7.154 | — | 7.16 | — |
| 4 | 7.556 | 7.58 | 7.56 | 7.55 |
| 5 | 7.937 | — | 7.94 | — |
| 6 | 8.300 | 8.33 | — | 8.30 |
| 8 | 8.990 | 9.03 | — | — |
| 10 | 9.642 | 9.67 | — | 9.64 |

There is very close agreement between ABC and the other results.

Initial mesh of characteristics for $kB/c_0 = 6$:

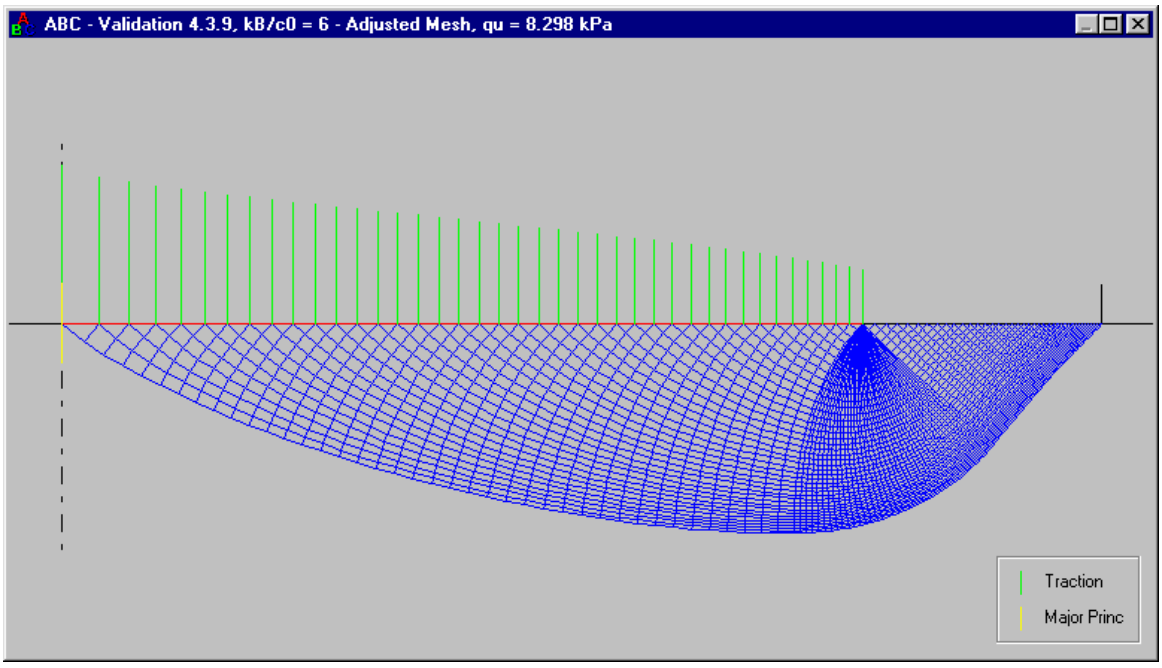

*4.3.10 Rough circular footing on non-homogeneous, undrained clay ($\phi = 0$)*

The bearing capacity is independent of $\gamma$ and is given by:

$$q_u = c_0 N_c + q \quad \text{where} \quad N_c = f\left(kB/c_0\right)$$

This problem has been studied previously by Salençon & Matar (1982a), Houlsby & Wroth (1983), Martin (1994) [see also Houlsby & Martin (2003)], and Tani & Craig (1995).

It is convenient to fix $c_0 = 1\,\text{kPa}$, $\phi = 0$, $\gamma = 0$ (or any other value), $B = 1\,\text{m}$ and $q = 0$, then choose $k$ to give the desired $kB/c_0$; the average bearing pressure $q_u$ then corresponds directly to the bearing capacity factor $N_c$. Converged results from ABC, with numerical results from other studies:

| $kB/c_0$ | $N_c$ | | | |
|---|---|---|---|---|
| | ABC | H. & W. (1983) | Martin (1994) | T. & C. (1995) |
| 0 | 6.048 | 6.05 | 6.05 | 6.34 |
| 1 | 6.946 | — | 6.95 | — |
| 2 | 7.626 | 7.61 | 7.63 | 7.70 |
| 3 | 8.211 | — | 8.21 | — |
| 4 | 8.740 | 8.71 | 8.73 | 8.77 |
| 5 | 9.232 | — | 9.23 | — |
| 6 | 9.695 | 9.67 | — | 9.72 |
| 8 | 10.56 | 10.54 | — | — |
| 10 | 11.37 | 11.33 | — | 11.38 |

In general there is close agreement between ABC and the other results. For small $kB/c_0$ the results of Tani & Craig (1995) are a little high, but their procedure for integrating the stresses acting on the 'false head' is suspect (Martin & Randolph, 2001).

Unfortunately the results of Salençon & Matar (1982a) are only presented in chart form, but they agree with ABC to within curve-reading accuracy.

Initial mesh of characteristics for $kB/c_0 = 6$:

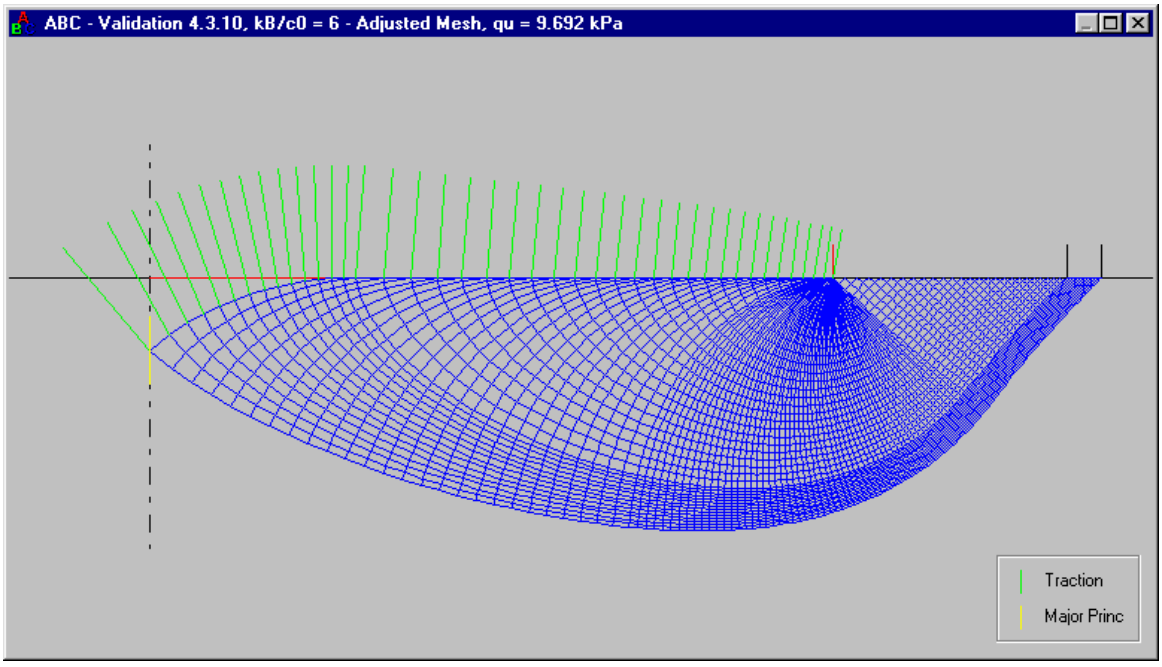

*4.3.11 Smooth circular footing on general cohesive-frictional soil*

Cox (1962) considered a series of problems involving a smooth circular footing on a general *c*-ϕ-γ soil. He defined a "relative cohesion" $c^*$ which in the present notation is equivalent to $c_0 + q\tan\phi$, the term that appears in the denominator of $F$ in equation (4.1). To characterise the relative importance of self-weight and cohesion/surcharge, he used a dimensionless ratio

$$G = \frac{\gamma B/2}{c^*}$$

Since Cox was only concerned with homogeneous soil ($k = 0$), there is a simple relationship between his $G$ the dimensionless ratio $F$ used here, namely $F = 2G\tan\phi$.

In Cox (1962) the results are presented as average bearing pressures, normalised with respect to $c^*$:

TABLE 1. VALUES OF THE MEAN YIELD-POINT PRESSURE $p_3/c^*$ FOR PUNCH INDENTATION

| $\phi$ \ $G$ | 0 | $10^{-2}$ | $10^{-1}$ | 1 | 10 |
|---|---|---|---|---|---|
| 0° | 5·69 | 5·69 | 5·69 | 5·69 | 5·69 |
| 10° | 9·98 | 9·99 | 10·0 | 10·4 | 13·8 |
| 20° | 20·1 | 20·1 | 20·3 | 22·4 | 38·8 |
| 30° | 49·3 | 49·4 | 50·5 | 60·6 | 141 |
| 40° | 164 | 165 | 173 | 237 | 754 |

Since the results in the first column had already been obtained by Cox et al. (1961), and the bearing capacity for $\phi = 0$ is independent of $G$, only 16 new calculations were required (Cox, 1962).

To reproduce these analyses in ABC it is convenient to fix $c_0 = 1\,\text{kPa}$, $k = 0$, $B = 2\,\text{m}$ and $q = 0$; the unit weight γ then corresponds directly to $G$, and the average bearing pressure $q_u$ corresponds directly to the normalised pressure in Cox's table. Converged results from ABC:

| ϕ (°) | $G$ | | | | |
|---|---|---|---|---|---|
| | 0 | $10^{-2}$ | $10^{-1}$ | 1 | 10 |
| 0 | 5.689 | 5.689 | 5.689 | 5.689 | 5.689 |
| 10 | 9.987 | 9.992 | 10.03 | 10.44 | 13.81 |
| 20 | 20.08 | 20.10 | 20.32 | 22.39 | 38.81 |
| 30 | 49.28 | 49.41 | 50.50 | 60.59 | 140.8 |
| 40 | 164.7* | 165.5* | 172.7* | 237.2* | 754.9 |

There is very close agreement between the two sets of results. Some of the solutions for $\phi = 40°$, indicated by *, involve crossing β characteristics (see Section 3.6.2).

*4.3.12 Rough circular footing on general cohesive-frictional soil*

Salençon & Matar (1982b) considered a series of problems involving a rough circular footing on a general *c*-ϕ-γ soil. The parameters for these problems, including the dimensionless ratio *F* defined in equation (4.1), were as follows:

| Problem[7] | $c_0$ (kPa) | $k$ (kPa/m) | ϕ (°) | γ (kN/m$^3$) | $B$ (m) | $q$ (kPa) | $F$ |
|---|---|---|---|---|---|---|---|
| A4 | 1 | 2.5 | 0 | 16 | 4 | 0 | 10 |
| A5 | 1 | 2.5 | 4 | 16 | 4 | 0 | 14.48 |
| A6 | 1 | 2.5 | 10 | 16 | 4 | 0 | 21.28 |
| B1 | 0 | 0.6 | 0 | 16 | 40 | 0 | ∞ |
| B2 | 0 | 0.6 | 4 | 16 | 40 | 0 | ∞ |
| B3 | 0 | 0.6 | 10 | 16 | 40 | 0 | ∞ |
| C | 16 | 0 | 30 | 18 | 4 | 18 | 1.575 |

The A and C problems can be solved without difficulty, but the B problems require special treatment because $F = \infty$. For problem B1, $\phi = 0$ and $F = \infty$ so the analytical solution $q_u = kB/6 + q$ is applicable (see Section 4.3.6). Problems B2 and B3 also have $F = \infty$, but now $\phi > 0$ so the situation is analogous to that of the '$N_\gamma$ problem' considered in Section 4.3.8. To solve these problems using ABC it is first necessary to introduce a nominal $c_0$ (or a nominal $q$) to make $F$ very large, but not greater than the permitted maximum of $10^{12}$ that applies when $\phi \geq 1°$. The analyses below were performed with $c_0 = 10^{-9}$ kPa, giving $F$ values of $6.9 \times 10^{10}$ for problem B2 and $1.4 \times 10^{11}$ for B3. Converged results from ABC, with numerical results from Salençon & Matar (1982b):

| Problem | $q_u$ (kPa) | |
|---|---|---|
| | ABC | S. & M. (1982b) |
| A4 | 11.37 | 11.3 |
| A5 | 18.33 | 17.7 |
| A6 | 39.19 | 39.1 |
| B1 | 4† | 4† |
| B2 | 27.26 | 27.0 |
| B3 | 125.1 | 126.2 |
| C | $2.517 \times 10^3$ | $2.52 \times 10^3$ |
| | † analytical | † analytical |

There is very close agreement between the two sets of results. Note that exact agreement would not be expected because Salençon & Matar (1982b) used the method of characteristics to produce a series of charts in terms of ϕ and (in the present notation) *F*. Their results for the example problems were based on factors read back from these charts, and not on a direct solution of each problem using the method of characteristics, as is done in ABC.

[7] Problems A1 to A3 involved a soil layer of limited depth.

## APPENDIX A. HOW ABC WORKS (REALLY)

It is useful to define the following constants:

$$c_0^* = c_0 + q\tan\phi \tag{A.1}$$

$$k^* = k + \gamma\tan\phi \tag{A.2}$$

Instead of developing the solution in terms of $x$, $z$, $\sigma$ and $\theta$ as described in Chapter 2, the back end of ABC works in terms of the normalised variables $\bar{x}$, $\bar{z}$, $\bar{\sigma}^*$ and $\theta$, where

$$\bar{x} = \frac{x}{B} \tag{A.3}$$

$$\bar{z} = \frac{z}{B} \tag{A.4}$$

$$\bar{\sigma}^* = \frac{\sigma^*}{c_0^*} \tag{A.5}$$

In equation (A.5), $\sigma^*$ denotes the mean stress relative to the geostatic stress field:

$$\sigma^* = \sigma - q - \gamma z \tag{A.6}$$

Equations analogous to (2.1) and (2.2) can be written as follows:

$$R^* = c^*\cos\phi + \sigma^*\sin\phi \tag{A.7}$$

where

$$c^* = c_0^* + k^* z \tag{A.8}$$

It is also useful to define a normalised Mohr's circle radius:

$$\begin{aligned}\bar{R}^* &= \frac{R^*}{c_0^*} \\ &= \frac{c^*\cos\phi + \sigma^*\sin\phi}{c_0^*} \\ &= \left(1 + F\bar{z}\right)\cos\phi + \bar{\sigma}^*\sin\phi\end{aligned} \tag{A.9}$$

In the last line the dimensionless ratio

$$F = \frac{k^* B}{c_0^*} \tag{A.10}$$

has been introduced. Equations (A.1) and (A.2) show that this is the same as the ratio referred to throughout the manual, namely

$$F = \frac{kB + \gamma B\tan\phi}{c_0 + q\tan\phi} \tag{A.11}$$

Noting that $R^*$ in equation (A.7) is equal to $R$ in equation (2.1), it is possible to recast the equations of Chapter 2 in dimensionless form using just $\phi$, $F$ and the normalised variables. As before the problem is assumed to be static, so that the body forces are $\gamma_x = 0$ and $\gamma_z = \gamma$.

In plane strain, equations (2.4) and (2.5) along the characteristics become:

$$\frac{\mathrm{d}\bar{x}}{\mathrm{d}\bar{z}} = \tan\left(\theta \pm \varepsilon\right) \tag{A.12}$$

and

$$\mathrm{d}\bar{\sigma}^* \pm \frac{2\bar{R}^*}{\cos\phi}\mathrm{d}\theta = \mp F\mathrm{d}\bar{x} \tag{A.13}$$

In axial symmetry, equations (2.7) and (2.8) along the characteristics become:

$$\frac{\mathrm{d}\bar{x}}{\mathrm{d}\bar{z}} = \tan\left(\theta \pm \varepsilon\right) \tag{A.14}$$

and

$$\mathrm{d}\bar{\sigma}^* \pm \frac{2\bar{R}^*}{\cos\phi}\mathrm{d}\theta = \mp F\mathrm{d}\bar{x} + \left(\bar{\gamma}_x^* \mp \bar{\gamma}_z^* \tan\phi\right)\mathrm{d}\bar{x} + \left(\bar{\gamma}_z^* \pm \bar{\gamma}_x^* \tan\phi\right)\mathrm{d}\bar{z} \tag{A.15}$$

where

$$\begin{aligned} \bar{\gamma}_x^* &= \frac{\bar{R}^*\left(\cos 2\theta - 1\right)}{\bar{x}} \\ \bar{\gamma}_z^* &= -\frac{\bar{R}^* \sin 2\theta}{\bar{x}} \end{aligned} \tag{A.16}$$

The first of equations (2.10), defining the mean stress on the free surface, becomes:

$$\bar{\sigma}_{\text{passive}}^* = \frac{\cos\phi}{1-\sin\phi} \tag{A.17}$$

It is also easy to express equation (2.21) in terms of the normalised variables.

When converting the finite difference formulation in Section 2.4, it is largely a matter of making the replacements $x \to \bar{x}$, $z \to \bar{z}$, $\sigma \to \bar{\sigma}^*$ and $R \to \bar{R}^*$, along with appropriate modifications to the finite difference equations. For example equations (2.13) become:

$$\begin{aligned} \bar{\sigma}_{\text{C}}^* - \bar{\sigma}_{\text{A}}^* + \frac{\bar{R}_{\text{A}}^* + \bar{R}_{\text{C}}^*}{\cos\phi}\left(\theta_{\text{C}} - \theta_{\text{A}}\right) &= -F\left(\bar{x}_{\text{C}} - \bar{x}_{\text{A}}\right) \\ \bar{\sigma}_{\text{C}}^* - \sigma_{\text{B}}^* - \frac{\bar{R}_{\text{B}}^* + R_{\text{C}}}{\cos\phi}\left(\theta_{\text{C}} - \theta_{\text{B}}\right) &= F\left(\bar{x}_{\text{C}} - \bar{x}_{\text{B}}\right) \end{aligned} \tag{A.18}$$

Equations (2.24), relating $\sigma$ and $\theta$ on the degenerate characteristic, become:

$$\begin{aligned} \bar{\sigma}^* &= \bar{\sigma}_{\text{passive}}^* + 2\left(\theta_{\text{passive}} - \theta\right) && \text{if } \phi = 0 \\ \bar{\sigma}^* &= \left(\cot\phi + \bar{\sigma}_{\text{passive}}^*\right) e^{2\tan\phi\left(\theta_{\text{passive}} - \theta\right)} - \cot\phi && \text{if } \phi > 0 \end{aligned} \tag{A.19}$$

The average bearing pressure $q_{\text{u}}$ is evaluated from:

$$\begin{aligned} q_{\mathrm{u}} &= q + 2c_0^* \oint_C \bar{\sigma}_{zz}^* \mathrm{d}\bar{x} - \bar{\tau}_{xz}^* \mathrm{d}\bar{z} && \text{plane strain} \\ q_{\mathrm{u}} &= q + 8c_0^* \oint_C \bar{\sigma}_{zz}^* \bar{x}\mathrm{d}\bar{x} - \bar{\tau}_{xz}^* \bar{x}\mathrm{d}\bar{z} && \text{axial symmetry} \end{aligned} \tag{A.20}$$

The curve $C$ is as defined in Section 2.10. If $x_0 \neq 0$ (see Section 3.4.6) the expression for axial symmetry becomes

$$q_{\mathrm{u}} = \left[1 - \left(2\bar{x}_0\right)^2\right] q + 8c_0^* \oint_C \bar{\sigma}_{zz}^* \bar{x}\mathrm{d}\bar{x} - \bar{\tau}_{xz}^* \bar{x}\mathrm{d}\bar{z} \tag{A.21}$$

where, cf. equation (A.3),

$$\bar{x}_0 = x_0 / B \tag{A.22}$$

In equations (A.20) and (A.21) the stress components are evaluated from the second and third of the following (cf. equations (2.3)/(2.6)):

$$\begin{aligned} \bar{\sigma}_{xx}^* &= \bar{\sigma}^* - \bar{R}^* \cos 2\theta \\ \bar{\sigma}_{zz}^* &= \bar{\sigma}^* + \bar{R}^* \cos 2\theta \\ \bar{\tau}_{xz}^* &= \bar{R}^* \sin 2\theta \end{aligned} \tag{A.23}$$

Having determined $q_{\mathrm{u}}$, the bearing capacity as a force $Q_{\mathrm{u}}$ can now be obtained from:

$$\begin{aligned} Q_{\mathrm{u}} &= q_{\mathrm{u}} \cdot B && \text{plane strain} \\ Q_{\mathrm{u}} &= q_{\mathrm{u}} \cdot \pi B^2 / 4 && \text{axial symmetry} \end{aligned} \tag{A.24}$$

Once the mesh has been constructed and the bearing capacity has been calculated, the actual values of $\sigma_{xx}$, $\sigma_{zz}$ and $\tau_{xz}$ at certain solution points need to be recovered for drawing and reporting purposes. These can be found from the normalised stress components of equation (A.23) via:

$$\begin{aligned} \sigma_{xx} &= c_0^* \bar{\sigma}_{xx}^* + q + \gamma B \bar{z} \\ \sigma_{zz} &= c_0^* \bar{\sigma}_{zz}^* + q + \gamma B \bar{z} \\ \tau_{xz} &= c_0^* \bar{\tau}_{xz}^* \end{aligned} \tag{A.25}$$

**REFERENCES**

Bishop, J.F.W. (1953). On the complete solution to problems of deformation of a plastic-rigid material. *J. Mech. Phys. Solids*, Vol. 2, pp 43-53.

Bolton, M.D. & Lau, C.K. (1993). Vertical bearing capacity factors for circular and strip footings on Mohr-Coulomb soil. *Can. Geotech. J.*, Vol. 30, pp 1024-1033.

Caquot, A. & Kerisel, J. (1953). Sur le terme de surface dans le calcul des fondations en milieu pulvérulent. *Proc. 3rd Int. Conf. on Soil Mech. and Found. Eng., Zurich*, Vol. 1, pp 336-337.

Cassidy, M.J. & Houlsby, G.T. (2002). Vertical bearing capacity factors for conical footings on sand. *Géotechnique*, Vol. 52, No. 9, pp 687-692.

Cox, A.D. (1962). Axially-symmetric plastic deformation in soils—II. Indentation of ponderable soils. *Int. J. Mech. Sci.*, Vol. 4, pp 371-380.

Cox, A.D., Eason, G. & Hopkins, H.G. (1961). Axially symmetric plastic deformation in soils. *Proc. R. Soc. London (Ser. A)*, Vol. 254, pp 1-45.

Davis, E.H. & Booker, J.R. (1971). The bearing capacity of strip footings from the standpoint of plasticity theory. *Proc. 1st Australia-New Zealand Conf. on Geomech., Melbourne*, pp 276-282.

Davis, E.H. & Booker, J.R. (1973). The effect of increasing strength with depth on the bearing capacity of clays. *Géotechnique*, Vol. 23, No. 4, pp 551-563.

Eason, G. & Shield, R.T. (1960). The plastic indentation of a semi-infinite solid by a perfectly rough circular punch. *J. Appl. Math. Phys. (ZAMP)*, Vol. 11, pp 33-43.

Etzel, M. & Dickinson, K. (1999). *Digital Visual Fortran programmer's guide*. Oxford: Digital Press.

Hansen, B. & Christensen, N.H. (1969). Discussion of "Theoretical bearing capacity of very shallow footings" by A.L. Larkin. *J. Soil Mech. and Found. Div., ASCE*, Vol. 95, No. 6, pp 1568-1572.

Hencky, H. (1923). Über einige statisch bestimmte Fälle des Gleichgewichts in plastischen Körpern. *Zeit. angew. Math. Mech.*, Vol. 3, pp 241-251.

Houlsby, G.T. (1982). Theoretical analysis of the fall cone test. *Géotechnique*, Vol. 32, No. 2, pp 111-118.

Houlsby, G.T. & Wroth, C.P. (1983). Calculation of stresses on shallow penetrometers and footings. *Proc. IUTAM / IUGG Symp. on Seabed Mech., Newcastle upon Tyne*, pp 107-112.

Houlsby, G.T. & Martin, C.M. (2003). Undrained bearing capacity factors for conical footings on clay. *Géotechnique*, Vol. 53, No. 5, pp 513-520.

Lundgren, H. (1953). Discussion of Session 4. *Proc. 3rd Int. Conf. on Soil Mech. and Found. Eng., Zurich*, Vol. 3, pp 153-154.

Lundgren, H. & Mortensen, K. (1953). Determination by the theory of plasticity of the bearing capacity of continuous footings on sand. *Proc. 3rd Int. Conf. on Soil Mech. and Found. Eng., Zurich*, Vol. 1, pp 409-412.

Martin, C.M. (1994). *Physical and numerical modelling of offshore foundations under combined loads*. D.Phil. thesis, University of Oxford.

Martin, C.M. & Randolph, M.F. (2001). Applications of the lower and upper bound theorems of plasticity to collapse of circular foundations. *Proc. 10th Int. Conf. on Comp. Meth. and Adv. in Geomech., Tucson*, Vol. 2, pp 1417-1428.

Martin, C.M. (2003). New software for rigorous bearing capacity calculations. *Proc. British Geotech. Assoc. Int. Conf. on Foundations, Dundee*, pp 581-592.

Martin, C.M. (2004). Discussion of "Calculations of bearing capacity factor $N_\gamma$ using numerical limit analyses" by B. Ukritchon, A.J. Whittle & C. Klangvijit. *J. Geotech. and Geoenv. Eng., ASCE*, Vol. 130, No. 10, pp 1106-1107.

Michalowski, R.L. (1997). An estimate of the influence of soil weight on bearing capacity using limit analysis. *Soils and Foundations*, Vol. 37, No. 4, pp 57-64.

Moré, J.J., Garbow, B.S. & Hillstrom, K.E. (1980). User guide for MINPACK-1. *Tech. Rep. ANL-80-74*, Argonne National Laboratory.

Powell, M.J.D. (1970). A hybrid method for nonlinear algebraic equations. In *Numerical methods for nonlinear algebraic equations* (ed. P. Rabinowitz), pp 87-114. London: Gordon and Breach.

Prandtl, L. (1921). Über die Eindringungsfestigkeit (Härte) plastischer Baustoffe und die Festigkeit von Schneiden. *Zeit. angew. Math. Mech.*, Vol. 1, pp 15-20.

Salençon, J. & Matar, M. (1982a). Capacité portante des fondations superficielles circulaires. *J. de Mécanique théorique et appliquée*, Vol. 1, No. 2, pp 237-267.

Salençon, J. & Matar, M. (1982b)[1]. Bearing capacity of circular shallow foundations. In *Foundation engineering* (ed. G. Pilot), pp 159-168. Paris: Presses de l'ENPC.

Shield, R.T. (1955). On the plastic flow of metals under conditions of axial symmetry. *Proc. R. Soc. London (Ser. A)*, Vol. 233, pp 267-287.

Sokolovskii, V.V. (1965). *Statics of granular media.* New York: Pergamon.

Tani, K. & Craig, W.H. (1995). Bearing capacity of circular foundations on soft clay of strength increasing with depth. *Soils and Foundations*, Vol. 35, No. 4, pp 21-35.

Ukritchon, B., Whittle, A.J. & Klangvijit, C. (2003). Calculations of bearing capacity factor $N_\gamma$ using numerical limit analyses. *J. Geotech. and Geoenv. Eng., ASCE*, Vol. 129, No. 6, pp 468-474.

[1] This is basically a translation of the preceding reference, but it includes additional worked examples.